Karlsruhe Institute of Technology

Lattice design of a transfer line for ultra-short bunches from FLUTE to cSTART

Master's Thesis of

Jens Schäfer

at the Department of Physics
Laboratory for Applications of Synchrotron Radiation

Reviewer:	Prof. Dr. Anke-Susanne Müller
Second reviewer:	Prof. Dr. Ulrich Husemann
Supervisor:	Dr. Bastian Härer

October 2019

I declare that I have developed and written the enclosed thesis completely by myself, and have not used sources or means without declaration in the text.

Karlsruhe, October 7, 2019

.....
(**Jens Schäfer**)

This thesis has been accepted by the first reviewer of the master's thesis.

Karlsruhe, October 7, 2019

.....
(**Prof. Dr. Anke-Susanne Müller**)

Zusammenfassung

Teilchenbeschleuniger sind wertvolle Werkzeuge für Wissenschaft und Technologie. Sie werden zum Beispiel als Quellen für Licht eingesetzt, welches mit seinen einzigartigen Eigenschaften vielfältig Verwendung findet. Für den Bereich der Spektroskopie sind insbesondere Beschleuniger zur Produktion von kurzen Elektronenpakete (genannt Bunche) interessant, da diese kurze Lichtpulse abstrahlen und somit eine hohe zeitliche Auflösung der Spektroskopie ermöglichen. Das Project **c**ompact **St**orage ring for **A**ccelerator **R**esearch and **T**echnology, kurz cSTART, wird die Dynamik von ultrakurzen Bunche in einem Speicherring untersuchen und neue Beschleunigertechnologien zur Erhaltung der Bunchlänge testen. Das **F**erninfrarot **L**inac- **u**nd **T**est-**E**xperiment FLUTE wird als einer von zwei Vollenergieinjektoren für cSTART verwendet, das Experiment erzeugt ultrakurze Bunchen mit einer geplanten Wiederholrate von zehn Hertz. Damit die Bunche von FLUTE in cSTART injiziert werden können, ist eine besondere Transferlinie nötig. Die Transferlinie wird die Bunche von FLUTE horizontal sowie vertikal ablenken müssen, da cSTART und FLUTE übereinander in einer vorhandenen Halle installiert werden. Aufgrund der dispersiven Effekte der Ablenkungen ändert sich das longitudinale Bunchprofil und die ultrakurze Bunchlänge kann nicht erhalten werden. Damit bei cSTART dennoch kurze Bunche injiziert werden können, wird der Bunch nicht zum Ende von FLUTE komprimiert, sondern die dispersiven Effekte während der Transportwege werden so ausgenutzt, dass der Bunch zum Injektionspunkt hin komprimiert wird. Die kürzeste Bunchlänge ergibt sich, wenn die Teilchenverteilung im longitudinalen Phasenraum linear und vertikal ausgerichtet ist. Das wird am Injektionspunkt erreicht, wenn die longitudinale Optik der Transferlinie die Bedingung für Vollkompression in erster und zweiter Ordnung erfüllt. Dazu muss die longitudinale lineare Optik der Transferlinie so ausgerichtet werden, dass der Bunch im longitudinalen Phasenraum von seiner initialen Schräglage in eine aufrechte Position geschert wird. Des Weiteren muss die longitudinale Optik in zweiter Ordnung so eingestellt werden, dass der Bunch während des Transportes keine Krümmung im longitudinalen Phasenraum entwickelt. Um die Bedingungen der Vollkompression erfüllen zu können, werden verschiedene achromatische Module der Magnetstruktur auf ihre longitudinalen Eigenschaften untersucht. Eine geschickte Kombination verschiedener Module ermöglicht das Erfüllen beider Kompressionsbedingungen, wodurch die Bunche zum Injektionspunkt hin komprimiert werden.

Mit dieser Strategie werden zwei Transferlinien entwickelt, von denen Layout A in einen der nahe gelegenen und Layout B in einen der entfernt gelegenen Symmetriepunkte von cSTART injiziert. Bedingt durch die Geometrie muss die Transferlinie in Layout A vertikal in cSTART injizieren. Die Entwicklung eines vertikalen Injektionsschemas ist nicht Teil dieser Arbeit und steht aus als eine künftige Herrausforderung. Daraus folgt, dass die transversalen Strahlparameter innerhalb dieser Arbeit nicht an cSTART angeknüpft werden können. Die Geometrie von Layout B andererseits ermöglicht ein horizontales Injektionsschema. Damit können die transversalen Strahlparameter an die Optik von cSTART angeknüpft werden konnte. Für Layout B können damit die transversalen Strahlparameter

am Injektionspunkt so abgestimmt werden, dass die Fortführung der Strahlparameter durch cSTART der periodischen Lösung entsprechen. Beide Transferlinien erfüllen die Bedingung für Vollkompression in erster und zweiter Ordnung. Ein Testbunch, der aus Simulationen von FLUTE stammt, wird für tracking Simulationen durch beide Strukturen verwendet. Diese Studien zeigen, dass der Bunch am Ende beider Transportwege im longitudinalen Phasenraum tatsächlich vertikal ausgerichtet und linearisiert ist. Der Transport durch Layout A resultiert in einer finale Bunchlänge von 70 fs. Die hohen Dispersionsamplituden bedingen Effekte höherer Ordnungen, wodurch der Bunch eine Aufweitung im longitudinalen Phasenraum erfährt. Die Transferlinie in Layout B bietet genug Platz für die Verwendung von dispersionsärmeren Modulen. Dadurch kann im Vergleich zu Layout A die maximale Dispersion halbiert und damit die finale Bunchlänge auf 17 fs reduziert werden. Zusätzlich bietet Layout B offene Freiheitsgrade in der longitudinalen Optik um den Bunch während des Transports zusätzlich zu modulieren, sodass das Erscheinungsbild des Bunche am Injektionspunkt nachjustiert werden kann.

Im Rahmen dieser Arbeit werden die Simulationsumgebungen und die Geometrien für zwei Transferlinien entwickelt, welche starke Ablenkungen in beiden transversalen Ebenen durchführen und dem begrenzten Raum sowie den technischen Rahmenbedingungen genügen. Für beide Versionen ist die transversal gekoppelte Optik sowie die longitudinale Optik in erster und zweiten Ordnung berechnet. Trackingsimulationen die Randeffekte, Strahlungseffekte und Apperturbegrenzungen berücksichtigen, ergeben eine Transmissionseffizienz von 100%. Die Arbeit zeigt, dass es möglich ist, einen Bunch aus FLUTE mit einer ultrakurzen Bunchlänge von weniger als 20 fs in cSTART zu injizieren. Somit stellt diese Arbeit einen wichtigen Beitrag zu dem Projekt cSTART dar, welches auf eine neue Generation von Lichtquellen hinarbeitet.

Abstract

This Master's Thesis discusses the lattice design of a transfer line for ultra short bunches from FLUTE to cSTART. The **c**ompact **St**orage ring for **A**ccelerator **R**esearch and **T**echnology cSTART is a test facility for novel techniques of storing ultra short bunches. The goal of cSTART is to develop a new generation of compact light sources which combine the benefits of linear and circular accelerator facilities, the radiation of short light pulses with a high repetition rate. The **F**erninfrarot **L**inac- **u**nd **T**est-**E**xperiment FLUTE serves as a full energy injector for cSTART, providing bunches with a length of only a few femtoseconds and stable beam parameters. As a consequence of the spatial arrangement of injector and storage ring, a transfer line is required which deflects the bunches in both transverse planes. The unavoidable dispersion affects the path length for off-energy particles and consequentially increases the bunch length. A concept for guiding the FLUTE bunches and avoiding the longitudinal spreading is developed in this thesis, taking into account the technical limitations, coupled transverse optics and non-linear longitudinal beam dynamics. In addition, tracking simulations including radiation effects prove the compression performance of the transfer line.

Contents

1. Introduction

This thesis presents the lattice design for a transfer line for ultra-short bunches from the **F**erninfrarot **L**inac- **u**nd **T**est-**E**xperiment FLUTE [1] to **c**ompact **St**orage ring for **A**ccelerator **R**esearch and **T**echnology cSTART [2]. The research facility cSTART investigates the dynamics of ultra-short electron bunches in a storage ring and therefore is a step towards a next generation of synchrotron light sources.

The electromagnetic radiation emitted by an electron beam is called synchrotron radiation and has unique features such as a high intensity and a wide spectrum ranging from hard x-rays to THz radiation. One of the many areas of application of this radiation is spectroscopy, where the temporal resolution is limited to the length of the light pulse, which is proportional to the bunch length in the accelerator. As a consequence, short bunches are of great interest. Accelerators built for the purpose of providing radiation are called light sources and can be separated into two main categories:

1. Free Electron Lasers (FEL) based on linear accelerators can produce ultra-short bunches in the order of femtoseconds but with a low repetition rate of a few hertz due to single shot operation. Examples of such machines are the European XFEL [3] at DESY, Germany, and SwissFEL [4] at PSI, Switzerland.
2. Synchrotron light sources store multiple bunches. The accumulation and the circular trajectory greatly increases the repetition rate of the emitted synchrotron light. On the other hand, the natural energy spread of a bunch leads to a larger bunch length in the equilibrium state which typically is in the order of picoseconds. Examples of these facilities are KARA [5] at KIT, Germany, or MAX IV [6] at MAX-lab, Sweden.

A light source combining both benefits could not be built yet but is of great interest for the community. The research facility cSTART is a first step towards this goal. It will investigate the evolution of a stored, ultra-short bunch with a length of only a few femtoseconds and provides a test bench for new technologies trying to conserve the short bunch length.

In addition, cSTART keeps the required space at a minimum with a circumference of only 44 m for a beam energy of 50 MeV. The compact design allows to save space and magnetic elements, this makes the facility cost and energy efficient. For further reduction of the project's footprint, a laser wake field accelerator (LWFA) will be used as full energy injector. A LWFA provides accelerating voltages in the range of GV/m, which is a thousand times higher than the accelerating voltage of today's RF technology. This allows to shrink down the accelerating structures by a factor of 10^3. In addition, this new technology can provide ultra-short bunches [8] which makes it an excellent component for this new generation of light sources. Yet bunches produced by an LWFA accelerator have a large momentum spread and shot-to-shot variance of the beam parameters, therefore they could not be stored so far. The lattice of cSTART is specialized for accepting these difficult bunches and demonstrates that they can be stored.

As a second injector with stable beam parameters FLUTE will be used. FLUTE provides ultra-short electron bunches with a repetition rate of 1 Hz based on conventional accelerator

technologies. It is located at the ground floor of the same experimental hall where cSTART will be installed. The guidance of the short bunches from FLUTE to the storage ring requires a special transfer line [9]. The limited space in the experimental hall requires the transfer line to deflect the beam several times in the horizontal and vertical plane. Yet each deflection spreads the bunch in the transverse plane, which results in different path lengths for each particle. As a consequence, the short bunch length cannot be maintained during deflections. The challenge of the transfer line is to guide the bunches to the injection point of cSTART where they should arrive as short as possible. Th discussions in this Thesis include coupled transverse and non-linear longitudinal beam dynamics. An 3-D impression of the project including the footprint of the experimental hall, FLUTE, one possible transfer line layout and cSTART is shown in Fig. 1.1.

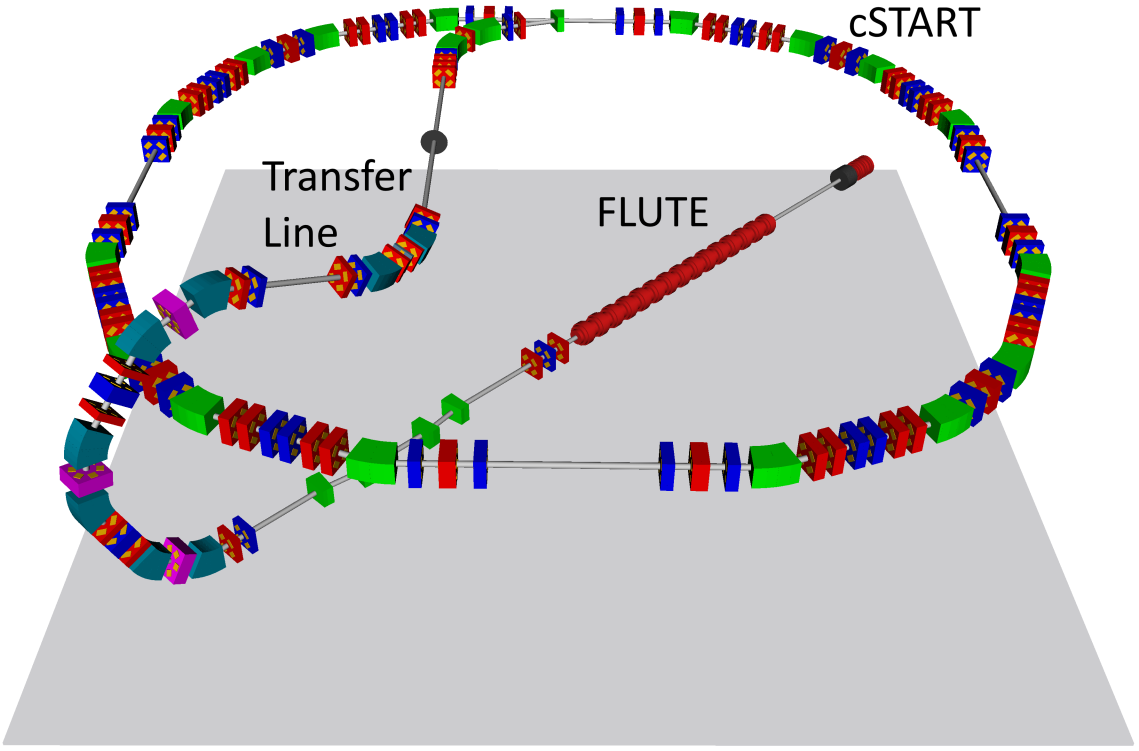

Figure 1.1.: Footprint of the experimental hall in gray. FLUTE at the ground floor orientated diagonally. The transfer line, presented in Layout B, guides the bunches from FLUTE to the injection point in a straight section of cSTART. The storage ring has a circumference of 44 m, it is horizontally aligned 2 m above FLUTE. The 3-D image was created by using the program view3dscene from the SDDStoolkit [7].

2. Accelerator physics for single-pass structures

This chapter will give an introduction into basic accelerator physics with emphasis on propagating a particle ensemble and its corresponding beam parameters through a single-pass structure with deflection in both the horizontal and the vertical plane. The discussion follows [10], [11] and [12].

2.1. Coordinate system

A particle accelerator is designed to guide particles with a given energy along a predefined trajectory. This reference orbit is taken by the reference particle with exactly the reference energy and without an initial spatial offset. In order to simplify the calculations of beam dynamics not the laboratory frame is used but the Frenet-Serret coordinate system, which moves along the reference orbit. Its origin is the position of the reference particle at every point in time, while the right handed axes are $\hat{x}$ and $\hat{y}$ for the transverse plane and $\hat{z}$ along the trajectory as shown in Fig. 2.1.

2.2. Accelerator elements

Steering and focusing of charged particles is done by the Lorentz force

$$\vec{F_L} = e\left(\vec{E} + \vec{v} \times \vec{B}\right) = \dot{\vec{p}}. \tag{2.1}$$

The beam of FLUTE consists of electrons with an energy of about 41.5 MeV, which leads to a velocity close to the speed of light.

$$\gamma = 1 + \frac{E_{\text{kin}}}{m_e c^2} = 81 \tag{2.2}$$

$$\beta = \sqrt{1 - \gamma^{-2}} = 0.99992 \tag{2.3}$$

$$v = \beta c = (1 - 8 \times 10^{-5})c \tag{2.4}$$

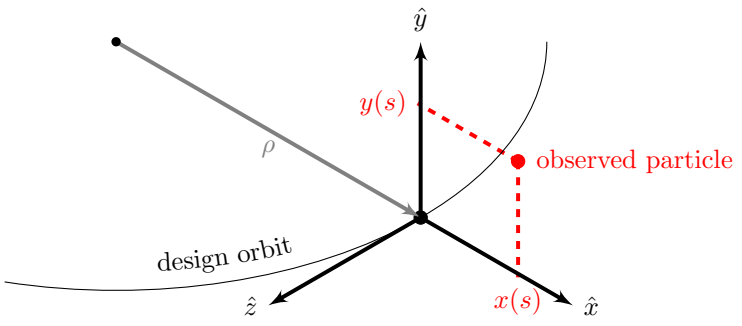

Figure 2.1.: Frenet-Serret coordinate system used in accelerator physics. $\hat{x}$, $\hat{y}$, and $\hat{z}$ form the right-handed orthogonal basis, ρ is the local bending radius [13].

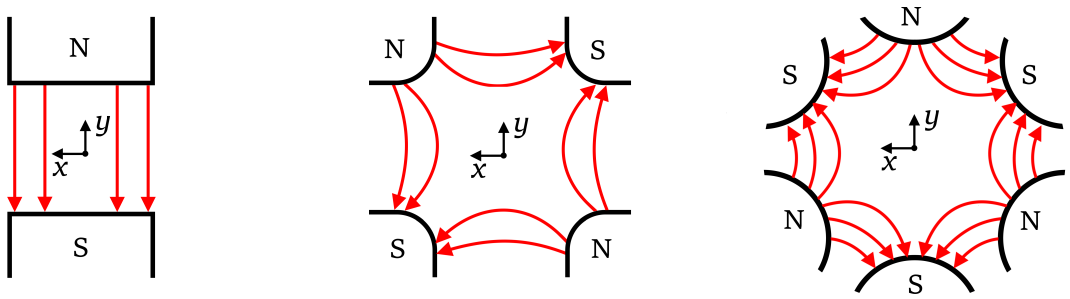

Figure 2.2.: Geometry of the yoke and the magnetic field lines within a dipole (a), a quadrupole (b) and a sextupole (c).

In this relativistic case a magnetic field of $B = 1\,\mathrm{T}$ perpendicular to the particle's velocity applies a comparable force to an electric field of $E \approx 3 \times 10^8\,\mathrm{V/m}$. While a magnetic field in the order of one Tesla is possible to build, a comparable electric field exceeds today's technological capabilities. Therefore the guidance and focusing of the beam is done by magnets. Electric fields are still used to increase the particles energy. This is achieved by cavities housing electric fields oscillating at radio frequency (RF).

The magnets are installed along the design orbit with their magnetic center at $x = y = 0$. In this case, the magnetic field can be expanded into a Taylor series around the magnet's center:

$$B_y(x) = \sum_{n=0}^{\infty} \frac{x^n}{n!} \frac{\partial^n B_y}{\partial x^n} = B_0 + x\frac{\partial B_y}{\partial x} + \frac{x^2}{2}\frac{\partial^2 B_y}{\partial x^2} + \dots \tag{2.5}$$

This can be rewritten as

$$B_y(x) = \frac{p}{e}\left(K_0 + xK_1 + \frac{x^2}{2}K_2 + \dots\right) \tag{2.6}$$

with the reference momentum p_0 and the multipole strengths K_n.

$$\text{Dipole} \qquad K_0 = \frac{e}{p_0}B_0 = \frac{1}{\rho} \qquad \left[m^{-1}\right] \tag{2.7}$$

$$\text{Quadrupole} \qquad K_1 = \frac{e}{p_0}\frac{\partial B_y}{\partial x} \qquad \left[m^{-2}\right] \tag{2.8}$$

$$\text{Sextupole} \qquad K_2 = \frac{e}{p_0}\frac{\partial^2 B_y}{\partial x^2} \qquad \left[m^{-3}\right] \tag{2.9}$$

Dipole magnets are used for steering, quadrupoles for focusing divergent particles and sextupoles for compensating chromatic effects. The geometries of the iron yokes of the first three multipoles are shown in Fig. 2.2. The optics of lattices consisting of dipoles and quadrupoles are called linear because of the magnetic fields rising only linearly with a transverse offset.

2.3. 6-D transport matrix formalism

The trajectories of particles along a magnetic lattice can be calculated with a simple matrix formalism. Each particle is described by its six dimensional state vector

$$\vec{\chi} = \begin{bmatrix} x \\ x' \\ y \\ y' \\ z \\ \delta \end{bmatrix}. \tag{2.10}$$

The positions x, y and z and the transverse slopes $x' = \frac{dx}{dz}, y' = \frac{dy}{dz}$ are expressed in the Frenet-Serret coordinate system. The relative momentum deviation $\delta = \Delta p/p_0$ is calculated with respect to the reference momentum p_0.

All accelerator elements can be parameterized as a square transport matrix R. A particle traveling through or being affected by an element simply changes its state vector according to

$$\vec{\chi}(S_2) = R\vec{\chi}(S_1). \tag{2.11}$$

R can be the transport matrix of a single element or a longer section of the lattice, which is then a product of many transfer matrices.

The full transport matrix is a 6×6 matrix.

$$R = \begin{bmatrix} R_{11} & R_{12} & R_{13} & R_{14} & R_{15} & R_{16} \\ R_{21} & R_{22} & R_{23} & R_{24} & R_{25} & R_{26} \\ R_{31} & R_{32} & R_{33} & R_{34} & R_{35} & R_{36} \\ R_{41} & R_{42} & R_{43} & R_{44} & R_{45} & R_{46} \\ R_{51} & R_{52} & R_{53} & R_{54} & R_{55} & R_{56} \\ R_{61} & R_{62} & R_{63} & R_{64} & R_{65} & R_{66} \end{bmatrix} \tag{2.12}$$

Not all matrix elements are free parameters. In the case of the transfer line, the generic transport matrix can be simplified a lot. Without RF cavities the transfer line has no time dependent elements. The initial z position must not have an influence on the transformation except an offset in the final z position. Therefore, R simplifies to

$$R = \begin{bmatrix} R_{11} & R_{12} & R_{13} & R_{14} & 0 & R_{16} \\ R_{21} & R_{22} & R_{23} & R_{24} & 0 & R_{26} \\ R_{31} & R_{32} & R_{33} & R_{34} & 0 & R_{36} \\ R_{41} & R_{42} & R_{43} & R_{44} & 0 & R_{46} \\ R_{51} & R_{52} & R_{53} & R_{54} & 1 & R_{56} \\ R_{61} & R_{62} & R_{63} & R_{64} & 0 & R_{66} \end{bmatrix}. \tag{2.13}$$

If the energy loss due to synchrotron radiation is very small, it can be neglected and energy is conserved. The matrix's sixth row is simplified accordingly:

$$R = \begin{bmatrix} R_{11} & R_{12} & R_{13} & R_{14} & 0 & R_{16} \\ R_{21} & R_{22} & R_{23} & R_{24} & 0 & R_{26} \\ R_{31} & R_{32} & R_{33} & R_{34} & 0 & R_{36} \\ R_{41} & R_{42} & R_{43} & R_{44} & 0 & R_{46} \\ R_{51} & R_{52} & R_{53} & R_{54} & 1 & R_{56} \\ 0 & 0 & 0 & 0 & 0 & 1 \end{bmatrix} \tag{2.14}$$

Without transversally tilted elements and sextupoles the optics stays uncoupled in the horizontal and the vertical plane. This means that the dynamics in x, x' is not dependent on the values of y, y' and vice versa, therefore the off-diagonal blocks become zero.

$$R = \begin{bmatrix} R_{11} & R_{12} & 0 & 0 & 0 & R_{16} \\ R_{21} & R_{22} & 0 & 0 & 0 & R_{26} \\ 0 & 0 & R_{33} & R_{34} & 0 & R_{36} \\ 0 & 0 & R_{43} & R_{44} & 0 & R_{46} \\ R_{51} & R_{52} & R_{53} & R_{54} & 1 & R_{56} \\ 0 & 0 & 0 & 0 & 0 & 1 \end{bmatrix} \tag{2.15}$$

All accelerator elements discussed so far only apply conservative forces on the particles. As a consequence of Liouville's theorem the phase space volume of the bunch is conserved during the transport and the transport matrices R fulfill the symplecticity condition.

$$R^T U R = U \qquad \text{with} \qquad U = \begin{bmatrix} 0 & I_n \\ -I_n & 0 \end{bmatrix} \tag{2.16}$$

Products of symplectic matrices stay symplectic. This condition further reduces the fifth row:

$$R = \begin{bmatrix} R_{11} & R_{12} & 0 & 0 & 0 & R_{16} \\ R_{21} & R_{22} & 0 & 0 & 0 & R_{26} \\ 0 & 0 & R_{33} & R_{34} & 0 & R_{36} \\ 0 & 0 & R_{43} & R_{44} & 0 & R_{46} \\ R_{26} & R_{16} & R_{46} & R_{36} & 1 & R_{56} \\ 0 & 0 & 0 & 0 & 0 & 1 \end{bmatrix} \tag{2.17}$$

The 36 matrix elements are reduced to 13 parameters which can be assigned to horizontal optics ($R_{11}, R_{12}, R_{21}, R_{22}$), vertical optics ($R_{33}, R_{34}, R_{43}, R_{44}$) and longitudinal optics ($R_{16}, R_{26}, R_{36}, R_{46}, R_{56}$). As long as x-y coupling is avoided, transport matrices of single elements and any combination thereof will stay in the shape of Eq. (2.17).

The following sections will present a few examples of transport matrices and how they modify the particle state vector $\vec{\chi}$.

2.3.1. Drifts

A drift space with length L_D is represented by the transport matrix R_{Drift}. For tracking a single arbitrary particle through a drift space the matrix R_{Drift} is multiplied with the state vector $\vec{\chi}$ resulting in

$$\vec{\chi}(S_1 + L_D) = R_{\text{Drift}} \times \vec{\chi}(S_1) = \begin{bmatrix} 1 & L_D & 0 & 0 & 0 & 0 \\ 0 & 1 & 0 & 0 & 0 & 0 \\ 0 & 0 & 1 & L_D & 0 & 0 \\ 0 & 0 & 0 & 1 & 0 & 0 \\ 0 & 0 & 0 & 0 & 1 & 0 \\ 0 & 0 & 0 & 0 & 0 & 1 \end{bmatrix} \times \begin{bmatrix} x \\ x' \\ y \\ y' \\ z \\ \delta \end{bmatrix} = \begin{bmatrix} x + x' L_D \\ x' \\ y + y' L_D \\ y' \\ z \\ \delta \end{bmatrix}. \tag{2.18}$$

The transverse offset changes with the product of the offset slope and the drift length while the remaining elements of the state vector stay the same.

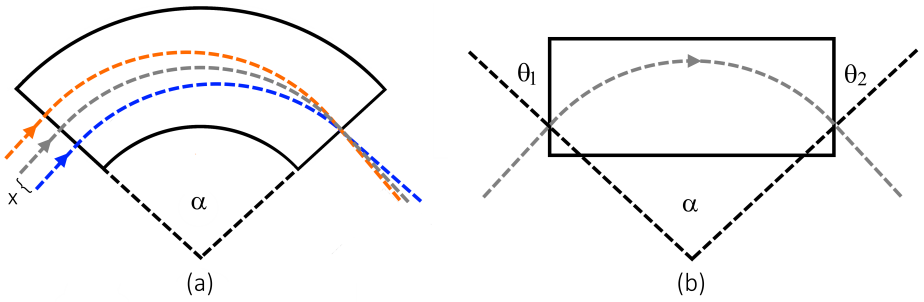

Figure 2.3.: Geometry of a sector dipole (a) and a rectangular dipole (b). The three trajectories belong to particles which differ only in the initial horizontal offset x. The positive (negative) offset of the orange (blue) trajectory causes a slightly longer (shorter) path through the dipole and therefore a larger (smaller) deflection angle. This brings their trajectories closer together to the reference trajectory (gray), this effect is called geometric focusing. The geometry of the rectangular dipole differs by the entrance and exit angle $\theta_{1,2}$ of the reference trajectory.

2.3.2. Dipoles

A dipole deflects the reference particle by a given angle α_r, with the length of the trajectory called L. The trajectory enters and exits the field of a sector dipole perpendicular of its pole face as shown in Fig. 2.3. With α_r given in radian, its transport matrix with the sine and cosine function $S = \sin(\alpha_r)$, $C = \cos(\alpha_r)$ as well as its deflection radius $\rho = L/\alpha_r$ is given by

$$R_{\text{Sectorbend}} = \begin{bmatrix} C & \rho S & 0 & 0 & 0 & \rho\,(1-C) \\ -\frac{1}{\rho}S & C & 0 & 0 & 0 & S \\ 0 & 0 & 1 & L & 0 & 0 \\ 0 & 0 & 0 & 1 & 0 & 0 \\ S & \rho\,(1-C) & 0 & 0 & 1 & \rho\,(\alpha_r - S) \\ 0 & 0 & 0 & 0 & 0 & 1 \end{bmatrix}. \tag{2.19}$$

A particle with the reference energy but an initial horizontal offset x also gets deflected by the radius ρ but the offset causes a slight change in its path length through the dipole and therefore also a different deflection angle. The trajectory is bent towards the reference trajectory as shown in Fig. 2.3 (a). This effect is called geometric focusing and appears in every dipole geometry. Mathematically it is described by the first diagonal block of the transport matrix. In the vertical plane the dipole acts as a drift space.

The geometry of a rectangular dipole differs by the entrance and exit angle $\theta_{1,2}$ of the reference trajectory as seen in Fig. 2.3 (b). This also changes the effective bend length for offset particles, which results in an additional horizontal and vertical focusing effect which is called edge focusing. It can be described by additional edge effect matrices.

$$R_{\text{edge}}(\theta) = \begin{bmatrix} 1 & 0 & 0 & 0 & 0 & 0 \\ \tan(\theta)/\rho & 1 & 0 & 0 & 0 & 0 \\ 0 & 0 & 1 & 0 & 0 & 0 \\ 0 & 0 & \tan(\theta)/\rho & 1 & 0 & 0 \\ 0 & 0 & 0 & 0 & 1 & 0 \\ 0 & 0 & 0 & 0 & 0 & 1 \end{bmatrix} \tag{2.20}$$

The transport matrix of a rectangular bend is given by:

$$R_{\text{Rectangularbend}} = R_{\text{edge}}\,(\theta_2 = \alpha/2) \times R_{\text{Sectorbend}}\,(\alpha) \times R_{\text{edge}}\,(\theta_1 = \alpha/2) \tag{2.21}$$

2.3.3. Quadrupoles

With the notation $S = \sin(L\sqrt{|K_1|})$ and $C = \cos(L\sqrt{|K_1|})$ and accordingly Sh and Ch for the hyperbolic functions the transfer matrix for a horizontal focusing quadrupole ($K_1 > 0$) is given by

$$R_{\text{Quad}} = \begin{bmatrix} C & \frac{S}{\sqrt{|K_1|}} & 0 & 0 & 0 & 0 \\ -S\sqrt{|K_1|} & C & 0 & 0 & 0 & 0 \\ 0 & 0 & Ch & \frac{Sh}{\sqrt{|K_1|}} & 0 & 0 \\ 0 & 0 & Sh\sqrt{|K_1|} & Ch & 0 & 0 \\ 0 & 0 & 0 & 0 & 1 & 0 \\ 0 & 0 & 0 & 0 & 0 & 1 \end{bmatrix}. \tag{2.22}$$

For a vertical focusing quadrupole ($K_1 < 0$) the matrix is rotated by 90°, this transposes the upper and middle diagonal block. Further matrices, for example for sextupole magnets, rotations or radiation can be found in the referenced literature.

2.4. Beam parametrisation

A particle accelerator usually does not guide a continuous beam but dense packages of 10^6 to 10^9 particles called bunches. Propagating the whole bunch is as simple as propagating a reference particle, this is called particle tracking.

If the collective motion of a bunch through a lattice is traced using tracking, statistical parameters to describe the bunch from the particle ensemble can be derived at any position. The transverse beam size $\sigma_{x,y}$ for instance is defined as the root mean square value of the offset of each particle.

$$\sigma_x = \sqrt{\frac{1}{n}\sum_{i=0}^{n} x_i^2} \qquad \sigma_y = \sqrt{\frac{1}{n}\sum_{i=0}^{n} y_i^2} \tag{2.23}$$

Although tracking is powerful, it is very time consuming even if only a representative share of particles per bunch is used. In many cases tracking and analyzing of a particle ensemble is neither feasible nor reasonable. Instead, the beam can be characterized with a set of parameters which are propagated instead of the whole ensemble. The beam size then can be derived directly from the beam parameters. These analytical optics calculations are much faster than tracking especially for optimization routines where a large number of different optics are investigated.

2.4.1. Beta function and emittance

For linear optics the equation of motion for an individual particle without energy offset is given by Hill's equation

$$\frac{\partial^2 x(s)}{\partial s^2} - K_1(s)x(s) = 0, \tag{2.24}$$

which is solved by

$$x(s) = \sqrt{\epsilon_x \beta_i(s)}\cos(\Psi(s) + \phi_i). \tag{2.25}$$

The individual particle oscillates around the reference trajectory with the amplitude $\sqrt{\epsilon\beta_i(s)}$ while being guided through a particle accelerator. This transverse motion is called the betatron oscillation. The individual beta function $\beta_i(s)$ and the betatron phase $\Psi(s)$ are

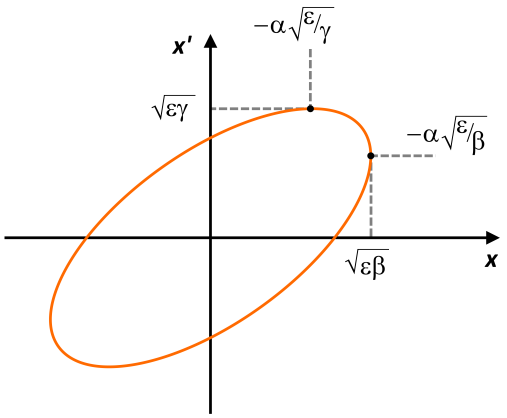

Figure 2.4.: Phase ellipse as a contour of one standard deviation of the bunches particle distribution in horizontal phase space. The parameters α, β and γ are defined by the ellipse form, ϵ by its area.

determined by the optics and the phase offset ϕ_i is a property of the particle's individual motion.

With each particle having an individual discrete state in the x-x' plane one can formulate an ellipse which encloses one standard deviation of the bunch's particles. While traveling along the accelerator each particle performs its individual betatron oscillation and changes its position in the transverse phase space. This leads to a rotation and reshaping of the collective phase ellipse along the accelerator. According to Liouville's theorem the area of the phase ellipse A stays invariant in the presence of only conservative forces. The emittance $\epsilon = A/\pi$ is a measure of the ellipse area and therefore a constant during transport.

The phase ellipse amplitude in x along the accelerator defines the beam envelope $\left[-\sqrt{\epsilon\beta}; +\sqrt{\epsilon\beta}\right]$. The beam size follows directly for each transverse plane with

$$\sigma_{x,y}(s) = \sqrt{\epsilon_{x,y}\beta_{x,y}(s)}. \tag{2.26}$$

The beam beta function $\beta_{x,y}(s)$ and the other two Twiss parameters

$$\alpha_x(s) = -\frac{1}{2}\frac{\partial\beta_x(s)}{\partial s} \tag{2.27}$$

$$\text{and} \qquad \gamma_x(s) = \frac{1+\alpha_x^2(s)}{\beta_x(s)} \tag{2.28}$$

describe the phase ellipse's shape given by the elliptical equation

$$A_x/\pi = \gamma_x(s)x^2(s) + 2\alpha_x(s)x(s)x'(s) + \beta_x(s)x'^2(s) = \epsilon_x. \tag{2.29}$$

The Twiss parameters describe the transverse dynamics of the bunch and can be formulated independently for the horizontal and vertical plane. The parameters can be combined to the beam matrix

$$B_{x,y}(s) = \begin{bmatrix} \beta_{x,y}(s) & -\alpha_{x,y}(s) \\ -\alpha_{x,y}(s) & \gamma_{x,y}(s) \end{bmatrix}. \tag{2.30}$$

A set of Twiss parameters can be calculated from a given particle ensemble using the covariance matrix C of the beam [14].

$$C = \begin{bmatrix} C_{xx} & C_{x\tilde{x}} \\ C_{\tilde{x}x} & C_{\tilde{x}\tilde{x}} \end{bmatrix} = \begin{bmatrix} \epsilon_x\beta_x & -\epsilon_x\alpha_x \\ -\epsilon_x\alpha_x & \epsilon_x\gamma_x \end{bmatrix} = \epsilon_x B_x \tag{2.31}$$

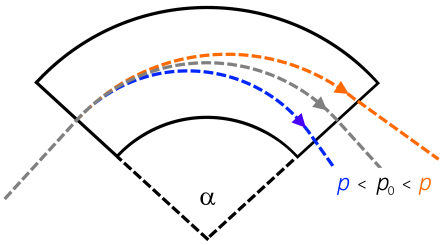

Figure 2.5.: Trajectories of three particles with different energies through a sector bend. The dipole splits the particles according to their momentum.

With the horizontal offset x and the angle of the trajectory $\tilde{x}$[1] for each particle of the ensemble, the four covariance matrix elements C_{ij} can be calculated using

$$C_{ij} = \langle ij \rangle - \langle i \rangle \langle j \rangle \tag{2.32}$$

with $\langle i \rangle$ is the average of the value i. Recalling the definition of γ from Eq. (2.28), the determinant of the covariance matrix equals the square of the emittance.

$$\det C = \epsilon_x^2 \left(\beta_x \gamma_x - \alpha_x^2 \right) \tag{2.33}$$

$$= \epsilon_x^2 \left(\beta_x \times \frac{1 + \alpha_x^2}{\beta_x} - \alpha_x^2 \right) \tag{2.34}$$

$$= \epsilon_x^2 \tag{2.35}$$

With the emittance value derived, the Twiss parameters can be calculated from the covariance matrix elements in Eq. (2.31). This method also holds for the vertical plane, leading to the vertical Twiss parameters.

As the initial Twiss parameters are known, both the horizontal and vertical beta matrix can be propagated through a lattice. Therefore the matrices M_x and M_y are used, both are extracted directly from the 6×6 transfer matrix R

$$\begin{bmatrix} B_x(S_2) & 0 \\ 0 & B_y(S_2) \end{bmatrix} = \begin{bmatrix} M_x & 0 \\ 0 & M_y \end{bmatrix} \times \begin{bmatrix} B_x(S_1) & 0 \\ 0 & B_y(S_1) \end{bmatrix} \times \begin{bmatrix} M_x & 0 \\ 0 & M_y \end{bmatrix}^T \tag{2.36}$$

$$M_x = \begin{bmatrix} R_{11} & R_{12} \\ R_{21} & R_{22} \end{bmatrix} \qquad M_y = \begin{bmatrix} R_{33} & R_{34} \\ R_{43} & R_{44} \end{bmatrix} \tag{2.37}$$

The conservation of the emittance $\epsilon_{x,y}$ is obtained by the symplecticity of the transport matrices.

2.4.2. Dispersion

A dipole guides a particle with the reference energy along the desired deflection radius. This is achieved by setting a certain magnetic field in the dipole according to $B = \frac{p}{e\rho}$. A particle with an energy offset follows another radius as shown in Fig. 2.5. The different trajectories result in a transverse offset for the off-energy particle and in a difference of its path length.

The dispersion function η[m] describes the transverse offset for particles depending on their momentum deviation. No dispersion means that there is no correlation between the

[1] The parameter x' in a particles state vector represents the particle's slope in the horizontal plane. The trajectory's angle then is given by $\tilde{x} = \arctan x' \approx x'$, since the angles are very small.

horizontal position and momentum while a positive dispersion describes that particles with positive momentum deviation $\delta > 0$ have offset $x > 0$ and particles with $\delta < 0$ accordingly a negative one. A single particle then performs its betatron oscillation not around the reference orbit but around the dispersion orbit

$$x_\eta(s) = \eta_x(s)\delta. \tag{2.38}$$

As a consequence, the transverse beam size increases in dispersive sections of the lattice:

$$\sigma_{x,y}(s) = \sqrt{\epsilon_{x,y}\beta_{x,y}(s) + \eta_{x,y}^2(s)\delta_\mathrm{B}^2} \tag{2.39}$$

With the momentum spread δ_B for the bunch as the standard deviation of the relative momentum deviation of all particles.

The propagation of the dispersion matrix D can be calculated with the same matrices $M_{x,y}$ used to propagate the beta matrices.

$$D(s) = \begin{bmatrix} \eta_x(s) \\ \eta_x'(s) \\ \eta_y(s) \\ \eta_y'(s) \end{bmatrix} \tag{2.40}$$

$$D(S_2) = \begin{bmatrix} M_x & 0 \\ 0 & M_y \end{bmatrix} \times D(S_1) + \begin{bmatrix} R_{16} \\ R_{26} \\ R_{36} \\ R_{46} \end{bmatrix} \tag{2.41}$$

As seen in Eq. (2.41), if no initial dispersion is present, a dispersion can only be introduced if the transport matrix has finite values in R_{16}, R_{26}, R_{36} or R_{46}, which only is the case for a dipole magnet. The propagation and alteration of an already existing dispersion $D(1) \neq 0$ on the other hand happens in every element and is calculated with the $M_{x,y}$ matrices. A quadrupole however cannot split the beam by its energy because of its 180° rotation symmetry and therefore cannot introduce a dispersion. Yet, if dispersion already is present, a quadrupole affects the dispersion's derivative $\eta' = \frac{\partial \eta}{\partial s}$. A drift space simply propagates the dispersion and changes its amplitude by $\eta' \times L$.

The important effect of dispersion is not the transverse offset but the unavoidable change of the path length Δz with respect to the momentum. Since the transfer line focuses on the longitudinal compression the dispersion is the most important optical parameter in this thesis.

2.5. Synchrotron radiation

A charged particle emits electromagnetic radiation while being accelerated. In synchrotrons, where the beam is forced on a circular orbit, synchrotron radiation (SR) is the main source of energy loss. The radiated energy for a particle deflected by 360° with the radius ρ is given by

$$\Delta E = \frac{e^4}{3\epsilon_0 (m_0 c^2)^4} \frac{E^4}{\rho}. \tag{2.42}$$

For ultra relativistic electrons the formula can be reduced to

$$\Delta E\,[\mathrm{keV}] = 88.5 \frac{E^4\,[\mathrm{GeV}^4]}{\rho\,[\mathrm{m}]}. \tag{2.43}$$

Both formulae include a lot of simplifications and assumptions. All higher order magnets and longitudinal accelerations are neglected. Also it only takes into account the radiation

of the deflection within dipoles, ignoring higher order magnets. Still Eq. (2.42) provides a good approximation for the order of magnitude of the radiation. It is extremely sensitive to the energy of the particles and also for very small deflection radii.

Assuming all deflection angles of the transfer line would add up to 360°, Eq. (2.43) can be used for a rough estimation of the energy loss in the transfer line. With a deflection radius of about 1 m an electron with an energy of 50 MeV would only lose 0.5 eV. Despite the small bending radii in the transfer line, the synchrotron radiation is very small because of the low beam energy provided by FLUTE.

The radiation power of a single electron deflected by radial forces is given by:

$$p_{\mathrm{SR}} = \frac{e^2 c}{6\pi\epsilon_0 \left(m_0 c^2\right)^4} \frac{E^4}{\rho^2}. \tag{2.44}$$

Since the synchrotron radiation is a pure single particle effect the total radiated power P_{SR} of the bunch simply equals the product of the number of electrons N times the radiated single electron power p_{SR}.

$$P_{\mathrm{SR}} = p_{\mathrm{SR}} N \tag{2.45}$$

2.5.1. Coherent synchrotron radiation

The phenomenon of coherent synchrotron radiation (CSR) is a collective effect of the bunch. The power radiated by the bunch is strongly enhanced for photons with a wavelength in the same order of magnitude of the bunch length. This effect depends on the shape of the bunch and the amount of particles in it. For N relativistic electrons forming a Gaussian shaped bunch with the bunch length σ_s the total radiated power per unit wavelength λ is given by

$$P_{\mathrm{CSR}}(\lambda) = p_{\mathrm{SR}} N^2 e^{-4\pi^2 \sigma_s^2/\lambda^2}. \tag{2.46}$$

The exponential function is very sensitive to short bunch lengths and to the ratio between bunch length and emitted wave length. Also the total radiated power depends on N^2, which becomes dominant for large N. As the transfer line aims for ultra-short bunches, CSR is expected to have a larger effect than SR.

Beside the higher radiation losses, the bunch can interfere with its own radiation wake if the trajectory of the bunch and the direction of its wake do cross each other. Then single electrons can absorb the CSR photons which leads to an uncontrolled energy increase. As a consequence of this, so called CSR self interaction the new trajectory might become unstable and the particle can get lost. In order to avoid CSR radiation, the transfer line will avoid short bunch lengths before reaching the injection point.

3. The simulation tool *elegant*

The accelerator simulation software *elegant* [15], version 34.4.1, was used for all simulations in the context of in this thesis. *Elegant* is a tool for lattice design and beam optics simulation, it also includes particle tracking and optics optimization routines. The C-based software uses binary data in the SDDS format for input and output, which is post processed and converted into ASCII by the SDDStoolkit [7]. The relevant notations, tools and definitions will be explained in this chapter.

3.1. Longitudinal nomenclature

In *elegant*, each particle is defined as a 6-D state vector similar to the one given in Eq. (2.10) except for the longitudinal position. *Elegant* uses the total longitudinal distance s_i traveled by an individual particle to describe its longitudinal position instead of using the relative longitudinal distance to the reference particle like the Frenet-Serret coordinate system does. The following parameters can be used to describe the longitudinal particle dynamics in *elegant*.

- s_i: Absolute path length of an individual particle
- t_i: Absolute travel time of an individual particle
- δt_i: Relative time delay with respect to the reference particle
- z_i: Relative longitudinal position with respect to the reference particle
- S: Absolute path length of the reference particle

The differences are illustrated in Fig. 3.1. Additional care has to be taken in the correlation between time and space. In the ultra relativistic case every particle travels at the speed of light, then the path length and the time required are linked via the speed of light c. With electrons with an energy of 41 MeV, differences in the velocity of single particles are still noticeable. Therefore not the speed of light but the instantaneous velocity needs to be taken and it is $s = \beta ct$. At this low relativistic case particles with an energy offset pass the transfer line with different time of flight. As a consequence time of flight effects need to be

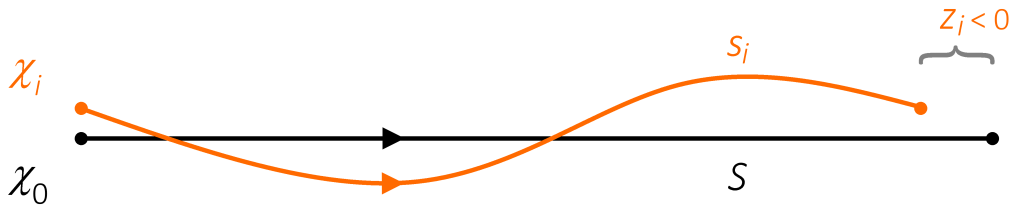

Figure 3.1.: Longitudinal notation in *elegant*. While the reference particle χ_0 follows the reference trajectory S, the particle χ_i with different energy follows another path with path length s_i. Their relative longitudinal distance is given by z_i.

taken into account and the longitudinal parameters needs to be distinguished carefully by aiming at ultra-short bunches.

3.2. Lattice definition

In order to perform beam optics calculations *elegant* has to know the lattice of the accelerator. All elements have to be defined and a beam line has to specify the sequence of the elements used. A lattice can contain an arbitrary composition of single elements like drift spaces and magnetic structures. *Elegant* offers multiple definitions for most of the common magnets with different calculation methods for several purposes. For this thesis only so called canonical kicker magnets were used which handle off-energy particles with the highest precision. Canonical kickers use the exact Hamiltonian for correct calculation of all orders in momentum offset during tracking. In addition, only canonical kicker elements support CSR simulations. The following paragraphs explain the elements used in the context of this thesis. If parameters are not specified, they remain at default values or are set to recommended settings.

The parameter L of all magnets defines the pole length of a magnet. The physical elements usually require more space because of cooling pipes, wires and the physical fixiation of the magnet. In all lattices discussed in this thesis two adjacent magnets are therefore always separated by a drift space of at least 15 cm.

Drift: The element CSRDRIF implements a drift space defined via its length L and allows the simulation of coherent synchrotron radiation. After a CSR wake is created by a previous dipole, the wake propagates through a consecutive CSRDRIF element. The drift is split into N_KICKS equally long slices. After each slice the propagation and reshaping of the wake is calculated as well as possible interactions of the wake with the bunch.

Dipoles: All dipoles are simulated with the canonical kicker element CSRCSBEND. Canonical kicker magnets are most precise in handling the trajectory of off-energy particles. Further a CSRCSBEND is the only element supporting the simulation of coherent synchrotron radiation. Between several possible models to simulate CSR radiation the method of [16] was choosen. According to the *elegant* manual it provides the most accurate results.

By default, a CSRCSBEND is a sector bend with its geometry defined by the horizontal deflection angle $ANGLE$ given in units of radians and the length L of the curved reference trajectory. A rectangular bend geometry can still be simulated by altering the entrance and exit angles θ_1, θ_2[1]. In case of a rectangular geometry the length of the desired rectangular magnet L_R differs from the length of the trajectory L inside the magnet. As L is used for the implementation of a CSRCSBEND this parameter has to be adjusted as illustrated in Fig. 3.2.

A realistic dipole field differs from a rectangular hard edge field. The magnetic field needs space to build up, therefore by entering and exiting a dipole a particle has to cross a volume of a rising fringe field. The CSRCSBEND applies a linear fringe field model based on the theory of [17]. It is implemented as shown in Fig. 3.3 in order to simulate the same integrated magnetic field as a hard edge model would provide. Also a CSRSBEND allows the implementation of an additional quadrupole gradient K_1 to construct combined function magnets.

[1] In fact, *elegant* calls the entrance angle $E1$ and the exit angle $E2$. In order to prevent confusion with the energy the angle names are substituted to θ_1 and θ_2.

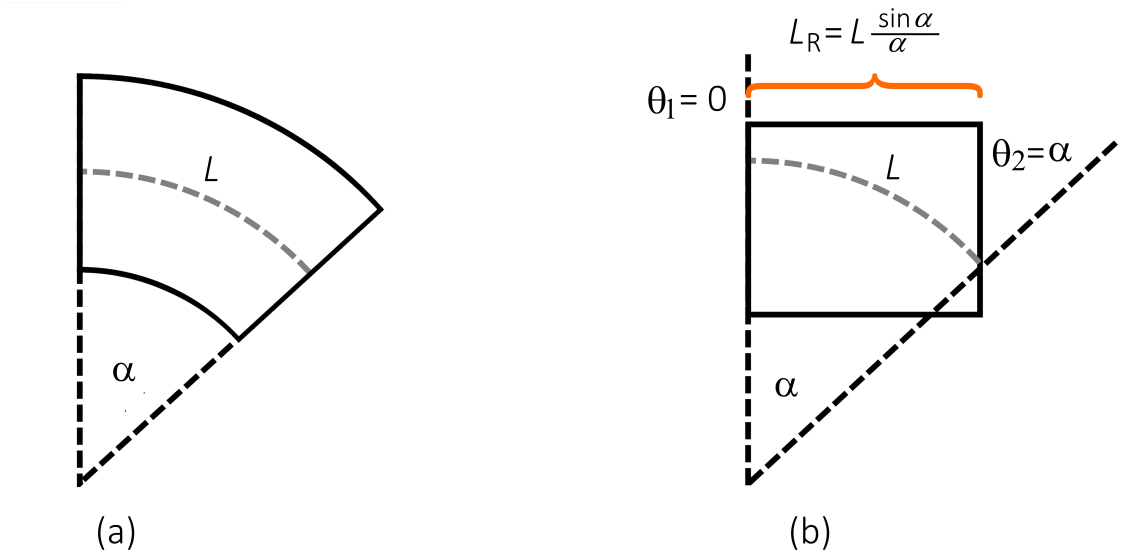

Figure 3.2.: Sector bend geometry definition in *elegant*. The left schematic shows its default sector geometry, the right schematic shows a possible implementation as a rectangular bend.

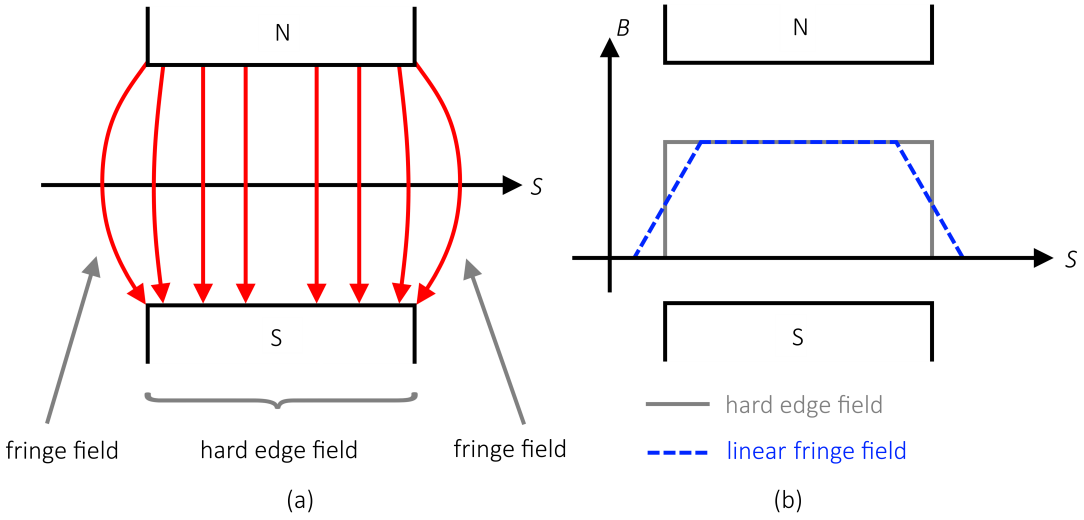

Figure 3.3.: Magnetic field of a dipole including the fringe field as it is implemented in *elegant*. The left schematic shows the field lines of a dipole along the longitudinal axis including the fringe field. The right schematic shows the magnetic field as a function of S including the fringe field to first order.

Quadrupoles:

The canonical kicker quadrupole KQUAD is implemented with a quadrupole strength K_1 and length L. It includes a linear entrance and exit fringe field.

For a combined function magnet with a quadrupole and a sextupole component the KQUSE element has to be used which does not provide a fringe field.

If a KQUAD or a KQUSE element is surrounded by CSRDRIF elements it acts like a CSRDRIF in case of a CSR simulation.

Sextupoles: A sextupole can be implemented as a KQUSE or a KSEXT element. Both are canonical kicker magnets and work similar to the KQUAD element but lack of the entrance and exit field effects.

Rotations and tilts: The ROTATE element rotates the 6-D phase space for every particle about the longitudinal axis. In addition, each element can have an individual TILT parameter which rotates just the single element about the longitudinal axis. This changes only the effect of the single element onto the optics while rotating a bunch will affect all its future manipulations.

By rotating the bunch or tilting elements by an angle unequal of a multiple of 90° the x and y plane get coupled. Without periodic boundary conditions like in a circular machine *elegant* cannot calculate coupled Twiss parameters. In this case tracking has to be used and the desired parameters have to be extracted from the tracked particle distribution.

Miscellaneous: Several additional elements are important although they do not have a direct effect on the beam dynamics:

- MAXAMP defines the inner diameter of the vacuum chamber for the hole lattice.
- MARK offers a fit point for the optimization routines.
- WATCH is a beam property and motion monitor. At its position all beam parameter are accessible.
- CHARGE implements the bunch charge. Every simulated particle then carries the same share of the total amount.

3.3. Synchrotron radiation

Elegant distinguishes between synchrotron radiation, incoherent synchrotron radiation and coherent synchrotron radiation which can be simulated independently while tracking.

- Synchrotron Radiation (SR) calculates the energy loss during deflection due to the single particle photon radiation. This effect only depends on the particle's energy and the deflection radius.
- Incoherent Synchrotron Radiation (ISR) simulates the effect of quantum excitation which is a consequence of SR.
- Coherent Synchrotron Radiation (CSR) simulates the self interaction of a bunch with its own radiation field. This effect depends on the bunch's dimensions, its energy, charge and trajectory.

As the effect of synchrotron radiation is expected to be very small, also the ISR as a side effect of SR will probably be negligible. CSR is considered in dipoles and drift spaces. Quadrupoles and sextupoles are substituted with drift sections in case of CSR simulations. In addition CSR simulations require an implementation of the CHARGE element before the first dipole.

4. Design Challenges

The following chapter discusses technical limitations, spatial dimensions and performance requirements for the transfer line, which define the boundary conditions for the simulation.

4.1. Magnetic fields and gradients

The transfer line's optics are defined by the multipole strengths of the dipoles ($K0 = \rho^{-1}$), quadrupoles (K_1) and sextupoles (K_2). The equations to derive the multipole strengths are given by Eq. (2.7) to Eq. (2.9). The parameters of these equations are discussed in order to estimate a realistic upper limit.

Momentum: The magnetic multipole strengths are not momentum independent but proportional to $\frac{e}{p_0}$. By changing the design energy the magnetic fields need to be adjusted in order to keep the multipole strengths unchanged. Although the reference momentum in the simulations is $p = 41.5\,\mathrm{MeV/c}$, for the calculation of the boundary conditions a momentum of $p_{\max} = 100\,\mathrm{MeV/c}$ is used. This gives an additional factor of two margin and should allow the possibility of future upgrades of the FLUTE's linac.

Magnetic field: The multipole strengths are limited by the maximum magnetic field at the element's pole tips. Conventional electromagnets can reach a field of up to 1.5 T. By getting closer to this limit the iron yoke starts saturating and the relation between the magnetic field and the electric current of the coil becomes non-linear. In order to stay in the linear regime a maximum magnetic field of $B_{\max} = 1\,\mathrm{T}$ is assumed.

Diameter: The equation for the quadrupole (sextupole) strength includes the first (second) derivative of the magnetic field $\frac{\partial B_y}{\partial r}$ $\left(\frac{\partial^2 B_y}{\partial r^2}\right)$ with respect to the distance of the poles to the geometric center r. For the estimation of the maximum possible multipole strength, the maximum magnetic field $B_{\max}$ is applied at the smallest possible ablation $r_{\min}$ of the pole tip.

$$K_{1,\max} = \frac{e}{p_{\max}} \frac{B_{\max}}{r_{\min}} \tag{4.1}$$

$$K_{2,\max} = \frac{e}{p_{\max}} \frac{B_{\max}}{r_{\min}^2} \tag{4.2}$$

The beam pipe of FLUTE has an outer radius of 2.5 cm. Including some margin the minimal possible pole tip distance from the quadrupoles (sextupoles) center is assumed to be $r_{\min} = 3\,\mathrm{cm}$. The discussed parameters lead to the following extremal multipole strengths:

- Minimum dipole deflection radius: $\rho_{\min} = 0.33\,\mathrm{m}$
- Maximum quadrupole strength: $K_{1,\max} = 99.9\,\mathrm{m}^{-2}$
- Maximum sextupole strength: $K_{2,\max} = 3331\,\mathrm{m}^{-3}$

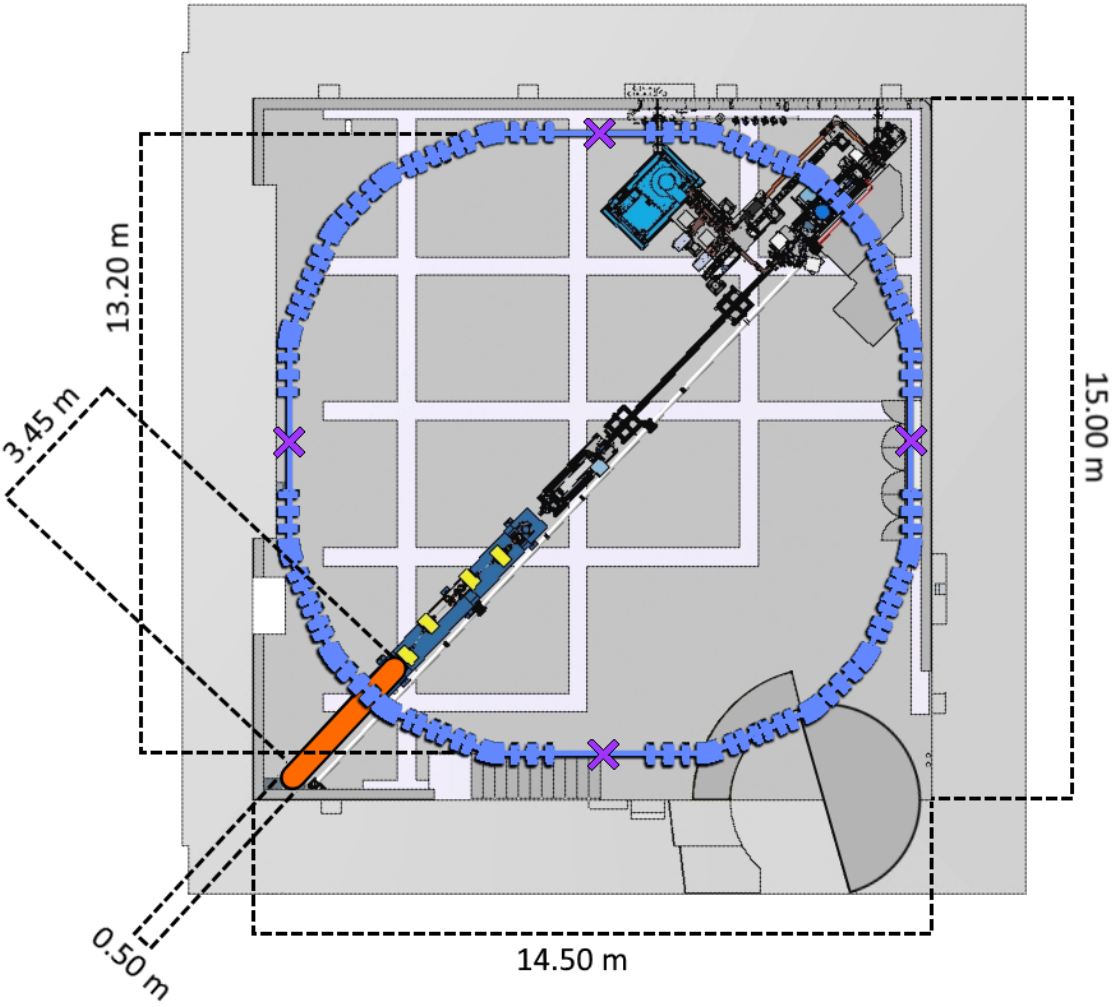

Figure 4.1.: Top view of the experimental hall with the footprints of FLUTE (black) and cSTART (blue). The four cSTART symmetry points are marked with the "X"es (purple). The transfer line starts after the bunch compressor (four yellow dipoles), its free space in the room's diagonal (orange) is only 3.45 m including a margin of 25 cm to the wall.

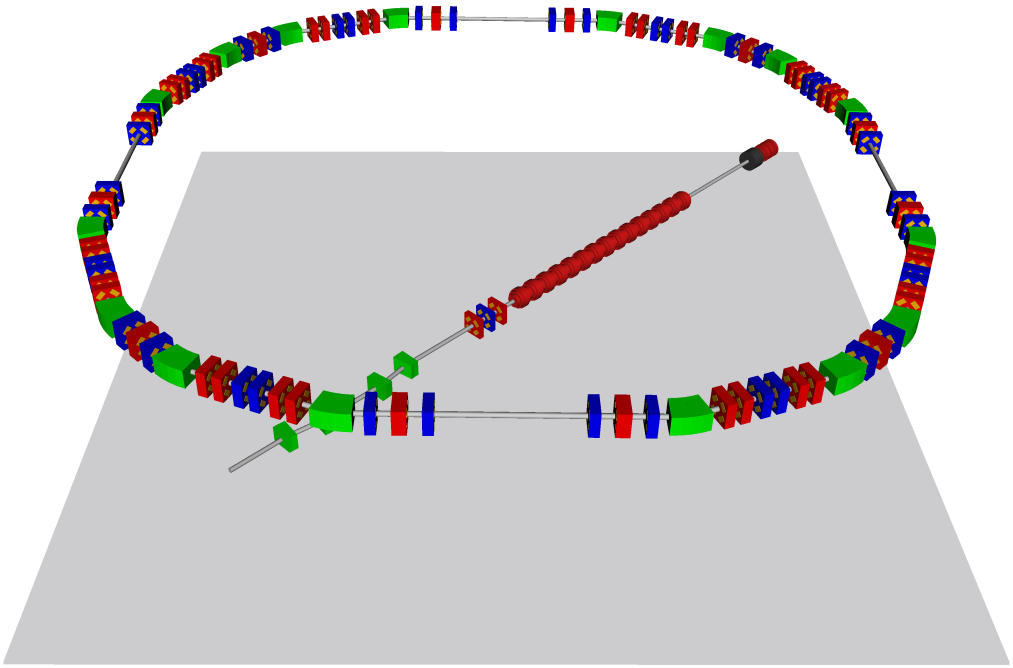

Figure 4.2.: Perspective view of the 3-D image of the FLUTE and cSTART lattices above the experimental hall's footprint (gray square). The visualized elements of FLUTE starting from the right top corner are the electron gun (red), solenoid (gray), linac (red), the quadrupole triplet (red: horizontal focusing, blue: vertical focusing) and the four dipole bunch compressor (green). Above cSTART is shown with dipoles and quadrupoles, its sextupoles are not visualized.

4.2. Civil engineering constraints

Both FLUTE and cSTART will be located inside a 15 m × 14.5 m experimental hall. FLUTE is positioned 1.2 m above the floor along the room's diagonal as shown in Fig. 4.1. In order to keep a minimal distance to the wall of 25 cm the transfer line has to include a turn within the first 3.45 m.

For visualizing the dimensions, the lattices of FLUTE and cSTART are converted into a 3-D image in x3d format with the software view3dscene from the SDDStoolkit. The geometries are positioned upon a square with the dimensions of the experimental hall footprint. A perspective view of the 3-D image is plotted in Fig. 4.2.

The cSTART storage ring is planned to have a diameter of 13.2 m and will be installed horizontally at a height of 3 m. The transfer line needs to connect the end of the FLUTE's bunch compressor (BC) with one of the symmetry points of cSTART, which are located at the center of one of the four long drift sections. Also the transfer line should not exceed an absolute height of 5 m to stay below the movable crane at the ceiling.

4.3. Initial beam parameters

The linear accelerator FLUTE is currently under construction [19], a schematic of its layout is given in Fig. 4.3. The electrons created in the electro-optical gun are focused with a solenoid and accelerated with a 5.2 m long linac. The phase of the linac's RF voltage is

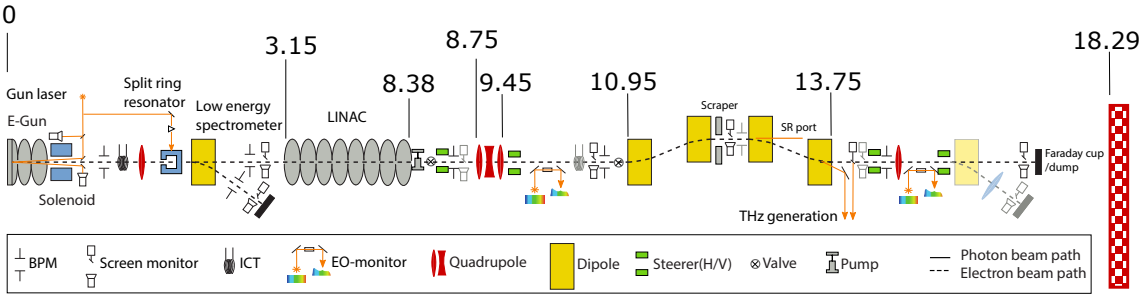

Figure 4.3.: Schematic layout of FLUTE including various diagnostics elements like beam position monitors (BPM), an integrated current transformers (ITC) and electro-optical (EO) monitors. The RF components are marked in gray and magnets in yellow and red[18].

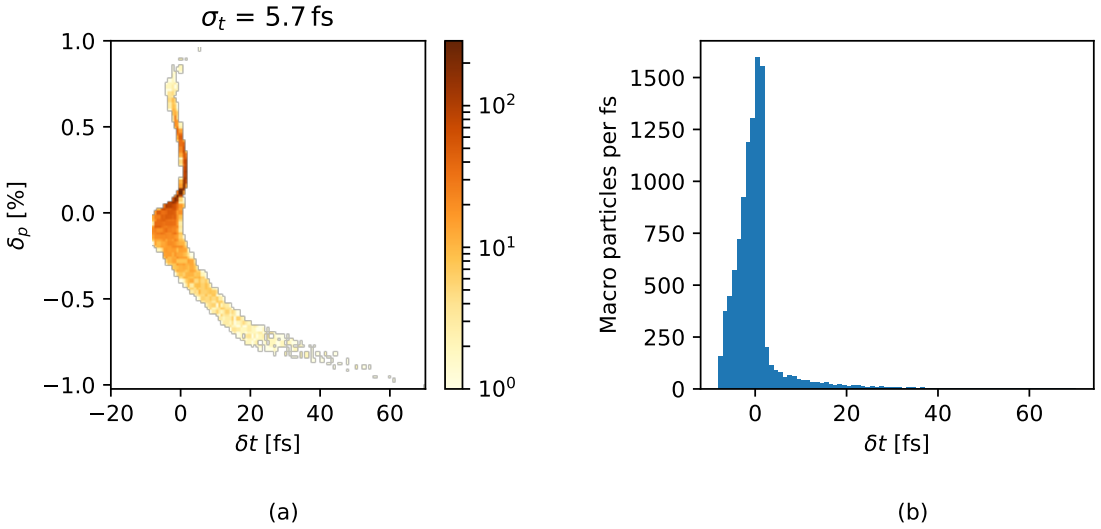

Figure 4.4.: (a): Longitudinal phase space of the bunch after the bunch compressor at $S = 14.75\,\mathrm{m}$ with the momentum deviation with respect to the reference momentum of $p_0 = 41.5\,\mathrm{MeV/c}$ as a 2-D histogram. (b): The corresponding bunch profile. The bunch length is only $\sigma_t = 5.7\,\mathrm{fs}$.

timed such that the bunch enters the accelerating voltage off-crest, which induces an energy spread correlated to the longitudinal position of the particle in the bunch. After the linac the bunch gets focused in the transverse planes by a quadrupole triplet and longitudinally compressed with a four dipole chicane. All parameters of FLUTE were optimized in order to create the shortest bunches possible [18].

The optimized FLUTE parameters lead to a bunch length of only 5.7 fs after the chicane. The bunch is shown in the longitudinal phase space in Fig. 4.4, subfigure (a) and its longitudinal profile in subfigure (b). The corresponding simulation was performed with the ASTRA simulation code [20] using particle tracking of 10,000 macro particles including space charge effects.

The outcome of the tracking simulation and parameter set resulting in the ensemble shown in Fig. 4.4 is the origin for all transfer line simulations. The distribution was not taken behind the bunch compressor but between the linac and the quadrupole triplet at $S = 8.5\,\mathrm{m}$ behind the gun. This is the starting point for the transfer line simulations which allows to include the quadrupole triplet and the bunch compressor to the optimization routines. At this point the bunch has passed the gun, solenoid and linac where it has been accelerated

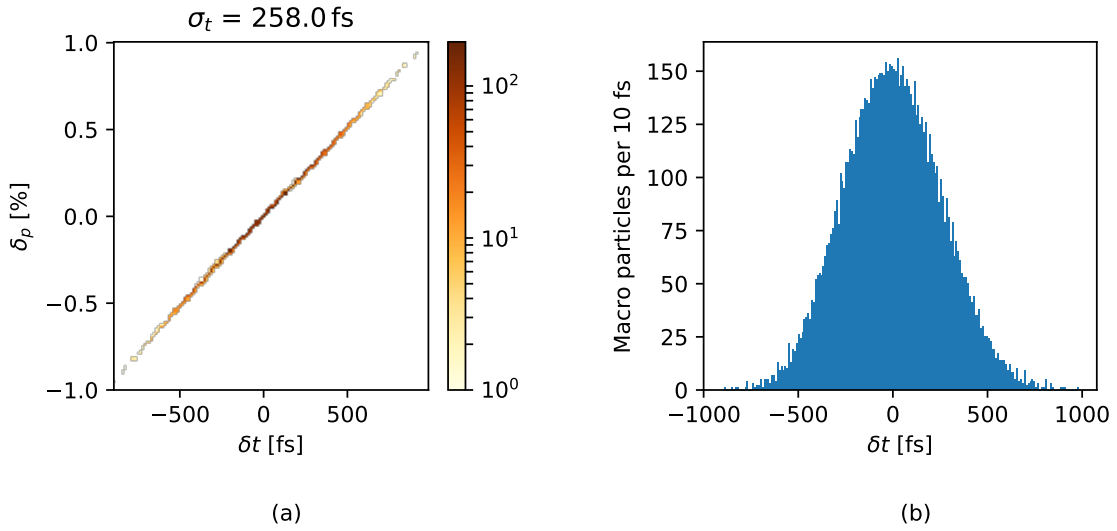

Figure 4.5.: (a): Longitudinal phase space of the bunch after the linac at $S = 8.5\,\mathrm{m}$ with the momentum deviation with respect to the reference momentum of $p_0 = 41.5\,\mathrm{MeV/c}$ as a 2-D histogram. (b): The corresponding bunch profile. The bunch length is $\sigma_t = 258\,\mathrm{fs}$.

to its final energy of 41.5 MeV. The correlated momentum spread can be seen in the longitudinal phase space in subfigure (a) of Fig. 4.5, the longitudinal profile in subfigure (b).

The particle distribution created and tracked with ASTRA up to $S = 8.5\,\mathrm{m}$ was converted into the *elegant* compatible SDDS format with the tool astra2elegant from the SDDStoolkit [7]. The tool sddsanalyzebeam can calculate the beam parameters listed in Tab. 4.1 and the optics parameters listed in Tab. 4.2 directly from the converted particle ensemble. Because the gun, solenoid and linac are rotationally-symmetric the particle distribution should be rotationally-symmetric too. Especially the dispersion function and its derivative should be zero for both transverse planes. Yet a finite dispersion function and derivative are present. The small values probably rise from a statistical uncertainty. For a charge of 1 pC six million electrons are required but only 10,000 were tracked. The down sampling of the distribution can lead to such binning effects.

The particle distribution at $S = 8.5\,\mathrm{m}$ is the result of the RF gun and linac optimized for the shortest possible bunch after the FLUTE chicane. It turned out that this distribution also performs well as initial distribution for the transfer line. Yet it is possible that another set of parameters in the gun and linac could provide an even better initial bunch for the transfer line. Open degrees of freedom to tune the initial bunch are the frequency, amplitude and phase of the accelerating voltage in the electron gun and linac. This is a possible open task for future investigations.

4.4. Final beam parameters

The cSTART storage ring has a lattice with a four-fold symmetry. Each of the four cells performs a 90° deflection with four equally deflecting rectangular bends. The bends are combined function magnets of a 22.5° deflecting dipole and a vertical focusing quadrupole. The lattice is specialized for accepting a beam with a wide momentum spread δ_B and large transverse beam sizes σ_x, σ_y [21]. In Fig. 4.6 the lattice and its linear optics functions for one cell are plotted. The cSTART lattice as implemented in *elegant* can be found in the appendix at A.3.

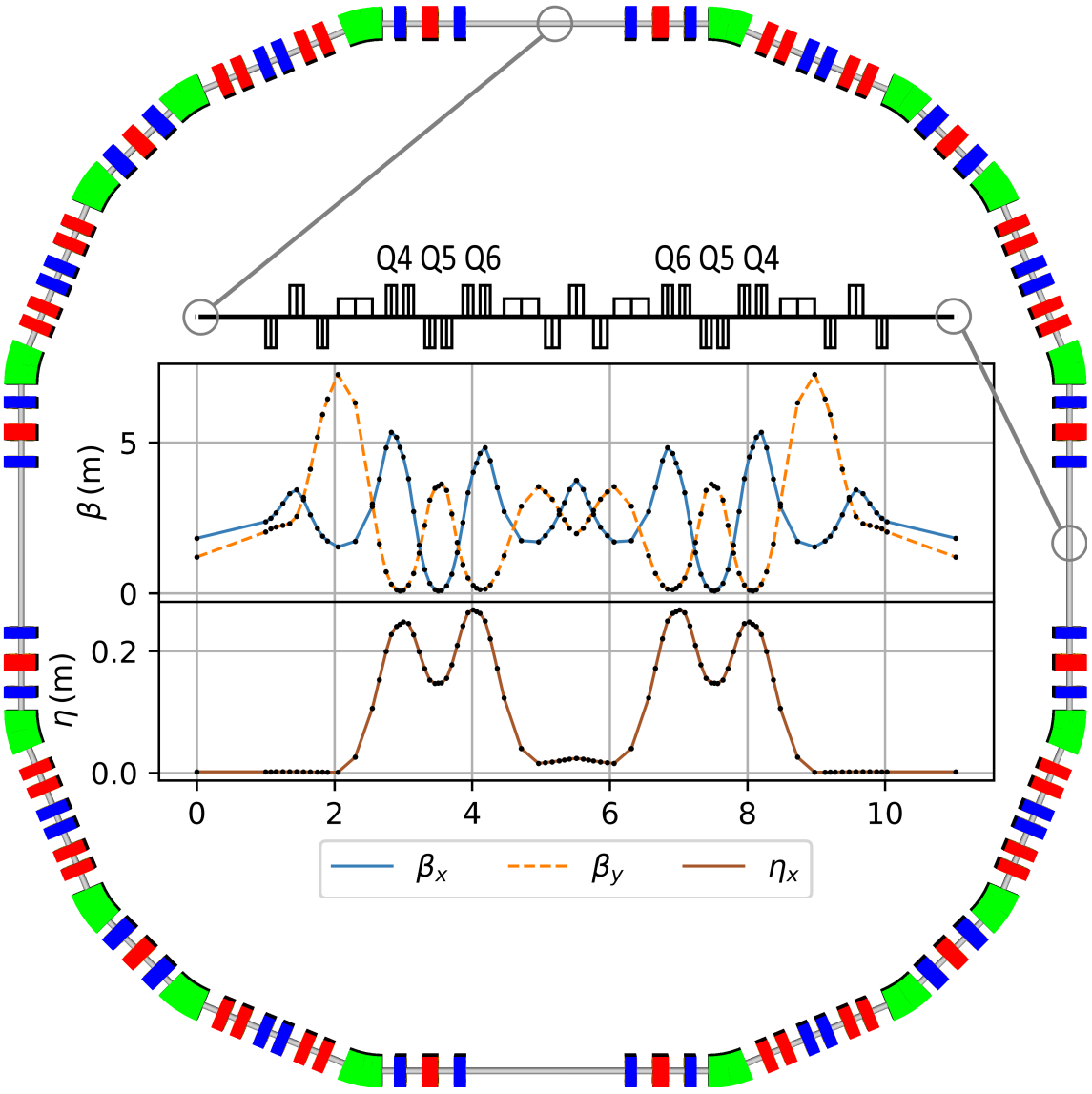

Figure 4.6.: Lattice and linear optics of the cSTART storage ring. The lattice shown consists of horizontal focusing (red) and defocusing (blue) quadrupoles and dipoles (green). The plot shows the linear optics for one cell with the dipoles (short) and quadrupoles (tall) visualized above. The quadrupoles Q4, Q5 and Q6 enclose thin sextupole elements (not visualized). Figure altered and provided from [2].

Table 4.1.: Beam parameters of the FLUTE electron bunch at $S = 8.5\,\mathrm{m}$ which was used as the initial particle distribution for the simulations of the transfer line.

Charge	q	1 pC
Mean energy	E_0	41.5 MeV
Energy spread	δ_B	0.27 %
Horizontal bunch size	σ_x	0.68 mm
Vertical bunch size	σ_y	0.68 mm
Bunch length	σ_t	258 fs

Table 4.2.: Optics parameters extracted from the particle distribution at $S = 8.5\,\mathrm{m}$ using the tool sddsanalyzebeam. The Twiss parameters and the emittances have the same values for the horizontal and vertical plane.

Beta function		$\beta_{x,y}$ (m)	1.43×10^{2}
Alpha function		$\alpha_{x,y}$	2.17
Emittance		$\epsilon_{x,y}$ (m rad)	3.3×10^{-9}
Dispersion function	horizontal	η_x (m)	1.7×10^{-4}
	vertical	η_y (m)	7.6×10^{-5}
Dispersion derivative	horizontal	η'_x	6.7×10^{-6}
	vertical	η'_y	9.3×10^{-6}

The transfer line needs to inject into one of the four symmetry points between the cells. The main focus lies on the bunch length, which should be as short as possible. In addition the injected beam should start a periodic trajectory within one cell. Therefore the transverse optics should match the periodic cSTART solution. The linear optics parameters of the periodic solution are listed in Tab. 4.3.

In this thesis the injection will be simplified to matching the linear optics. Yet a full discussion of a valid injection scheme requires more investigation in the beam dynamics like the aperture and the layout of the elements used.

Table 4.3.: Optics parameters at the symmetry point of the cSTART storage ring.

Beta function	horizontal	β_x (m)	1.8
	vertical	β_y (m)	1.2
Alpha function		$\alpha_{x,y}$	0
Dispersion function	horizontal	η_x (m)	1.8×10^{-3}
	vertical	η_y (m)	0
Dispersion derivative		$\eta'_{x,y}$	0

5. Longitudinal bunch compression

The transfer line focuses on a short bunch length at the injection point. The required deflections during the transport will create dispersion which changes the path length for off-momentum particles. Of course, the bunches created by FLUTE have a momentum spread. In order to prevent the bunch from being torn apart, the change in the path length for off-momentum particles needs to be studied.

5.1. Longitudinal dynamics

The transport matrix R of a single element or a whole section transforms a particles state vector from position S_1 to position S_2.

$$\vec{\chi}(S_2) = R \times \vec{\chi}(S_1) \tag{5.1}$$

The change in the relative longitudinal offset z of the particle $\vec{\chi}$ is obtained as:

$$z(S_2) = R_{51}\, x(S_1) + R_{52}\, x'(S_1) + R_{53}\, y(S_1) + R_{54}\, y'(S_1) + R_{55}\, z(S_1) + R_{56}\, \delta_p(S_1) \tag{5.2}$$

Without further specifications the calculation of $z(S_2)$ requires the knowledge of the particle's complete initial state vector.

5.1.1. The transport matrix element R_{56}

The mathematics simplifies a lot, if the section described by R fulfills the achromaticity criterion. A section is achromatic, if it does not raise dispersion or its derivative $\eta' = \frac{\partial \eta}{\partial z}$ when initially both are zero.

$$\text{Achromaticity criterion:} \qquad D(S_1) = \begin{bmatrix} \eta_x \\ \eta'_x \\ \eta_y \\ \eta'_y \end{bmatrix} = \begin{bmatrix} 0 \\ 0 \\ 0 \\ 0 \end{bmatrix} \quad \text{and} \quad D(S_2) = \begin{bmatrix} 0 \\ 0 \\ 0 \\ 0 \end{bmatrix} \tag{5.3}$$

The achromaticity criterion puts constraints on the elements of the transport matrix R. Recall Eq. (2.41) that describes the propagation of the dispersion function through the lattice.

$$D(S_2) = \begin{bmatrix} M_x & 0 \\ 0 & M_y \end{bmatrix} \times D(S_1) + \begin{bmatrix} R_{16} \\ R_{26} \\ R_{36} \\ R_{46} \end{bmatrix}$$

Insertion of Eq. (5.3) immediately yields

$$R_{16} = R_{26} = R_{36} = R_{46} = 0. \tag{5.4}$$

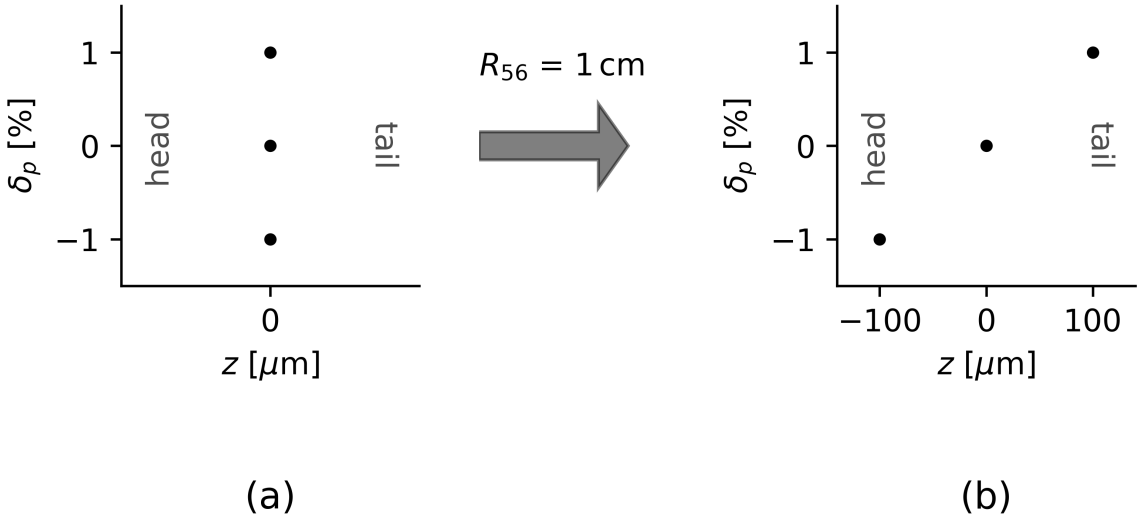

Figure 5.1.: Change of the relative longitudinal position z for off-momentum particles by passing an achromatic section with $R_{56} = 1\,\mathrm{cm}$. The particle's horizontal shift in the longitudinal phase space is directly proportional to R_{56}, as a result the bunch gets sheared clockwise (counterclockwise) for a positive (negative) R_{56}.

With the symplecticity of the transfer matrix R follows

$$R_{16} = R_{52}, \quad R_{26} = R_{51}, \quad R_{36} = R_{54} \quad \text{and} \quad R_{46} = R_{53}. \tag{5.5}$$

As a consequence for an achromatic section, the first four factors of Eq. (5.2) vanish.

As a last step the transfer line does not include time dependent elements, the initial longitudinal position $z(S_1)$ simply is an offset for the final longitudinal position, therefore $R_{55} = 1$. The change of the longitudinal relative position Δz only depends on a particle's momentum offset and the transport matrix element R_{56}. From Eq. (5.2) it follows

$$\Delta z = z(S_2) - z(S_1) = R_{56}\,\delta_p. \tag{5.6}$$

The off-energy particles of a bunch passing an achromatic section are shifted in the z-plane proportional to R_{56}. As a consequence, the bunch sheares clockwise for a positive R_{56} and counterclockwise for a negative R_{56} in the longitudinal phase space. This effect is illustrated in Fig. 5.1. For instance, an off-momentum particle with $\delta_p = 1\%$ passing an achromatic section with $R_{56} = 1\,\mathrm{cm}$ changes its z-position by $1\,\mathrm{cm} \times 1\% = 100\,\mu\mathrm{m}$ towards the tail of the bunch. Accordingly, a particle with $\delta_p = -1\%$ drifts the same distance towards the head of the bunch. With the longitudinal offset of each particle also the bunches length changes.

5.1.2. Full compression condition in first order

A bunch is sheared in the longitudinal phase space by R_{56}. In order to utilize this effect to achieve ultra-short bunches, a linear correlation between the longitudinal position and the energy spread is required. This is achieved by off-crest acceleration in the FLUTE linac. The shape of the bunch in the longitudinal phase space follows the sinusoidal wave form of the accelerating voltage at the phase the bunch enters the linac. The mechanism is visualized in Fig. 5.2, with the accelerating voltage in subfigure (a) and two bunches which were accelerated at opposing phases in (b) and (c). Both ensembles are identical except for their correlated energy spread which is mirrored in time. If the curvature of the sine wave

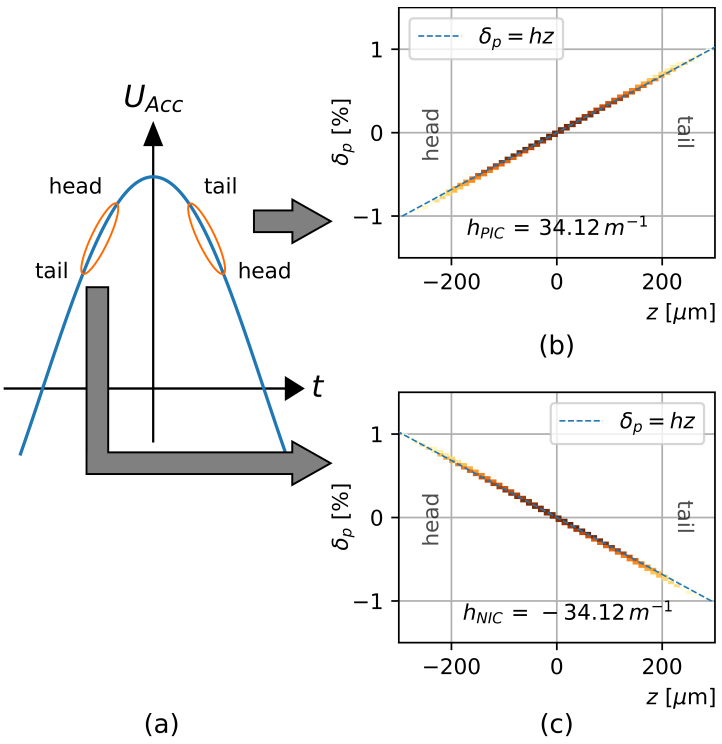

Figure 5.2.: (a) The bunch is accelerated off-crest in the FLUTE linac with the sinusoidal accelerating voltage U_{Acc}. This induces a sharp correlation between the momentum spread and the longitudinal plane, depending on the accelerating phase. The slope in the δ_p-z-plane is called chirp $h = \frac{\partial \delta_p}{\partial z}$, it is calculated with a linear fit. The particle distributions accelerated at the two marked phases have a positive initial chirp (PIC, subfigure b) or a negative initial chirp (NIC, subfigure c).

at the chosen phase is negligible, the particle distribution can be parameterized by a linear function in the δ_p-z-plane. The slope of this linear correlation is called chirp h.

$$h = \frac{\partial \delta_p}{\partial z} \tag{5.7}$$

FLUTE can provide both, a bunch with a positive initial chirp (PIC) or with a negative initial chirp (NIC).

The change of a particle's longitudinal offset is calculated according to Eq. (5.6). As a consequence also the chirp changes while the bunch is traveling from position S_1 to S_2. As the particle's energy is conserved, the chirp changes by

$$h(S_2) = \frac{\partial \delta_p}{\partial (z(S_1) + R_{56}\delta_p)}. \tag{5.8}$$

By inverting the equation,

$$h^{-1}(S_2) = \frac{\partial (z(S_1) + R_{56}\delta_p)}{\partial \delta_p} \tag{5.9}$$

$$= \frac{\partial z(S_1)}{\partial \delta_p} + \frac{\partial (R_{56}\delta_p)}{\partial \delta_p} \tag{5.10}$$

the first addend can be identified as the initial chirp.

$$h^{-1}(S_2) = h^{-1}(S_1) + \frac{\partial (R_{56}\delta_p)}{\partial \delta_p} \tag{5.11}$$

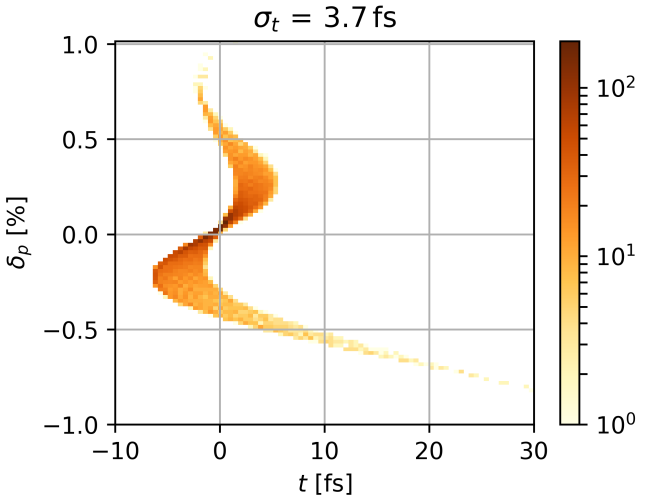

Figure 5.3.: Longitudinal phase space of the initial bunch after it was tracked through the verification matrix M_{verify}. The bunch is compressed to only 3.7 fs.

The inversive chirp of a bunch transforms simply by adding the R_{56} value.

$$h^{-1}(S_2) = h^{-1}(S_1) + R_{56} \tag{5.12}$$

This allows to formulate a condition for full compression, which is a powerful tool to optimize the transfer line towards short bunch lengths. If the bunch has a linear distribution in the longitudinal phase space, the shortest bunch length is obtained, when the bunch is aligned vertically. This implies an infinite chirp and therefore a vanishing inverse chirp. If the sum of the R_{56} parameters of all sections in the transfer line equal the initial inverse chirp, then the longitudinal phase space of the bunch is sheared into a vertical alignment at the end of the transport.

$$h_{\text{final}}^{-1} = h_{\text{init}}^{-1} + \sum R_{56} \stackrel{!}{=} 0 \tag{5.13}$$

$$\textbf{Full compression condition:} \quad \sum R_{56} = -h_{\text{init}}^{-1} \tag{5.14}$$

Validation test: The chirp of the two bunches created by FLUTE are calculated by a linear fit function using the least-squares method.

$$h_{\text{PIC}} = \frac{\partial \delta_p}{\partial z} = +34.12\,\text{m}^{-1} \qquad h_{\text{NIC}} = -34.12\,\text{m}^{-1} \tag{5.15}$$

In order to verify the full compression condition, the 10,000 particles of the PIC ensemble are tracked through a verification matrix M_{verify}, which is a unit matrix with the R_{56} parameter set to fulfill the full compression condition for the PIC bunch.

$$M_{\text{verify}} = \begin{bmatrix} 1 & 0 & 0 & 0 & 0 & 0 \\ 0 & 1 & 0 & 0 & 0 & 0 \\ 0 & 0 & 1 & 0 & 0 & 0 \\ 0 & 0 & 0 & 1 & 0 & 0 \\ 0 & 0 & 0 & 0 & 1 & -h_{\text{PIC}}^{-1} \\ 0 & 0 & 0 & 0 & 0 & 1 \end{bmatrix} \tag{5.16}$$

The result is plotted in Fig. 5.3, the bunch is compressed to a length of 3.7 fs, which is even shorter than the bunch length of 5.7 fs achieved by FLUTE with optimized setup. This shows that the full compression condition is a valid tool to optimize the linear optics towards short bunches. As the bunch gets very short, deviations from the linear distribution of the longitudinal phase space dominate the bunch length. This can be seen in Fig. 5.3.

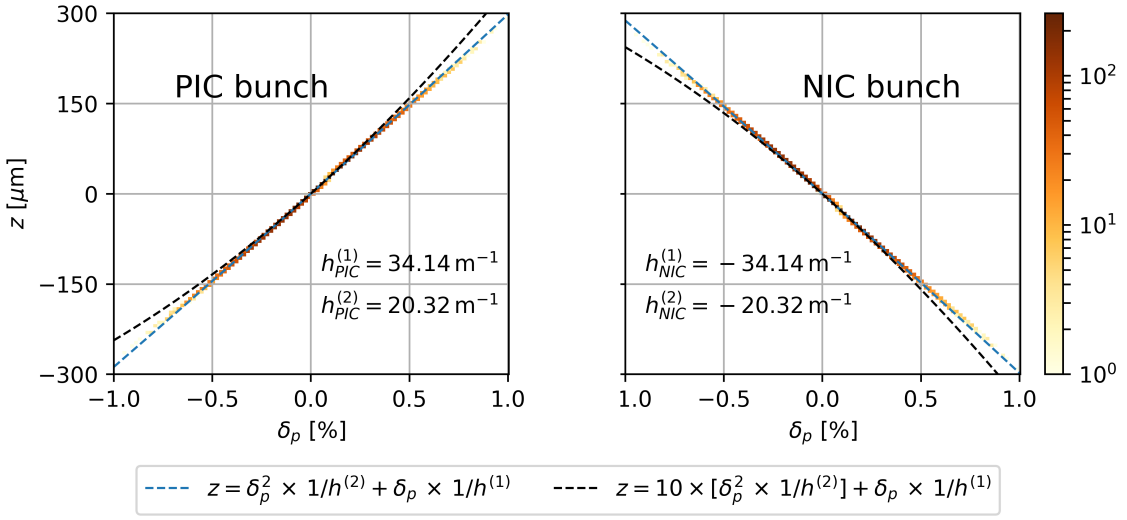

Figure 5.4.: NIC and PIC bunch in the z-δ_p-plane including a second order polynomial fit. For better visibility of the curvature, the fit function is plotted a second time in black with its curvature increased by a factor of ten.

5.1.3. Full compression condition in second order

In order to increase the precision of the compression performance of the transfer line, second order effects need to be taken into account. The longitudinal offset of each particle of the bunch is related to its momentum by the linear chirp as derived in Eq. (5.7).

$$z = \delta_p \times 1/h$$

A second order approximation of the bunch's longitudinal plane is derived by expanding the previous equation in δ_p.

$$z = \delta_p \times 1/h^{(1)} + \delta_p^2 \times 1/h^{(2)} \tag{5.17}$$

With the inverse chirp in first and second order is given by:

$$1/h^{(1)} = \frac{\partial z}{\partial \delta_p}, \tag{5.18}$$

$$\text{and} \qquad 1/h^{(2)} = \frac{\partial^2 z}{\partial \delta_p^2}. \tag{5.19}$$

The second order chirp represents a curvature of the z-position of the bunch in δ_p. Mind that the first order chirp represents the slope of the particle distribution in the δ_p-z-plane and the inverse slope in the z-δ_p-plane. Therefore the first order chirp can be calculated from the distribution's slope in both planes. The second order chirp as defined in Eq. (5.19) on the other hand can be calculated exclusively in the z-δ_p-plane. In this representation both, the PIC and NIC bunch are fitted by a second order polynomial function according to Eq. (5.17), the fit functions are shown in Fig. 5.4.

In the previous chapter the transformation of the linear chirp was discussed. A bunch passing an achromatic lattice module shears in the longitudinal phase space proportional to the modules R_{56} parameter, recall Eq. (5.6):

$$\Delta z = \delta_p \, R_{56}$$

As a consequence the inverse chirp of first order changes by adding the value of R_{56}. Basis for this mechanism are the 6×6 linear transport matrices R of each element. For second

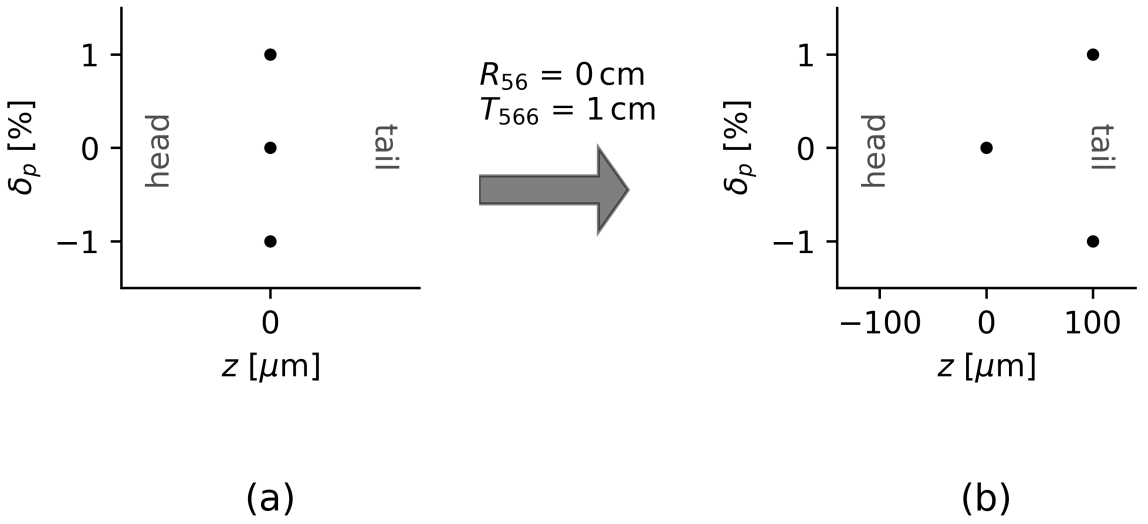

Figure 5.5.: Change of the relative longitudinal position z for off-momentum particles by passing an achromatic section with $R_{56} = 0\,\mathrm{cm}$ and $T_{566} = 1\,\mathrm{cm}$. The positive T_{566} warps the longitudinal phase space of the bunch. Both particles with $\delta_\mathrm{p} = +1\%$ and $\delta_\mathrm{p} = -1\%$ momentum offset change their longitudinal relative position by $\Delta z = +100\,\mu\mathrm{m}$ with respect to the reference particle.

order beam dynamics the matrix algorithm is expanded into a formalism with $6 \times 6 \times 6$ dimensional transport maps T. Similar to the first order, all effects on Δz which dependent on the momentum offset squared are summarized in a single matrix element T_{566} [22].

$$\Delta z = \delta_p \, R_{56} + \delta_p^2 \, T_{566} \tag{5.20}$$

and the inverse second order chirp also transforms by adding the T_{566} parameter.

$$1/h^{(2)}(S_2) = 1/h^{(2)}(S_1) + T_{566} \tag{5.21}$$

T_{566} contributes to Δz with the momentum offset squared, therefore particles with positive or negative δ_p are affected identically. A bunch passing a module with a finite T_{566} value changes its curvature in the longitudinal phase space, an illustration of this effect can be found in Fig. 5.5.

In theory, the bunch length becomes zero if the longitudinal offset of all particles completely vanish after the transport. The basis for the full compression condition therefore is

$$z_f \stackrel{!}{=} 0. \tag{5.22}$$

The initial longitudinal position of each particle z_i is calculated by Eq. (5.17):

$$z_i = \delta_p \times 1/h^{(1)}_\mathrm{Init} + \delta_p^2 \times 1/h^{(2)}_\mathrm{Init} \tag{5.23}$$

In order to satisfy the condition for full compression, Δz is required to cancel the initial longitudinal offset for every particle.

$$z_f = z_i + \Delta z \stackrel{!}{=} 0 \tag{5.24}$$

Inserting Eq. (5.20) results in

$$z_f = \delta_p \left[1/h^{(1)}_\mathrm{Init} + R_{56}\right] + \delta_p^2 \left[1/h^{(2)}_\mathrm{Init} + T_{566}\right] \tag{5.25}$$

This directly yields the full compression condition in first and second order.

$$\textbf{Full compression condition in first order:} \qquad \sum R_{56} = -1/h^{(1)}_{\text{Init}} \tag{5.26}$$

$$\textbf{Full compression condition in second order:} \qquad \sum T_{566} = -1/h^{(2)}_{\text{Init}} \tag{5.27}$$

In order to design a transfer line which results in exactly the required values of R_{56} and T_{566}, the longitudinal dynamics will be discussed in a phenomenological approach. This will provide insight into the origin of the parameters R_{56} and T_{566} and allows to find a strategy to manipulate their values.

5.1.4. Path length

While the previous sections discussed the change in path length Δz from the mathematical point of view, this section derives Δz phenomenologically, which will provide additional information about R_{56} and T_{566} and how to manipulate them.

The path length S for the reference particle is given by the length of all magnetic structures and drift spaces it passes. A particle with a transverse offset experiences a different arc length in dipoles as shown in subfigure (a) of Fig. 2.3. Its individual path length s changes from the reference path according to [23] with

$$s = \int_0^S \left(1 + \frac{x(s)}{\rho(s)}\bigg|_{\text{Dipole}}\right) \mathrm{d}s. \tag{5.28}$$

As the first addend represents the reference path length, the change of the relative longitudinal offset is given by

$$\Delta z = \int_0^S \frac{x(s)}{\rho(s)}\bigg|_{\text{Dipole}} \mathrm{d}s. \tag{5.29}$$

In the case of deflection in a dipole magnet, the transverse offset is a result of dispersion. Recalling the definition of the dispersion in Eq. (2.38)

$$x_\eta(s) = \eta_x(s)\delta_p \tag{5.30}$$

and applying it on Eq. (5.29) results in

$$\Delta z = \delta_p \int_0^S \frac{\eta_x(s)}{\rho_x(s)} \mathrm{d}s. \tag{5.31}$$

Again Δz is proportional to the momentum offset of a particle. For the achromatic case the integral can be identified as R_{56}.

$$\Delta z = \delta_p R_{56}\Big|_{\text{achromatic}} \qquad \text{with} \quad R_{56} = \int_0^S \frac{\eta(s)}{\rho(s)} \mathrm{d}s\Big|_{\text{achromatic}} \tag{5.32}$$

ρ is determined by the geometry of the lattice and therefore can not be varied. Quadrupoles on the other hand affect the dispersion without changing the design orbit and can be used to tune R_{56}.

Path length in second order:

In addition to the transverse offset x of a particle, also the transverse slope $x' = \frac{\partial x}{\partial s}$ of the trajectory affects the path length. The length of a sloped, straight path changes with respect

to the reference path by a factor of $\sqrt{1+x'}$. Multiplying this factor to the expression for the linear path length of Eq. (5.28) leads to

$$s = \int_0^S \left(1 + \frac{x(s)}{\rho(s)}\Big|_{\text{Dipole}}\right) \sqrt{1+x'^2}\,\mathrm{d}s. \tag{5.33}$$

This idea follows the discussion of [24].

Expanding the square root with

$$\sqrt{1+x'^2} \approx 1 + \frac{x'^2}{2} - \mathcal{O}(x'^3) + \ldots \tag{5.34}$$

allows to expand the integral as follows:

$$s = \int_0^S \left(1 + \frac{x(s)}{\rho(s)}\right)\left(1 + \frac{1}{2}x'^2\right)\,\mathrm{d}s \tag{5.35}$$

$$s = \int_0^S \left(1 + \frac{x(s)}{\rho(s)} + \frac{x'^2}{2} + \frac{x'^2}{2}\frac{x(s)}{\rho(s)}\right)\,\mathrm{d}s \tag{5.36}$$

This time, the transverse offset x is replaced with the dispersion function expanded to the second order.

$$x_\eta(s) = \eta_x^{(1)}(s)\delta + \eta_x^{(2)}(s)\delta^2 \tag{5.37}$$

Introducing the second order dispersion function as the second derivative of the transverse offset with respect to the momentum.

$$\eta_x^{(2)}(s) = \frac{\partial^2}{\partial\delta_p^2}x(s) = \frac{\partial}{\partial\delta_p}\eta_x^{(1)}(s) \tag{5.38}$$

Inserting Eq. (5.37) into Eq. (5.36) and ignoring terms of third and higher orders in δ_p leads to the following result.

$$\Delta z = \delta_p \int_0^S \frac{\eta_x^{(1)}(s)}{\rho_x(s)}\mathrm{d}s + \delta_p^2 \int_0^S \left(\frac{\eta_x^{(2)}(s)}{\rho_x(s)} + \frac{1}{2}\left[\eta_x'^{(1)}(s)\right]^2\right)\mathrm{d}s \tag{5.39}$$

The dispersion's slope η' again is the derivative of the dispersion with respect to s. The first integral equals the result of the first order approach given in Eq. (5.31). The second integral represents the changes in a particles path length which are proportional to the square of the momentum offset. Comparing Eq. (5.39) with Eq. (5.20) allows to identify the integrals as the parameters R_{56} and T_{566}.

$$R_{56} = \int_0^S \frac{\eta_x^{(1)}(s)}{\rho_x(s)}\mathrm{d}s \tag{5.40}$$

$$T_{566} = \int_0^S \left(\frac{\eta_x^{(2)}(s)}{\rho_x(s)} + \frac{1}{2}\left[\eta_x'^{(1)}(s)\right]^2\right)\mathrm{d}s \tag{5.41}$$

Like the first order dispersion, also the second order dispersion only contributes to Δz within a dipole $\rho \neq 0$. The first order dispersion's derivative in s can be altered by quadrupoles, therefore, quadrupoles are possible tools to alter the R_{56} value of an achromatic lattice module while keeping dipole magnets unchanged. Sextupole magnets within finite dispersion affect the second order dispersion and can be used to change the T_{566} value of a lattice module [25].

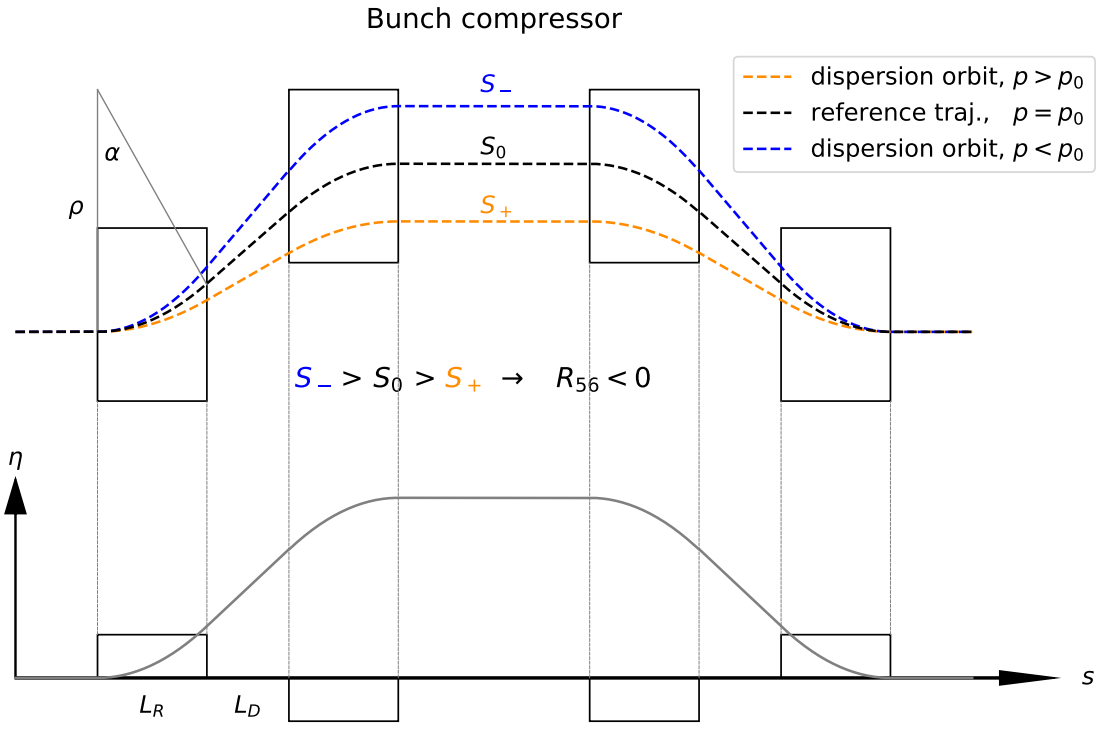

Figure 5.6.: Illustration of a generic four dipole bunch compressor. The upper part shows the geometry, the design orbit (dashed, black) and the trajectory for a particle with a negative (positive) δ_p in blue (orange). In the bottom half, the evolution of the dispersion function η along the lattice is plotted. The L_R long rectangular dipoles deflect the reference path with the radius ρ by the angle α. The outer and inner magnets are separated by L_D, the distance between the two inner magnets does not affect the linear beam dynamics.

5.2. Lattice modules

In the previous part of this chapter R_{56} and T_{566} were found to be the lattice properties which shear and warp the particle distribution in the longitudinal phase space. If the transfer line's total R_{56} and T_{566} values fulfill the full compression conditions, the bunch is expected to become ultra-short. Three lattice modules will be investigated in their R_{56} parameters in order to find a lattice for the transfer line that allows to fulfill the first order full compression condition.

5.2.1. Bunch Compressor

A bunch compressor (BC) is a common lattice module to longitudinally compress a positively chirped bunch. The geometry of a generic bunch compressor together with three exemplary trajectories for different energies are visualized in the upper part of Fig. 5.6. The module consists of four equally deflecting dipoles creating a chicane. A particle with a positive momentum offset will be deflected with a larger radius than the reference particle. As a consequence of the geometry, its trajectory is shorter than the reference path. This allows the particle to catch up with the bunch's head if its initial position is at the tail. A particle with a negative momentum offset on the other hand will fall back in the bunch. As a result of the different path lengths the longitudinal phase space gets sheared counterclockwise and R_{56} is negative.

This is confirmed from the mathematical point of view. All dipoles have the same deflection radius but the middle dipoles deflect in the opposite direction. Therefore, in case of

calculating R_{56}, they are considered to have a negative bending radius. The dispersion function defining the trajectory's transverse offset is shown in the lower part of Fig. 5.6. Since R_{56} is obtained from the relation of dispersion and deflection radius, the two middle dipoles contribute stronger and negative to R_{56} than the outer dipoles because of the larger dispersion.

$$R_{56,\mathrm{BC}} = \int_0^S \frac{\eta(s)}{\rho(s)} \mathrm{d}s \tag{5.42}$$

$$\propto \int_0^S \left[\frac{\eta_1}{\rho}\bigg|_{\mathrm{Bend1}} + \frac{\eta_2}{-\rho}\bigg|_{\mathrm{Bend2}} + \frac{\eta_2}{-\rho}\bigg|_{\mathrm{Bend3}} + \frac{\eta_1}{\rho}\bigg|_{\mathrm{Bend4}} \right] \mathrm{d}s \tag{5.43}$$

$$< 0 \qquad \text{with} \qquad \eta_1 < \eta_2 \tag{5.44}$$

For this geometry $R_{56,\mathrm{BC}}$ is always negative and the longitudinal phase space shears always sheared counter clockwise.

FLUTE bunch compressor: The FLUTE bunch compressor consists of four rectangular dipoles with a length of $L_\mathrm{R} = 20\,\mathrm{cm}$. It is designed to deflect a bunch with an energy of 42 MeV by an angle in the range of 0° to 11.3° [1] per dipole. Different angles are achieved by changing the magnetic field in the dipoles and by moving the inner dipoles in the horizontal plane in order to follow the design orbit. The outer and inner dipoles are positioned with a distance of $L_\mathrm{D} = 20\,\mathrm{cm}$ to each other, the drift space in the *elegant* model between these dipoles depends on the deflection angle and is given by $20\,\mathrm{cm}/\cos(\alpha)$.

The R_{56} value of this lattice was calculated by *elegant* for the possible angular range with a step size of 10 mrad. For each simulation step the definition of the dipole geometry and the drift length L_D was adjusted. The resulting R_{56} values are plotted against the deflection angle in Fig. 5.7. A polynomial fit function of second order represents the relation with

$$R_{56,\mathrm{BC}}(\alpha) = \left(-0.041\alpha^2 + 0.015\alpha\right)\ \mathrm{cm} \quad \text{with} \quad \alpha \in [0°; 11.3°] \tag{5.45}$$

For deflection angles in the range of $\alpha \in [0°; 11.3°]$ this results in values of

$$R_{56,\mathrm{BC}}(\alpha) \in [0\,\mathrm{cm}; -5.2\,\mathrm{cm}]. \tag{5.46}$$

5.2.2. Double Bend Achromat

A double bend achromat (DBA) is a common way to realize a net deflection while staying achromatic, which is vital for the transfer line geometry in order to keep R_{56} at a minimum. The geometry is shown in Fig. 5.8. The two dipoles are separated by a central quadrupole. In the first dipole dispersion is introduced. The central quadrupole changes the sign of the dispersions derivative such that the dispersion created by the first dipole is canceled by the second and the achromaticity criterion is fulfilled. The dispersion function can be found in the bottom subplot of Fig. 5.8. Further, there are four additional quadrupoles flanking the dipoles. At their position no dispersion is present, therefore they have no effect on the longitudinal dynamics. With their four additional degrees of freedom, they can be used to tune the transverse optics.

The dispersion in the center part of the DBA forces particles onto trajectories of different lengths depending on their momentum. Three exemplary trajectories of particles with different momenta are visualized along the DBA's geometry in the upper plot of Fig. 5.8, the corresponding dispersion function is shown in the bottom plot of the same figure.

From Eq. (5.32) follows that only the dispersion within a dipole contributes to $R_{56,\mathrm{DBA}}$. Therefore the DBA's R_{56} value equals twice the R_{56} value of the dipoles used. With the

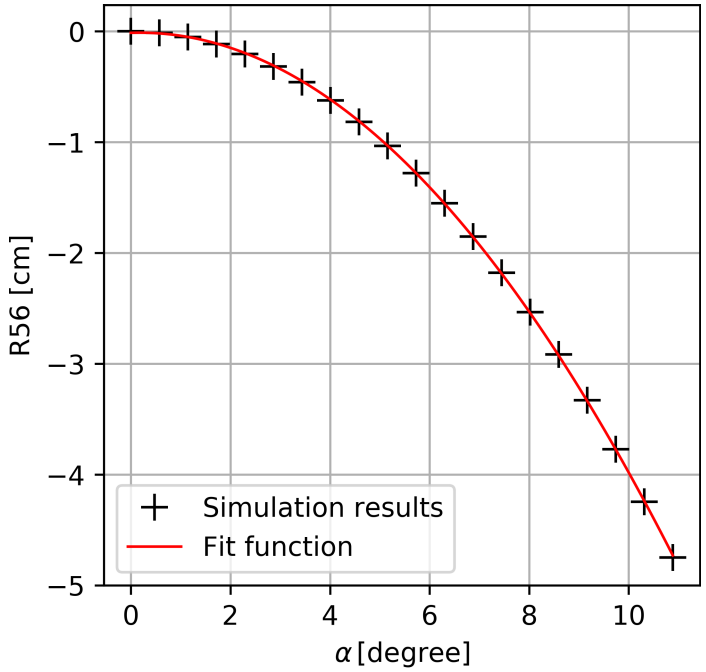

Figure 5.7.: R_{56} of the FLUTE bunch compressor for different deflection angles.

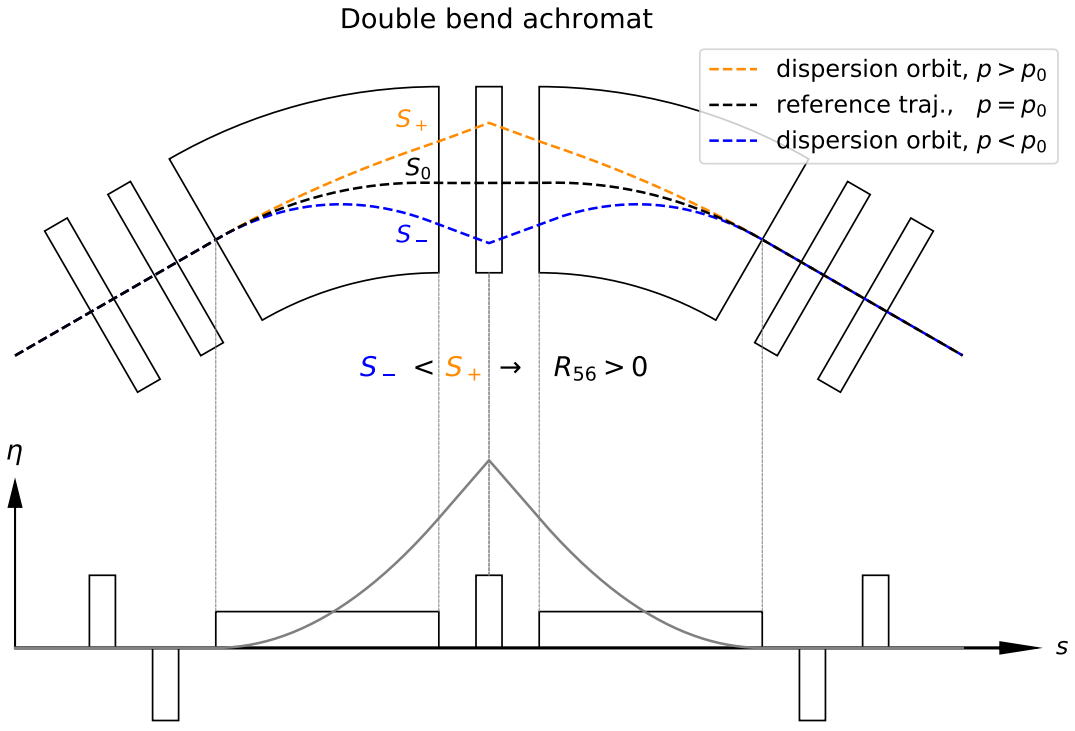

Figure 5.8.: Geometry and trajectories (top) and corresponding dispersion function (bottom) for a generic double bend achromat. The upper half shows the trajectory for a particle with a negative (positive) δ_p in blue (orange) and the reference trajectory in black. In the bottom half the evolution of the dispersion function along the lattice is plotted. The outer quadrupoles are required to focus the transversal optics but do not affect the dispersion.

transport matrix element of a sector dipole given in Eq. (2.19) follows:

$$R_{56,\mathrm{DBA}} = 2 \times R_{56,\mathrm{Sectorbend}} \tag{5.47}$$
$$= 2\rho\left(\alpha_{\mathrm{r,Sectorbend}} - \sin(\alpha_{\mathrm{r,Sectorbend}})\right) \tag{5.48}$$
$$= 2\rho\left(\frac{\alpha_\mathrm{r}}{2} - \sin\left(\frac{\alpha_\mathrm{r}}{2}\right)\right) \tag{5.49}$$

with the deflection radius ρ and the deflection angle for the DBA α_r [rad] twice as large as the angle of a single dipole $\alpha_{\mathrm{r,Sectorbend}}$ [rad].

The sine function can be expanded into a Taylor series:

$$R_{56,\mathrm{DBA}} = 2\rho\left(\frac{\alpha_\mathrm{r}}{2} - \sum_{n=0}^{\infty}(-1)^n\frac{(\alpha_\mathrm{r}/2)^{2n+1}}{(2n+1)!}\right) \tag{5.50}$$
$$= 2\rho\left(\frac{\alpha_\mathrm{r}}{2} - \frac{\alpha_\mathrm{r}}{2} + \frac{1}{8}\frac{\alpha_\mathrm{r}^3}{6} - \frac{1}{32}\frac{\alpha_\mathrm{r}^5}{120} + \dots\right) \tag{5.51}$$
$$= \rho \times \left(\frac{1}{24}\alpha_\mathrm{r}^3 - \frac{1}{1920}\alpha_\mathrm{r}^5 + \dots\right) \tag{5.52}$$

According to this relation R_{56} grows strictly monotonic for realistic configurations ($\alpha < 400°$). As a consequence of the angle contributing with the third power, a DBA's angle should be kept small. The deflection of large angles should be performed with multiple DBA cells with small bending radii in order to keep $R_{56,\mathrm{DBA}}$ as small as possible.

For example, consider a 90° turn performed by DBAs made of two sector dipoles with deflection radius of 1 m. A single DBA rises $R_{56,\mathrm{DBA}}(90°) = 16\,\mathrm{cm}$ while using two DBAs results in only $2 \times R_{56,\mathrm{DBA}}(45°) = 4\,\mathrm{cm}$. Yet splitting DBAs increases the space needed due to the required quadrupoles and drift sections.

5.2.3. Hexa Bend Achromat

A DBA is a good and simple lattice module for achromatic deflections for small angles. Yet its R_{56} value grows with the deflection angle in the third power. One of the two transfer line layouts which will be discussed require an arc with a total deflection angle in the order of 180°. Such an arc should not be built by one single DBA. The module used is made of three DBA cells. Because it includes six dipoles it is named hexa bend achromat (HBA) within this thesis. The HBA can deflect by angles in order of 180° with moderate R_{56} values in the order of 15 cm. Its geometry is shown in Fig. 5.9. The common DBA sequence foresees a quadrupole quartet (D,F,F,D) between the adjacent dipoles of two DBA cells. In order to reduce the length of the HBA, a quadrupole triplet (D,F,D) is used instead. The HBA needs to be understood as a single module instead of three DBA modules, with the possibility to install either the regular DBA optics within each cell or a new optics which will be called negative dispersion optics. The latter allows to tune R_{56} in a wide range and proved to be a powerful tool to fulfill the full compression condition.

DBA optics: If the achromaticity criterion is fulfilled for each DBA cell individually, the optics will be called DBA optics. Because the geometry for each cell is identical, also each central quadrupole needs to be set to the same strength to fulfill the achromaticity criterion correctly. R_{56} is strictly positive in this case.

Negative dispersion optics: This concept follows the idea of negative alpha optics in storage rings [26]. By increasing the strength of the three central quadrupoles simultaneously, the individual DBA cells lose their achromaticity. After the first cell the dispersion is not canceled but pushed to a negative value. The finite dispersion then is affected by

the quadrupole triplet before entering the second DBA cell. If the triplet is set correctly the dispersion's derivative becomes zero in the middle of the second DBA cell. Then the dispersion function evolves mirror symmetrically and the HBA fulfills the achromaticity criterion. This is called negative dispersion optics. The lower part of Fig. 5.9 shows the evolution of the dispersion along the HBA lattice in both, DBA optics and negative dispersion optics.

The R_{56} value of the HBA with DBA optics equals three times the R_{56} value of the single DBAs and as a consequence is strictly positive. For a total deflection angle α_{tot} [rad], the R_{56} value of the HBA in DBA optics can be approximated with the equation for a single DBA given in Eq. (5.52).

$$R_{56,\mathrm{HBA}}(\mathrm{DBA}) = 3 \times R_{56,\mathrm{DBA}}\left(\alpha_{\mathrm{tot}}/3\right) \tag{5.53}$$

$$= \rho \times \left(\frac{1}{216}\alpha_{\mathrm{tot}}^3 - \frac{1}{155520}\alpha_{\mathrm{tot}}^5 + \dots\right) \tag{5.54}$$

The negative dispersion optics, on the other hand, reduces R_{56} depending on the increased strength in the central quadrupoles.

$$R_{56,\mathrm{HBA}}(-\eta) \in [R_{56,\mathrm{HBA}}(\mathrm{DBA}); -\infty] \tag{5.55}$$

Of course R_{56} cannot be reduced infinitely. Increasing the amplitude of the dispersion function inflicts a larger transverse beam size which is limited by the dimensions of the vacuum chamber. Yet in case of the simulations R_{56} could be tuned to any reasonably desired numeric value without suffering particle loss.

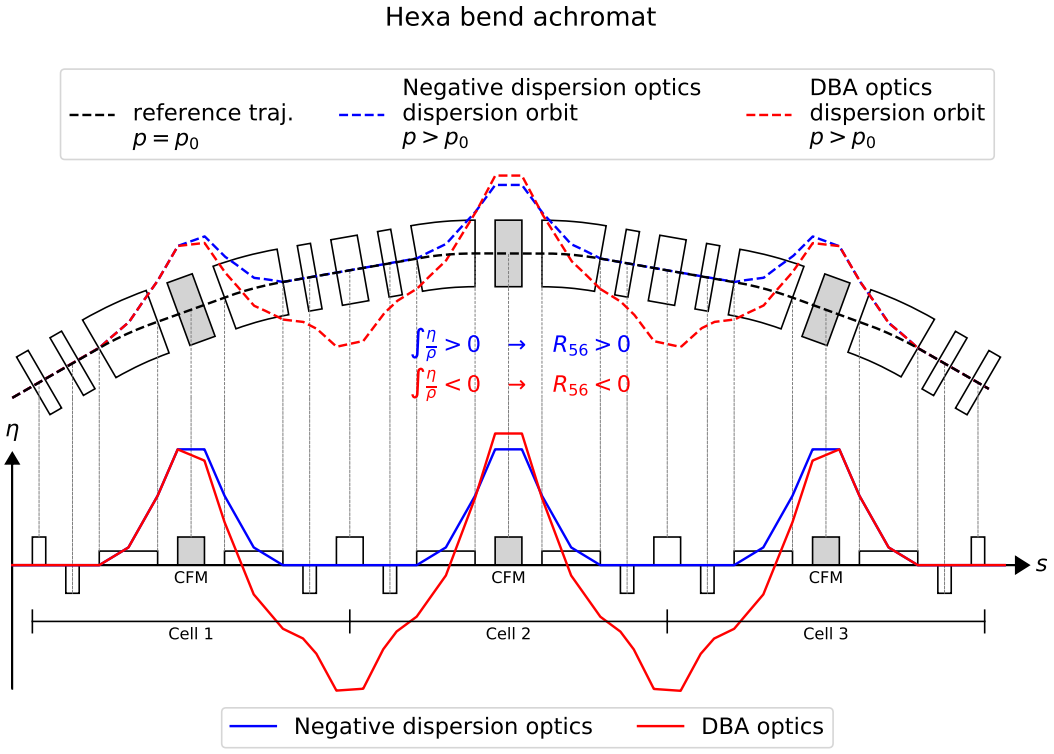

Figure 5.9.: Hexa bend achromat consisting of three cells based on a DBA structure. The upper part shows the geometry, the reference trajectory (black, dashed) and the orbit for a particle with a positive momentum offset for both, the DBA optics (blue) and the negative dispersion optics (red). In the bottom plot, the dispersion function along the lattice is shown for both corresponding optics. The central quadrupoles (gray) of each cell are prepared to apply a sextupole component.

5.3. Conclusion

The first section of this chapter discusses the longitudinal dynamics. It was found that the longitudinal phase space of a bunch changes by two effects while traveling through achromatic lattice modules.

1. The longitudinal phase space is sheared proportional to the R_{56} element of the module's linear transport matrix R.
2. The longitudinal phase space is warped proportional to the T_{566} element of the module's second order transport map T.

These two effects can be used in order to align the longitudinal phase space vertically and to linearize it. As a consequence the bunch length will be reduced to a minimum. With the FLUTE linac providing a linear chirped bunch, the requirements to the transfer line in the parameters R_{56} and T_{566} can be calculated and the two full compression conditions can be formulated.

$$\text{1st order (PIC):} \quad \sum R_{56,\mathrm{PIC}} = -1/h^{(1)}_{\mathrm{PIC}} = -2.9\,\mathrm{cm} \tag{5.56}$$

$$\text{1st order (NIC):} \quad \sum R_{56,\mathrm{NIC}} = -1/h^{(1)}_{\mathrm{NIC}} = +2.9\,\mathrm{cm} \tag{5.57}$$

$$\text{2nd order (PIC):} \quad \sum T_{566,\mathrm{PIC}} = -1/h^{(2)}_{\mathrm{PIC}} = -4.9\,\mathrm{cm} \tag{5.58}$$

$$\text{2nd order (NIC):} \quad \sum T_{566,\mathrm{NIC}} = -1/h^{(2)}_{\mathrm{NIC}} = +4.9\,\mathrm{cm} \tag{5.59}$$

The sign of the values depends on the orientation of the initial chirp and are derived by the second order polynomial fit shown in Fig. 5.4.

In the second section of this chapter three different achromatic lattice modules were discussed with emphasis on their longitudinal compression performance.

- The bunch compressor (BC) provides a negative R_{56} depending on the dipoles deflection angle.
- The double bend achromat (DBA) performs a net deflection, its R_{56} is defined by the module geometry and is always positive.
- The hexa bend achromat (HBA) also performs a net deflection. With DBA optics it has a positive R_{56} value which is defined by the geometry, similar to the DBA module. It is possible to apply negative dispersion optics which allow to reduce the R_{56} parameter. As a consequence, the HBA module has a finite positive R_{56} value, which can be reduced to lower or even negative values over a wide range.

The next two chapters will present two possible layouts of the transfer line connecting FLUTE with a nearby or a distant symmetry point of cSTART. Both layouts need to deflect the bunch multiple times. The required deflections can be performed with DBA and HBA modules. Together with the FLUTE bunch compressor a combination of modules is required, which fulfills the full compression condition in first order.

It turned out that each module discussed results in a positive T_{566} value. The installation of sextupoles within a dispersive region will be required to push T_{566} of single modules to negative values in order to fulfill the second order full compression condition, too.

6. Layout A: Injection into the nearby symmetry point

The transfer line Layout A provides the shortest possible lattice and requires a minimum of magnets. It is visualized in Fig. 6.1, the first part of FLUTE and cSTART are shown in light gray while the elements of the transfer line and the simulated part of FLUTE are colored. Right after the FLUTE bunch compressor two DBA cells deflect the beam by 90° and 100° with a deflection radius in the dipoles of 1 m. Between the two DBAs, the deflection plane has to be rotated by 45° in order to deflect the beam towards the symmetry point. As a result of the arc's total angle of 190° the following parts of the transfer line are heading downwards with a slope of 10°. A second bunch compressor is installed after the arc, its four rectangular dipoles have a length of 20 cm. The drift space between the outer and inner dipoles is 50 cm.

This transfer line layout requires vertical injection into cSTART. So far a vertical achromatic injection scheme that fits within the remaining space has not been found. Without achromaticity the vertical dispersion is not zero at the cSTART symmetry point. Therefore the simulations do not involve the injection scheme. For the 3-D image a simple sector dipole was used. The task of a valid injection scheme is left to further investigations.

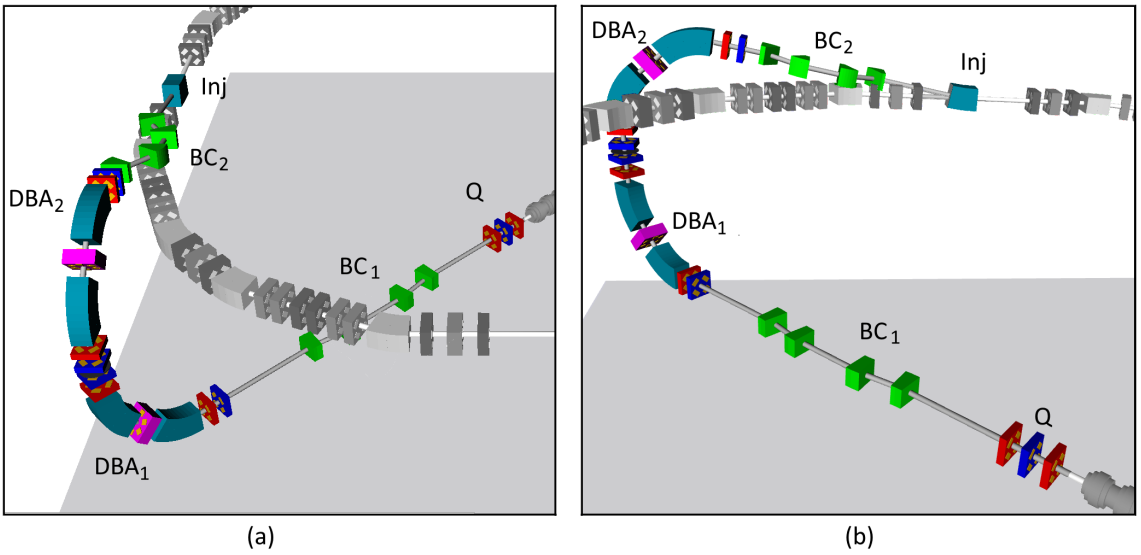

Figure 6.1.: Two perspectives of the transfer line in Layout A. The elements included to the simulations are colored, the remaining FLUTE modules and cSTART appear in gray shades. Shown are horizontal/vertical focusing quadrupoles (red/blue), horizontal/vertical deflecting dipoles (green/turquoise) and combined function magnets with quadrupole and sextupole components (pink).

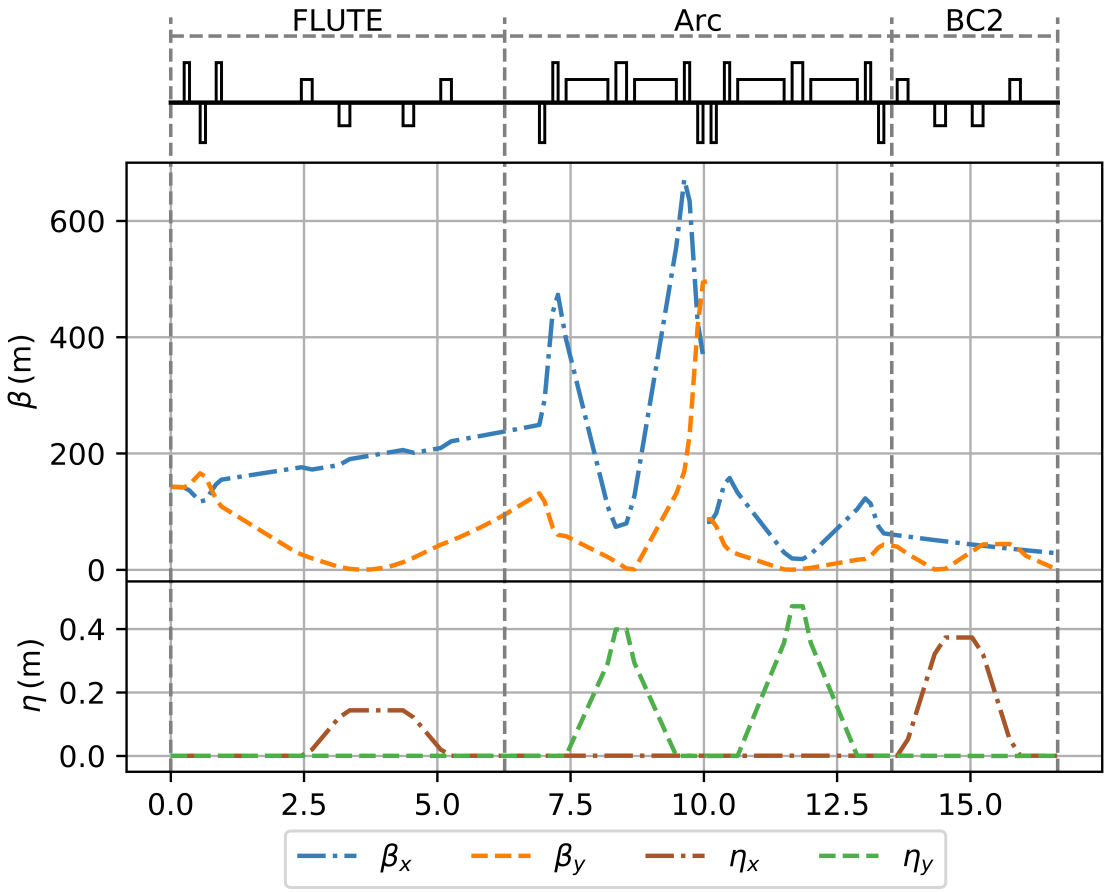

Figure 6.2.: Linear transverse optics of the transfer line in Layout A, fulfilling the first order full compression condition. The beta functions are shown in the top plot and the dispersion function in the bottom plot. Above the optics functions, the lattice is visualized with quadrupoles (and CFM) as tall and dipoles as flat squares. The rotation of the transfer line coordinate system at $S = 10\,\mathrm{m}$ results in a step in the optics functions.

6.1. Transverse optics

All simulations in this chapter start 8.5 m after the electron gun of FLUTE. This position is addressed as the starting point of the transfer line with $S = 0\,\mathrm{m}$. The initial particle ensemble is defined by the settings of the FLUTE gun, solenoid and linac. From the initial ensemble at the starting point, a set of Twiss parameters is extracted with the tool sddsanalyzebeam and propagated through the optics. The linear transverse optics parameters are plotted in Fig. 6.2, with the beta functions in the top and the dispersion functions in the bottom plot.

The first possibility to modify the beta functions for the transfer line is the FLUTE quadrupole triplet. The next module is the FLUTE bunch compressor, which is set to its maximum possible deflection angle, which will be subject of the upcoming section. However, it cannot be altered in order to match the transverse optics, yet it applies edge focusing in the vertical plane and geometric focusing in the horizontal plane. In the plot these two effects are barely visible due to the magnitude and slope of the beta functions. In the DBAs the central quadrupoles are tuned to fulfill the achromaticity criterion for each DBA cell. As a consequence they cannot be altered for transverse focusing either. Yet the dispersive part of both DBAs have a strong transverse focusing effect. The quadrupole doublets outside of the dispersive part of the two DBAs remain as open degrees of freedom in order to match the transverse beam parameters. The second bunch compressor also affects the

transverse plane only passively like the FLUTE bunch compressor. As a result, only the FLUTE quadrupole triplet and the four quadrupole doublets can be used to manipulate the transverse optics, which should be matched with the optics of cSTART at the symmetry point. However as long as the injection scheme is not decided, the linear optics cannot be propagated all the way to the symmetry point. The open degrees of freedom are set in order to prevent the beam from diverging transversely. When a valid injection scheme is found, it should be checked if the remaining quadrupoles are sufficient to match the linear optics to the optics required in cSTART or if additional magnets are required.

Transverse coupling: The step in the transverse optics at $S = 10\,\mathrm{m}$ shown in Fig. 6.2 comes from the rotation of the coordinate system. The initial Twiss parameters are propagated through the lattice until the rotation point at $S = 10\,\mathrm{m}$. This provides the data of the transverse optics for the first half of the lattice. The deflection plane of the second DBA is rotated by 45° with respect to the deflection plane of the first DBA, as shown in the 3-D image in Fig. 6.1. As a consequence of this rotated deflection plane, the dynamics in the transverse planes are no longer decoupled. *Elegant* is not able to calculate Twiss parameters for a non-periodic lattice if transverse coupling is present.

In order to find the Twiss parameters in the second half of the transfer line, the initial bunch was tracked to $S = 10\,\mathrm{m}$, where its coordinate system is rotated by 45°. With the particle ensemble described in the rotated coordinate system, it will experience only forces in parallel to its horizontal and vertical planes in the second half of the transfer line. Therefore the upcoming elements can be described as uncoupled in the rotated coordinate system. A visualization of the rotation of the bunch coordinate system is given in Fig. 6.3. A new set of Twiss parameters is calculated from the rotated particle ensemble at $S = 10\,\mathrm{m}$ using the covariance matrix method. For this case, the covariance matrix method has an advantage over the sddsanalyzebeam tool. After tracking the bunch through the first half of the transfer line, it got rearranged in such a way that the latter method misinterprets the transverse parameters. This new set of optics parameters then is propagated through the lattice from $S = 10\,\mathrm{m}$ to the injection dipole. This provides the data plotted in the second half in Fig. 6.2. The size of the step in the beta functions is conspicuously large. While a rotation of the coordinate system about 90° would exchange the amplitudes of the beta functions for the horizontal and vertical plane, the rotation of 45° is expected to make both beta functions amplitudes meet somewhere in between the initial values. Indeed the both new beta functions after the rotation have almost the same values, yet the rotation makes both beta function amplitudes drop several hundreds of meters.

The reason for this is that the Twiss parameters plotted between $S = 0\,\mathrm{m}$ and $S = 10\,\mathrm{m}$ originate from the propagation of the initial Twiss parameters, while the Twiss parameters after the rotation originate from a tracking simulation. While the Twiss propagation only considers linear optics and assumes the shape of the bunch stays Gaussian, the tracking simulation takes transverse coupling and non-linear effects into account. Therefore both approaches result in different values. Evaluating the beta functions before and after the rotation both from tracking leads to a more reasonable transition. The rotation makes the horizontal beta function drop from $\beta_{\mathrm{Init,track};x} = 65\,\mathrm{m}$ to $\beta_{\mathrm{Rot};x} = 47\,\mathrm{m}$ while the vertical beta function rises from $\beta_{\mathrm{Init,track};y} = 44\,\mathrm{m}$ to $\beta_{\mathrm{Rot};y} = 48\,\mathrm{m}$. Both pairs of values can be found in Tab. 6.1 together with the values from the Twiss propagation method. The huge differences between the two methods mainly rise inside the first double bend achromat, the reason for this is considered to be non-linear effects invoked by the high dispersion amplitude.

Although Twiss propagation method results in different quantities than the more precise tracking method, it still calculates the correct quality. The Twiss propagation still is a reliable tool to derive the optics of the transfer line.

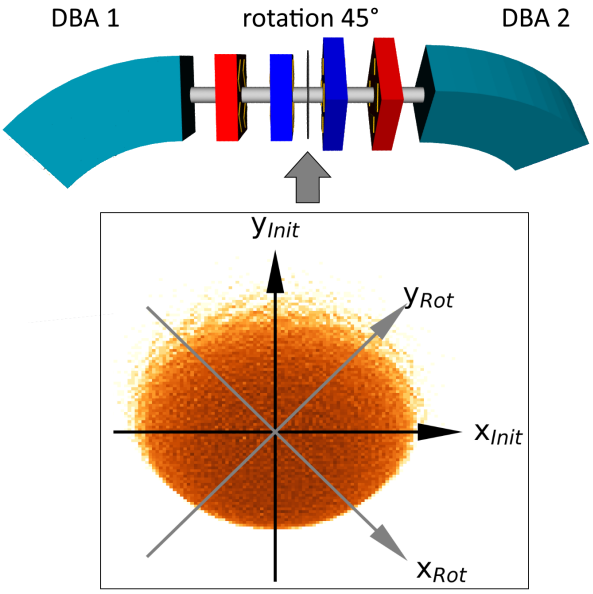

Figure 6.3.: End of the first DBA and start of the second DBA in the Arc section. The coordinate system of the bunch is rotated in between the DBAs at $S = 10\,\mathrm{m}$. The transverse plane of the bunch at this point is shown in the x-y-plane with both the initial and the rotated coordinate system.

Table 6.1.: Beta functions at the rotation point derived by propagating the initial Twiss parameters compared with the tracking method.

	before rotating Twiss propagation	before rotation tracking	after rotation tracking
Horizontal beta function	370 m	65 m	47 m
Vertical beta function	493 m	44 m	48 m

6.2. Longitudinal optics

The modules of the chosen layout raise the R_{56} and T_{566} values which are listed in Tab. 6.2. Both DBAs are required to deflect with large angles and therefore create large R_{56} values of 19 cm and 25 cm. Splitting them into multiple DBA cells would reduce their longitudinal impact. However, a split into three DBA cells is not possible due to the required rotation within the arc and a split into four DBAs would require too much space because of the additional quadrupoles and drift spaces needed. The DBA's unavoidable large R_{56} values are compensated by the two bunch compressors. The FLUTE bunch compressor is set to its maximum possible deflection angle of 11.3° which leads to $R_{56,\mathrm{BC}} = -5.1\,\mathrm{cm}$. The second bunch compressor is required to provide an R_{56} in order to fulfill the first order full compression condition. Recalling the full compression condition from Eq. (5.57) and Eq. (5.57):

$$\sum R_{56,\mathrm{PIC}} = -2.9\,\mathrm{cm} \qquad \sum R_{56,\mathrm{NIC}} = +2.9\,\mathrm{cm} \tag{6.1}$$

Matching the longitudinal optics for a PIC bunch would require the second bunch compressor to apply an even higher R_{56} value than for a NIC bunch. This would lead to larger non-linear effects. Therefore, the optics are optimized for the transport of a NIC bunch. With the second bunch compressor set to an deflection angle of 30.1°, it provides an R_{56} value of $-36\,\mathrm{cm}$. The sum of all R_{56} adds up to 3 cm which fulfills the first order full compression

Table 6.2.: R_{56} and T_{566} before and after second order correction for each achromatic section in the transfer line for transporting a NIC bunch.

Section	R_{56}	T_{566}	T_{566} after correction
FLUTE BC	−5.1 cm	7.9 cm	7.9 cm
Arc: DBA1	19.3 cm	42.3 cm	−53.4 cm
Arc: DBA2	25.2 cm	61.5 cm	−24.5 cm
2nd BC	−36.4 cm	61.5 cm	61.5 cm
Sum	3.0 cm	167.0 cm	−8.4 cm

condition with only a small divergence. All R_{56} values for this lattice are listed in the first column of Tab. 6.2. Each section also grows naturally a positive T_{566} value which can be found in the middle column of the table.

Second order: Since the naturally grown T_{566} value of all modules is positive, the second order full compression condition is not fulfilled. In order to reduce the sum of T_{566}, a sextupole component is added to the central quadrupole in both DBA modules. This changes the magnet type from quadrupoles to combined function magnets which are colored in pink in the artistic view in Fig. 6.1. The correct strength of the sextupoles were found by a optimization function performed by *elegant* using the simplex method. The optimization was set to find the best sextupole strengths in order to reduce the final bunch length. The results are $K_{2,\mathrm{DBA1}} = 220\frac{1}{\mathrm{m}^2}$ and $K_{2,\mathrm{DBA2}} = 100\frac{1}{\mathrm{m}^2}$, the reason for the asymmetry in these parameters has not been investigated in detail, but could be found in the rotated deflection plane. The sextupole components change the arc's T_{566} and the sum over all modules is reduced from 167 cm to −8 cm. This value is a consequence of the optimization for a short bunch length and differs from the value expected by the full compression condition of 5 cm. As a consequence, the final bunch is expected to have a small curvature corresponding to a T_{566} of −13 cm. Since the second order chirp contributes to the longitudinal offset of particles with the momentum deviation squared, this remaining second order chirp is much smaller than the longitudinal spread which grew during the transport. The lattice definition including the magnetic strengths set for the final tracking simulation of the transfer line in Layout A can be found in appendix A.1.

6.3. Tracking

The performance of the optics is investigated with a tracking simulation. The NIC bunch represented by 100,000 macro particles was tracked from the starting point in front of the FLUTE quadrupole triplet until the end of the second bunch compressor. The resulting distribution in the longitudinal phase space after tracking to the end of the transfer line is plotted in Fig. 6.4 for three different cases.
(a) Without sextupoles: The optics fulfill only the first order full compression condition, the bunch is compressed to a length of 89 fs. As each lattice module has a positive T_{566} value, the longitudinal phase space grew a curvature.
(b) Including sextupoles: The T_{566} corrections of the sextupoles make the bunch stay linear in the longitudinal phase space and the bunch length is further reduced to only 70 fs.
(c) Including radiation effects: The third tracking simulation uses the same optics like run (b) but includes coherent synchrotron radiation.
The negligible effect of the CSR radiation can be explained with the evolution of the bunch length. The bunch is compressed to its final length by passing the very last dipole of the

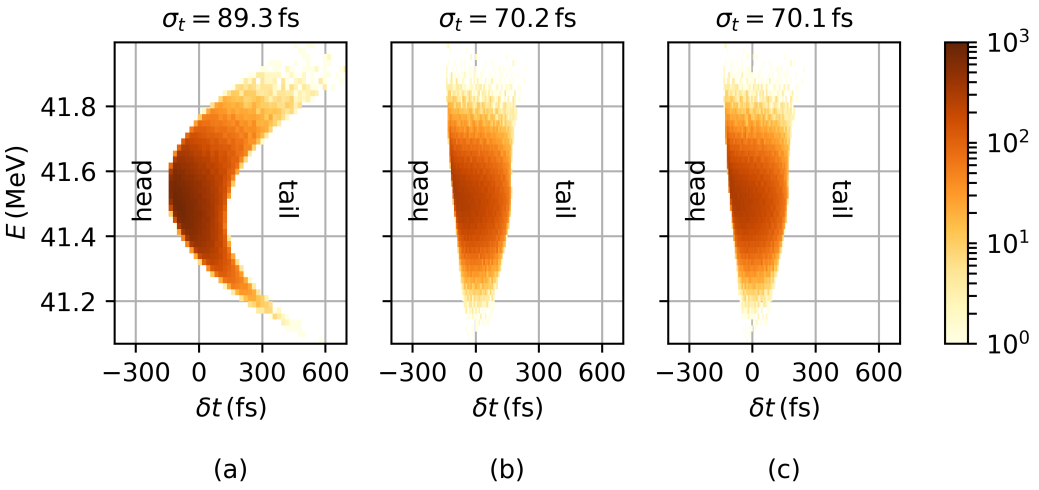

Figure 6.4.: Result of the tracking studies for Layout A. A NIC bunch was tracked throught the lattice with optics fulfilling only the first order full compression condition (a) and optics fulfilling the first and second order full compression condition (b and c). The tracking study resulting in the right hand plot also include CSR effects.

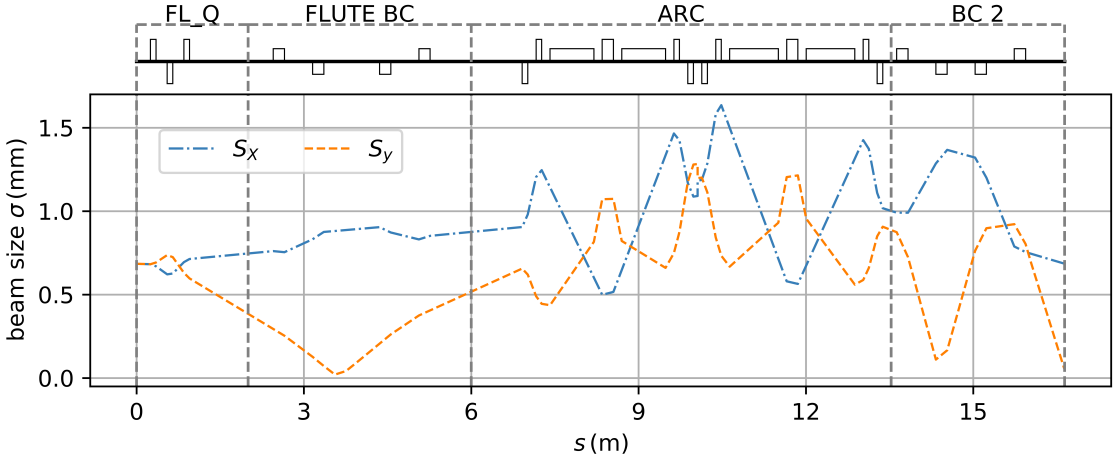

Figure 6.5.: Transverse beam size of the NIC bunch through the transfer line in Layout A, fulfilling both conditions for full compression. The data originate from tracking, including coherent synchrotron radiation.

second bunch compressor. Before, the bunch length was too large to emit a significant amount of coherent synchrotron radiation.

The transverse beam size of the bunch is plotted in Fig. 6.5. The data shown originate from the tracking simulation of run (c) but does not differ between the three tracking simulations. Since tracking is more precise and calculates the rotation correct, the beam size is the most reliable parameter to describe the transverse dynamics. Qualitatively the evolution of the transverse beam size is a superposition of the beta functions and the dispersion functions. This is clearly visible for example in both bunch compressors. While the vertical beam size is proportional to the vertical beta function, the horizontal beam size increases from the horizontal dispersion from the bunch compressor. The step in the horizontal and vertical beam size at $S = 10\,\mathrm{m}$ comes from the rotation. All tracking simulations consider edge effects in second order for each element (if possible) and the aperture limitation of the FLUTE vacuum chamber.

6.4. Conclusion

The Layout A of the transfer line is designed for shortest possible length and requires a minimum of magnets. In tracking simulations no particle exceeded the transverse aperture limitations, which means no particle was lost. In addition the longitudinal optics compresses the bunch to a length of 70 fs. By traveling through the transfer line, the longitudinal phase space of the initial bunch grew a wide spread, the sharp correlation achieved by the linac could not be conserved. However, if such a layout should be chosen, the following challenges still have to be addressed:

- The second bunch compressor deflects by 30°. For such large angles higher order effects need to be investigated in more detail.
- The transfer line approaches the injection point with an angle of 10°. This provides only little space for the physical elements of the transfer line and cSTART.
- A vertical achromatic injection scheme is required.
- The transverse optics need to be matched to cSTART's. It might be possible that additional degrees of freedom are required. This depends on the injection scheme that will be chosen.

In order to avoid the injection from in vertical plane another layout has been investigated.

7. Layout B: Injection into the distant symmetry point

In the previous chapter, layout A was found as a solution of transporting the beam to the nearest symmetry point of cSTART. Beside other difficulties, Layout A would require a vertical injection scheme which could not be found within this master's thesis. Another approach is given by Layout B, which injects into the distant symmetry point. The geometry allows a horizontal injection, it can be seen in Fig. 7.1 and in Fig. 7.2.

The transfer line of Layout B starts after the FLUTE bunch compressor with a vertical arc which deflects the beam by 200°, realized with an HBA module. The consecutive transfer line has the shape of a dogleg. Seen from a top view, the dogleg starts with a turn to the left (referenced as DLL) followed by a turn to the right (DLR). The DLL part is made of a modified DBA module with a split central quadrupole and a sextupole installed in between.

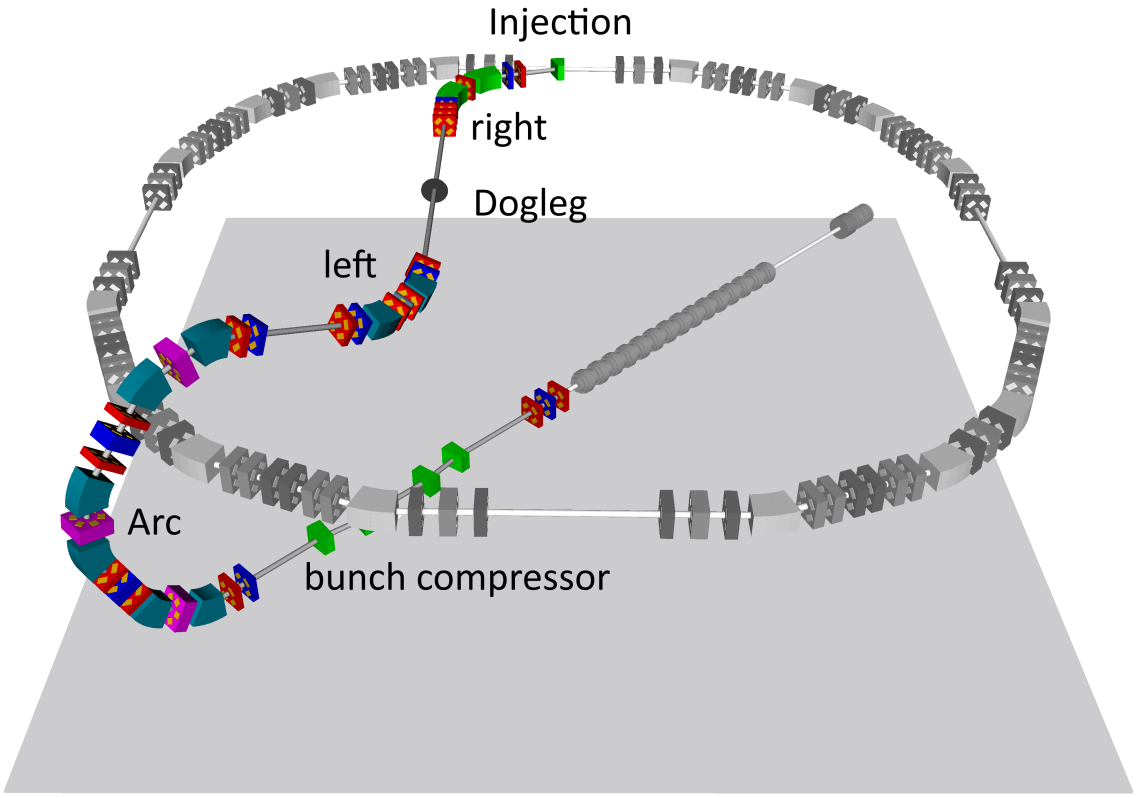

Figure 7.1.: Transfer line in Layout B. The elements included in the simulations are colored. Shown are horizontal/vertical focusing quadrupoles (red/blue), horizontal/vertical deflecting dipoles (green/turquoise) and combined function magnets with quadrupole and sextupole components (pink).

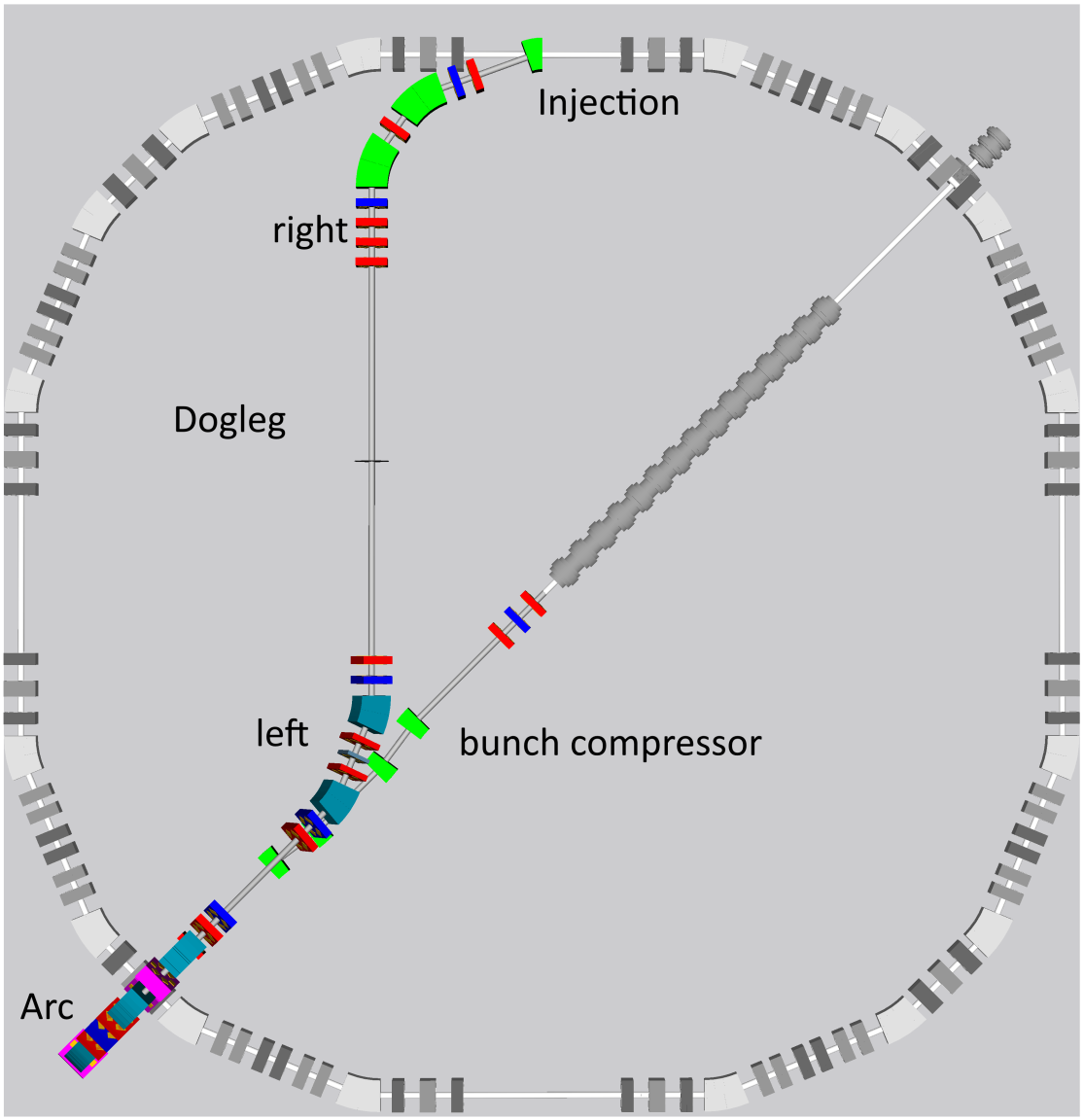

Figure 7.2.: Transfer line in Layout B from a top view.

Coming from the arc, the DLL module starts with a falling slope of 20°. Its deflection plane is rotated clockwise by 17.8° and the deflection angle is chosen such that after the DLL module the transfer line joins the horizontal plane of cSTART and is parallel to the wall of the experimental hall. The final DLR part is made by a common DBA module with an additional quadrupole doublet in front, which will be useful for matching the transverse optics to cSTART. Right after the DLR part, the beam reaches the horizontal injection section. In this layout, the injection is realized as a sector dipole representing the septum magnet with a small horizontal focusing component. A choice of parameters defining the geometry of each module is listed in Tab. 7.1, the full *elegant* input for the lattice definition can be found in appendix A.2.

Although the transfer line joins the horizontal plane of cSTART after the rotated DLL part, the local coordinate system of the bunch is not aligned with the cSTART coordinate system. In order to align the tilted coordinate system of the bunch to the horizontal coordinate system of cSTART, a second rotation of $-25.8°$ is required. The rotation is executed in between the DLL and DLR part. In the 3-D images the rotation point is represented as a black disc. An illustration of the evolution of the coordinate system along the transfer line

Table 7.1.: A selection of element parameters used in Layout B.

Arc	Deflection	33.3°
	Radius	0.75 m
DLL	Deflection	24.0°
	Radius	1 m
	Rotation	17.8°
DLR	Deflection	35.0°
	Radius	1 m
Injection	Deflection	20.0°
	Radius	0.57 m
	Focusing strength	$10\,\mathrm{m}^{-1}$

can be found in Fig. 7.3. In addition, the DLL part introduces transverse coupling, this will be discussed in more detail in the section about transverse optics. Like in the previous chapter, the simulations for this transfer line starts in front of the FLUTE quadrupole triplet. This position is located 8.5 m after the FLUTE electron gun and will be referenced as the starting point with $S = 0$ for all simulations.

7.1. Transverse optics

In the context of this thesis, the priority of the linear optics design lies in fulfilling the linear full compression condition. This defines the settings for all elements in dispersive parts of the transfer line. The remaining degrees of freedom are used to control the transverse optics, which is the subject of this section. The optics shown and discussed describe the so called reference optics, which solve the first and second order full compression condition.

Because of the rotated deflection plane in the DLL part, the horizontal and vertical planes are coupled with each other and an comprehensive calculation of the Twiss parameters for the whole transfer line is not possible. As already mentioned, *elegant* is not able to calculate coupled Twiss parameter in a non-periodic lattice. Tracking on the other hand can be calculated with rotated sections without a loss in precision. Therefore after each rotation, the Twiss parameters used in *elegant* start from values extracted from a particle ensemble which where tracked, rotated and analyzed.

Starting point → 1th rotation point: The first rotation is located between the arc and the DLL part. Up to this position the Twiss parameters can be calculated as an evolution from the initial parameters. A plot including both, the beta and dispersion functions for both planes in this first part is shown in Fig. 7.4. The FLUTE quadrupole triplet focuses the beta functions at the start of the arc section, taking into account the strong vertical focusing effect of the rectangular dipoles in the bunch compressor. As negative dispersion optics will be required in the HBA for fulfilling the full compression condition, the quadrupoles within the dispersive part of the HBA module cannot be altered without affecting the longitudinal dynamics. Details will be discussed later. The parameters of the first and last quadrupole doublet of the arc remain as open degrees of freedom. These are set to make the beta functions evolve symmetrically in the HBA module.

It was found that the sextupole components implemented in the center of the DBA cells perform well, if the transverse beam size at their position is small. As the transverse beam size is very small at the center of the DBA cells, the beam is strongly divergent because of the conservation of the phase ellipse's area. As a consequence, the beam diverges and the

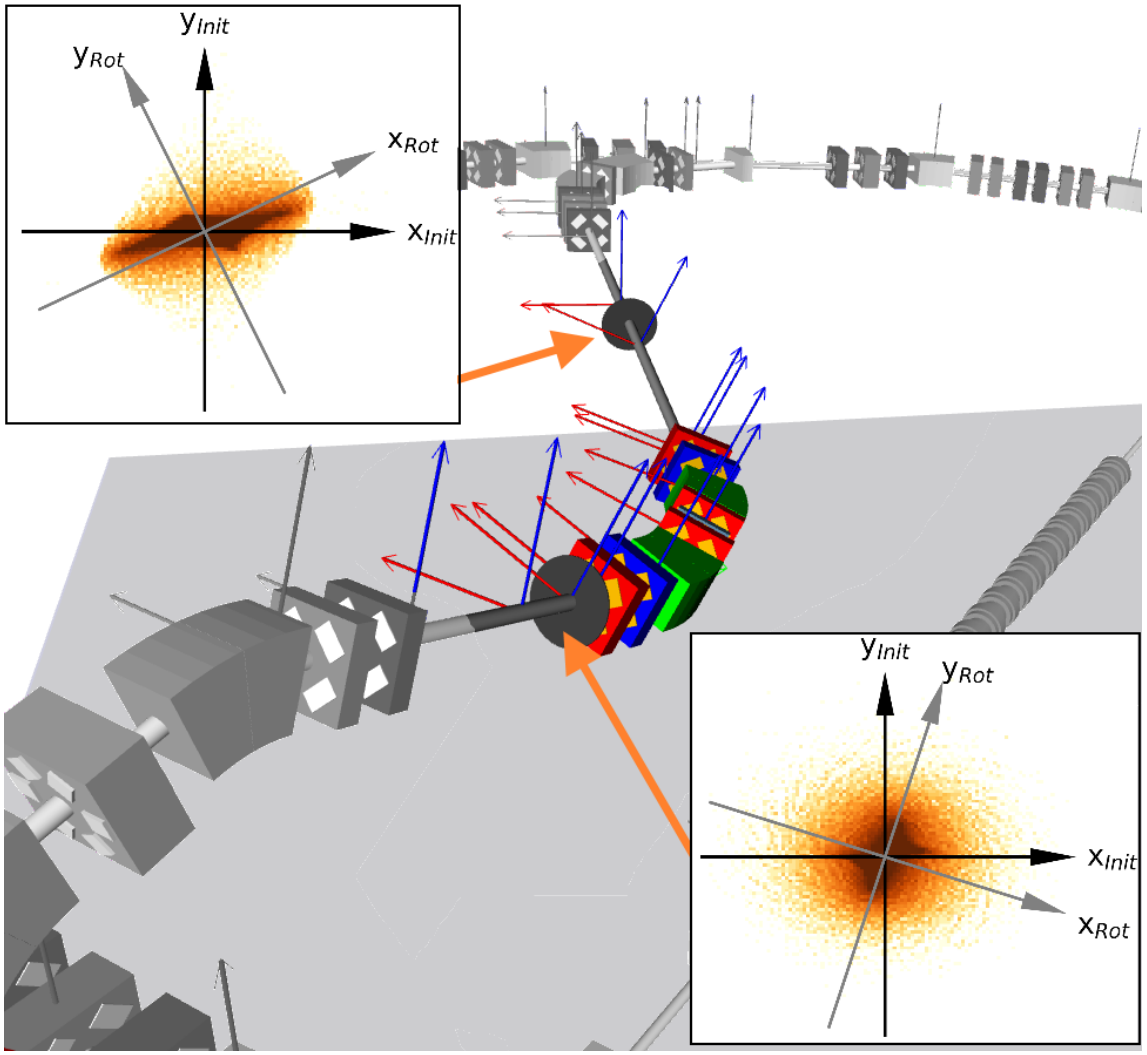

Figure 7.3.: Transfer line in Layout B with view on the dogleg section. Before and after the DLL part, the bunch has to be rotated in order to calculate the transverse Twiss parameters. The rotation points are visualized with black discs in the lattice. For both rotation points, the transverse plane of the bunch is shown with the (local) initial and the rotated coordinate system. Between the arc and the DLL part, the coordinate system of the bunch is rotated clockwise by 17.8° for the first time. In the middle of the five meter long drift between the DLL and DLR part, the coordinate system of the bunch is rotated counter clockwise by 25.8° into horizontal alignment.

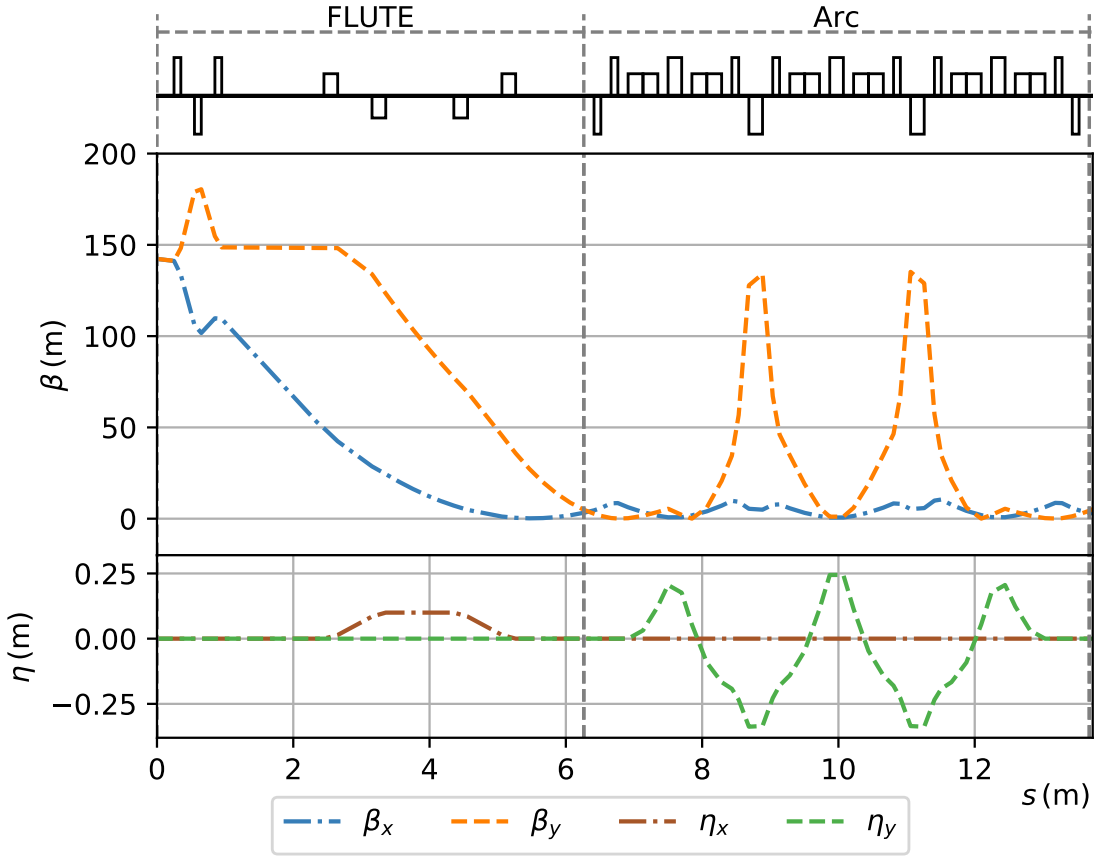

Figure 7.4.: Linear optics for Layout B from the starting point to the first rotation point. The beta functions are shown in the top plot and the dispersion function in the bottom plot. Above the optics functions, the lattice is visualized with quadrupoles (and CFM) as tall and dipoles as flat squares.

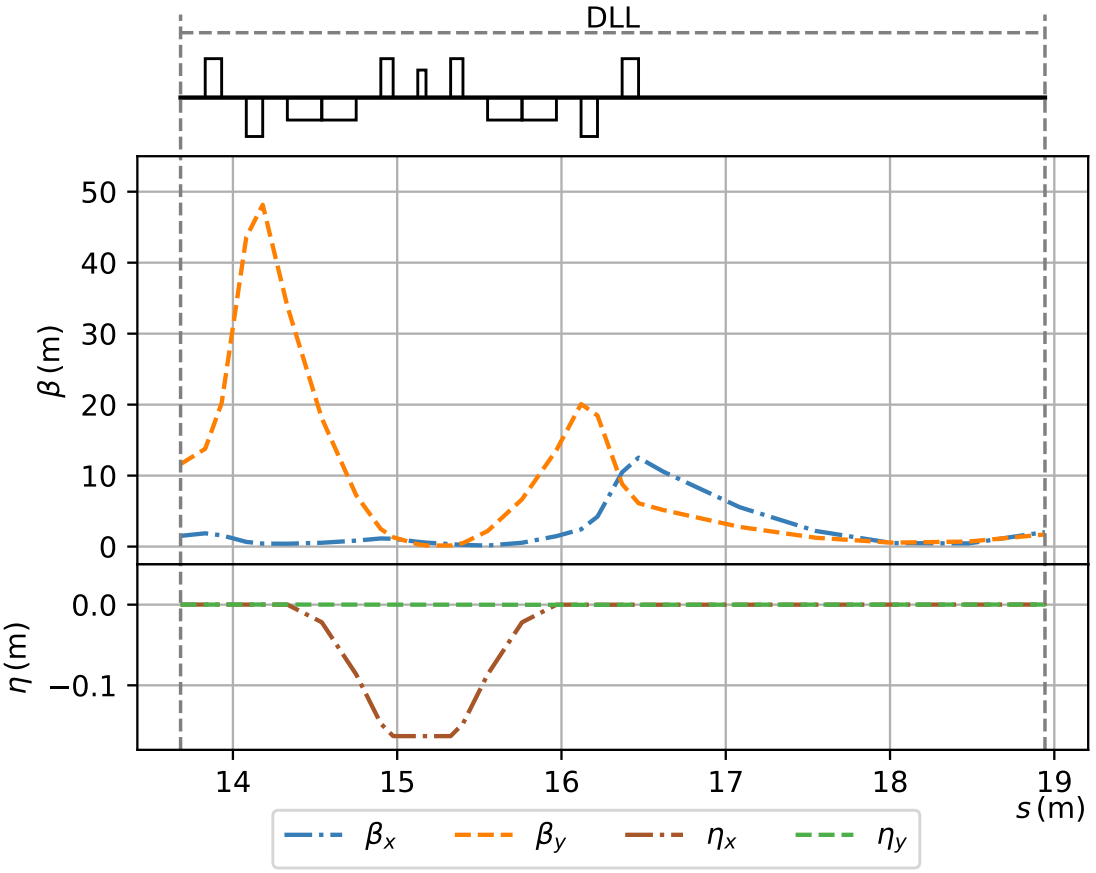

Figure 7.5.: Linear optics for Layout B from the first rotation point to the second rotation point. See Fig. 7.4 for plot description, mind the different axis scaling.

beta functions grow rapidly in between the DBA cells. After the arc, the beam is focused and passes over to the DLL part.

1th rotation point → 2nd rotation point: In front of the DLL part, the coordinate system is rotated by 17.8° as seen in Fig. 7.3. With the coordinate system aligned with the deflection plane, the section's transverse planes are uncoupled for the linear optics. The tracked bunch was rotated and analyzed at this position, this provides the Twiss parameters which then are propagated through the DLL part. A plot of their evolution can be found in Fig. 7.5. The section is made of a modified DBA module including a sextupole in between a quadrupole doublet instead of a single quadrupole in its center. The outer quadrupoles are set in order to focus the beam in the transverse planes to the middle of the five meter long drift space which connects the DLL and DLR part.

2nd rotation point → cSTART: This second rotation is executed in the middle of the five meters drift. As a consequence of this second rotation, the new transfer line coordinate system has its horizontal axis aligned in the horizontal plane of the experimental hall. Therefore the coordinate system of the transfer line equals the coordinate system of cSTART after the injection. The Twiss parameters for this section are again extracted from the tracked and rotated particle ensemble. The Twiss parameters are propagated through the DLR part, the injection dipole and also through the first cell of cSTART, their evolutions are plotted in Fig. 7.6. The DLR part is made of a common DBA module but will not be operated in DBA optics. Instead, the achromaticity criterion has to be fulfilled including the injection dipole. Therefore, they are considered as a single section which will be referenced as „DLR+Inj“. The dispersion can be found in the lower half of

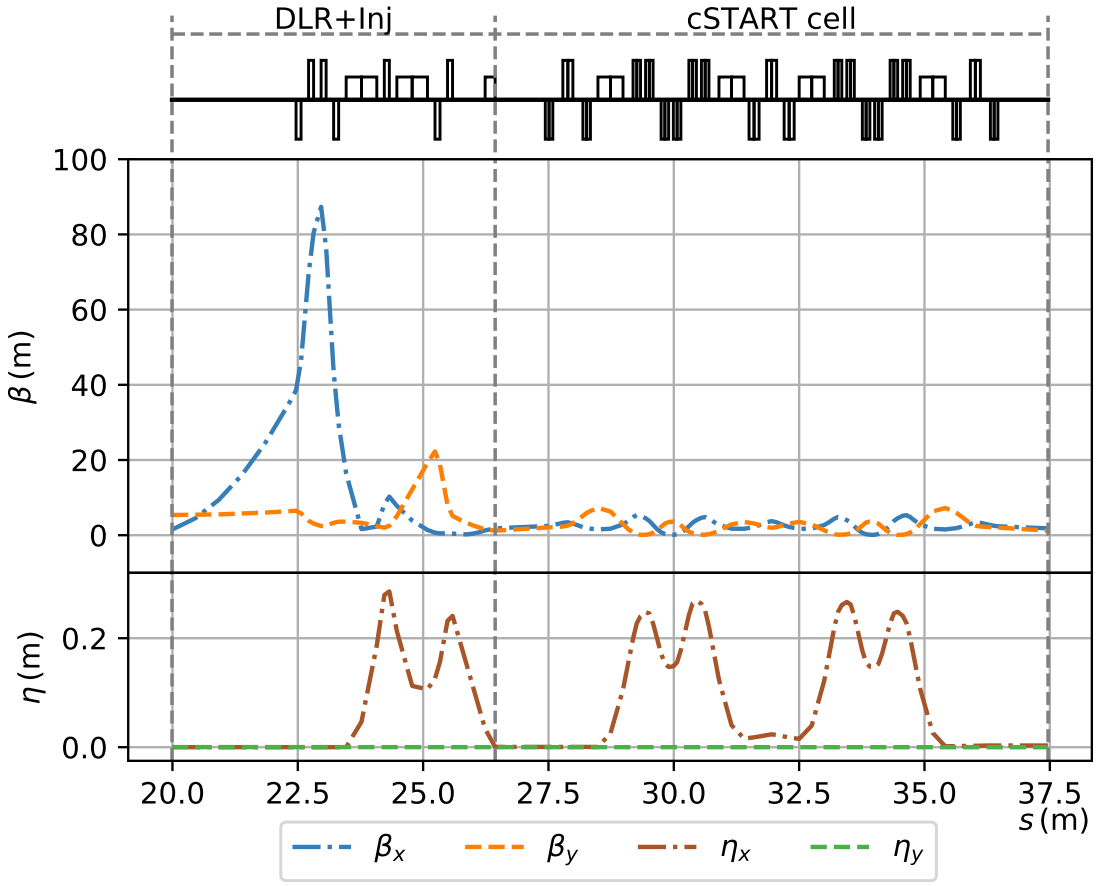

Figure 7.6.: Linear optics for Layout B from the second rotation point to the end of the first cell of cSTART. See Fig. 7.4 for plot description.

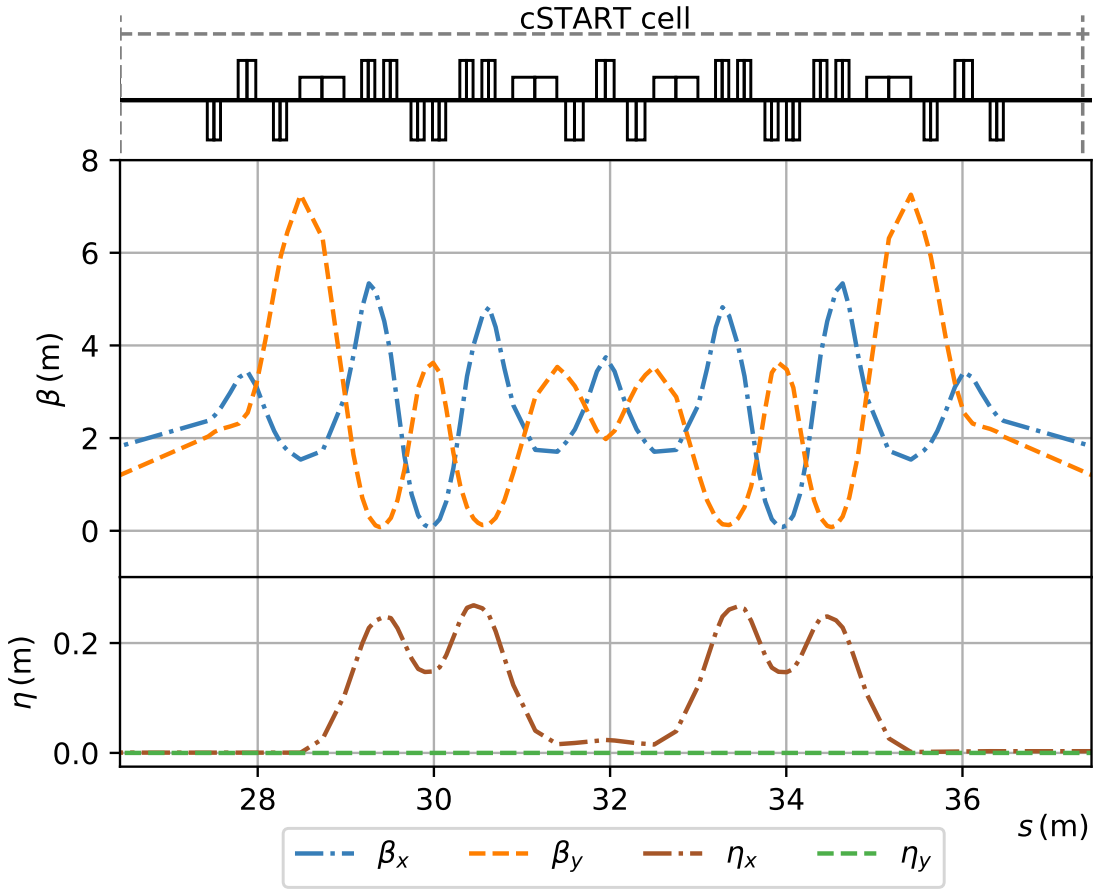

Figure 7.7.: Linear optics from the transfer line at the injection point propagated through the first cell of cSTART. See Fig. 7.4 for plot description.

Fig. 7.6, details will be discussed later. However, the quadrupoles within the dispersive part are required to fulfill the achromaticity criterion and cannot be used for matching the transverse beam parameters. The dispersive part of the DLR+Inj section still affects the transverse plane. It appears to have a small influence on the vertical beam size but a strong focusing effect on the horizontal beam size. In order to match the transverse beam parameters to cSTART, the horizontal beta function in front of the dispersive part has to be much larger than the vertical beta function. This is achieved by the quadrupole quartet in front of the DBA module. In principle, the matching of four parameters ($\beta_{x,y}$, $\alpha_{x,y}$) requires four degrees of freedom, therefore a quadrupole quartet was installed. Apparently, for these set of optics a quadrupole triplet would be sufficient as the two quadrupoles are both set to be horizontal focusing elements. The transverse beam parameters at the injection point are compared to the required values of cSTART in Tab. 7.2. For better readability, the optics within the cSTART cell are plotted a second time in Fig. 7.7.

This Layout B in the presented reference optics matches the transverse linear optics parameters to the periodic solution of the cSTART optics with only small deviations.

7.2. Longitudinal optics

The reference optics, discussed in the last section already fulfills the first order full compression condition. This section discusses in more detail, how the elements within the dispersive parts were set in this optics in order to achieve this goal.

Table 7.2.: Comparison of transverse optics parameters at the injection point between the required and achieved values.

Optics parameter		value	required value	achieved value
Beta function	(horizontal)	β_x (m)	1.8	1.83
	(vertical)	β_y (m)	1.2	1.20
Alpha function	(horizontal)	α_x	0	4×10^{-7}
	(vertical)	α_y	0	4×10^{-7}
Dispersion function	(horizontal)	η_x (m)	1.8×10^{-3}	5.3×10^{-4}
	(vertical)	η_y (m)	0	6.2×10^{-6}
Dispersion derivative	(horizontal)	η'_x	0	1×10^{-4}
	(vertical)	η'_y	0	-7×10^{-5}

FLUTE bunch compressor: As discussed in chapter 5, the FLUTE bunch compressor can provide a range of $R_{56\,\mathrm{BC}} \in [0\,\mathrm{cm}, -5\,\mathrm{cm}]$. In order to find a flexible solution of the transfer line optics, the R_{56} value is set at midrange to $-2.5\,\mathrm{cm}$, this is achieved with an deflection angle of 8°. This allows final adjustments of R_{56} in the range of $\pm 2.5\,\mathrm{cm}$.

Arc in DBA optics: The arc is made of a single HBA module, it is shown in Fig. 7.8 in a side view perspective. The central quadrupole of each DBA cell is realized as a combined function magnet and therefore prepared to include a sextupole component for later adjustments of T_{566}. In the 3-D model these combined function magnets are colored pink. The geometry of the HBA module leads to an R_{56} value of 14.5 cm for the DBA optics.

Dogleg left: The dogleg left part is made of a modified DBA module. With the achromaticity criterion fulfilled, it has a fixed R_{56} value of only defined by the geometry. The small deflection angles lead to a value of only $R_{56,\,\mathrm{DLL}} = 2.4\,\mathrm{cm}$. The deflection plane of the module is rotated by 17.9° from the horizontal plane, its dispersion function plotted in a coordinate system parallel to its deflection plane can be found in Fig. 7.5 in the bottom subplot. The built-in sextupole will later be used as a fine-tuning knob for the T_{566} value of the module, but it will not be considered for fulfilling the second order full compression condition in the first place. Instead it will remain an open degree of freedom for subsequent adjustments as like the bunch compressor for the first order.

Dogleg right and Injection: As already discussed, the DLR and Injection part act together as one single achromatic section. To achieve these optics, the DBA's central quadrupole is set to a lower strength than the common DBA optics would require. Then the second DBA dipole does not decrease the dispersion to zero and a finite dispersion propagates through the subsequent quadrupole doublet to the injection dipole. The dispersion after the final DBA dipole can be modified by the qudrupole doublet, such that the dispersion vanishes after the injection dipole and the whole module becomes achromatic. The integral of the dispersion function depends on the strength of the central DBA quadrupole. An optimization function found the values for this quadrupole strength that minimizes the dispersion integral for the DLR+Inj section while staying achromatic. It was found that an additional horizontal focusing component in the injection dipole and in the DBA's dipoles changes the optics such that the integrated dispersion function can be further reduced. Keeping in mind that the transverse optics are affected by the additional quadrupole component, these values are kept small. The quadrupole components $K_{1,\mathrm{DLR}} = -1\,\mathrm{m}^{-1}$ and $K_{1,\mathrm{Inj}} = +10\,\mathrm{m}^{-1}$ were found to be a good compromise between a low transverse influence and the reduction of the dispersion integral. With these qudarupole

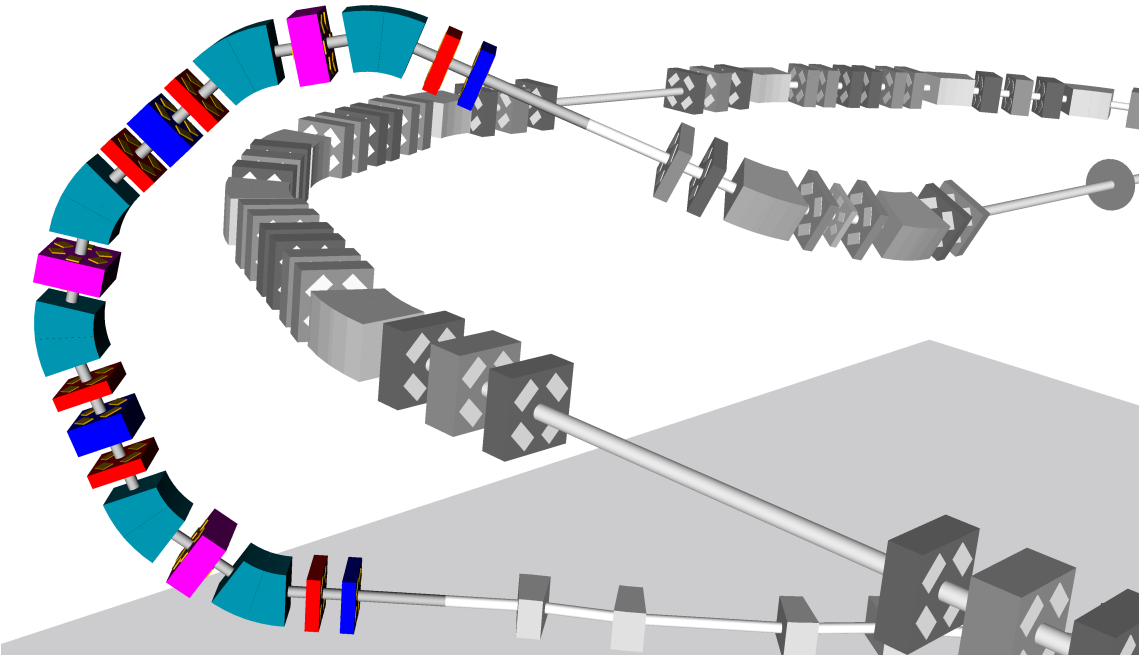

Figure 7.8.: Side view of the arc section made of an HBA module. The central quadrupoles of each DBA cell (pink) are considered as combined function magnets, including an additional sextupole component.

Table 7.3.: R_{56} and T_{566} for DBA optics in Layout B.

Section	R_{56}(DBA)	T_{566}(DBA)
BC	−2.5 cm	3.8 cm
Arc	14.5 cm	87.5 cm
DLL	2.4 cm	15.5 cm
DLR + Inj	12.0 cm	50.2 cm
Sum	26.5 cm	156.9 cm

components the sections R_{56} value results in 12 cm.

The R_{56} values for all modules are listed in the first column in Tab. 7.3. Since the HBA module was discussed in DBA optics so far, the table column is labeled as R_{56}(DBA) and the sum of R_{56} over all modules is positive. The corresponding T_{566} values for each module is listed in the second column of the same table. Without sextupole components, all modules have a positive T_{566} parameter. The arc is required to operate in negative dispersion optics to fulfill the first order full compression condition.

Negative dispersion optics: In order to find the optics which provide exactly the desired R_{56} value, multiple negative dispersion optics were simulated and analyzed. Starting from the DBA optics, the strength of the central quadrupoles in the DBA cells was increased step wise by 5%. For each step, the two quadrupole triplets in between the cells were readjusted to sustain the achromaticity criterion for the HBA module. The dispersion function for every second step is shown in Fig. 7.9.

For each simulated negative dispersion optics, the R_{56} value is calculated and plotted versus the change of the central quadrupoles, their correlation were found to be linear for the observed range. The corresponding data and the fit function are shown in Fig. 7.10. With

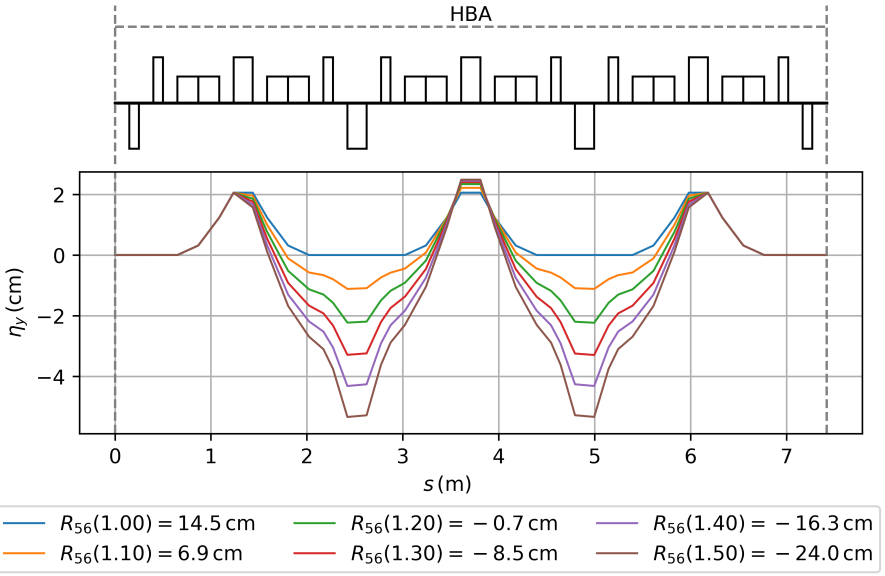

Figure 7.9.: Dispersion function in the HBA module while increasing the central quadrupole strengths step wise by 10% starting from the DBA optics.

this relation the optics in the HBA can be set to a precise R_{56} value as desired. Evaluating the full compression condition for Layout B and isolating the term of the arc section allows to find the R_{56} value of the negative dispersion optics required for full compression.

$$R_{56,\,\mathrm{HBA}}(-\eta) \stackrel{!}{=} -\left[R_{56,\,\mathrm{BC}} + R_{56,\,\mathrm{DLL}} + R_{56,\,\mathrm{DLR+Inj}}\right] - h_{\mathrm{Init}}^{-1} \tag{7.1}$$

The numerical value still requires the choice of the initial chirp of the bunch. The target values for both the PIC and NIC bunches are indicated by the gray lines in Fig. 7.10.

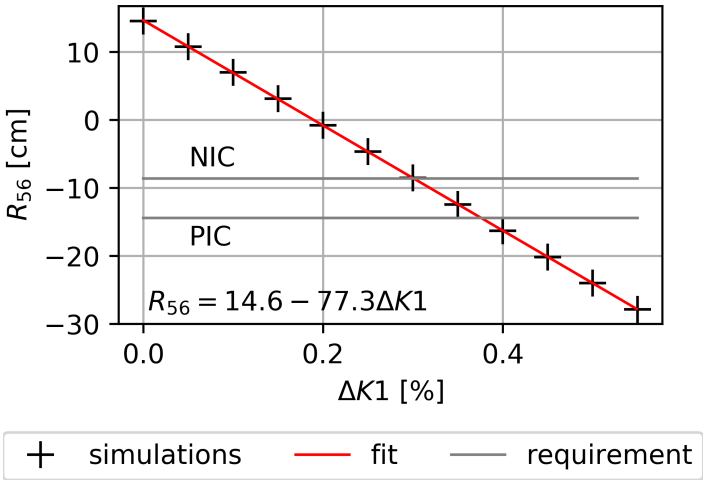

Figure 7.10.: R_{56} value of the HBA module for changing the central quadrupole strengths by ΔK_1 from the value required in DBA optics. The data are fitted by a linear function. The requirement to fulfill the full compression conditions for a PIC or a NIC bunch are inlcuded as gray horizontal lines.

Table 7.4.: R_{56} and T_{566} values of the transfer line in negative dispersion optics for a NIC bunch.

Section	$R_{56}(-\eta)$	$T_{566}(-\eta)$
BC	−2.5 cm	3.8 cm
Arc	−8.6 cm	269.3 cm
DLL	2.4 cm	15.5 cm
DLR + Inj	12.0 cm	50.2 cm
Sum	3.3 cm	338.7 cm

Choice of chirp: In principle both a NIC and a PIC bunch can be transported through the transfer line. The difference in the full compression condition can be compensated for both modes with the HBA module. Yet, the NIC bunch is more beneficial than the PIC bunch because of two effects:

1. From Eq. (7.1) immediately follows that transporting a PIC bunch would require the HBA to have a higher, negative, R_{56} value than for transporting a NIC bunch. A more negative R_{56} value is achieved with higher quadrupole fields, which implies higher non-linear effects and a higher dispersion function which results in a larger transverse beam size.

2. The DLL and the DLR+Inj part have a positive R_{56} value and shear the bunch clockwise into full compression. As a consequence, the arc needs to shear the particle distribution in the longitudinal phase space such that the resulting chirp is negative, independent on the initial bunch. This means that the PIC bunch will change from a positively chirped to a negatively chirped bunch during the transport. This might lead to an ultra-short bunch within the arc, which might emit intense coherent synchrotron radiation. In order to avoid such possible CSR outbursts, a NIC bunch should be chosen. The evolution of the longitudinal phase space for both a PIC and NIC bunch along the transfer line is shown in Fig. 7.11.

With the choice of the NIC bunch, the arc is required to result in in $R_{56,\,\mathrm{Arc}}(-\eta) = -8.6\,\mathrm{cm}$ The resulting values for all modules can be found in Tab. 7.4, labeled as $R_{56}(-\eta)$. The sum of all R_{56} contributions differs from the expected value for a NIC bunch $h_{\mathrm{NIC}}^{-1} = 2.9\,\mathrm{cm}$ on purpose. The difference compensates the time-of-flight effects discussed below.

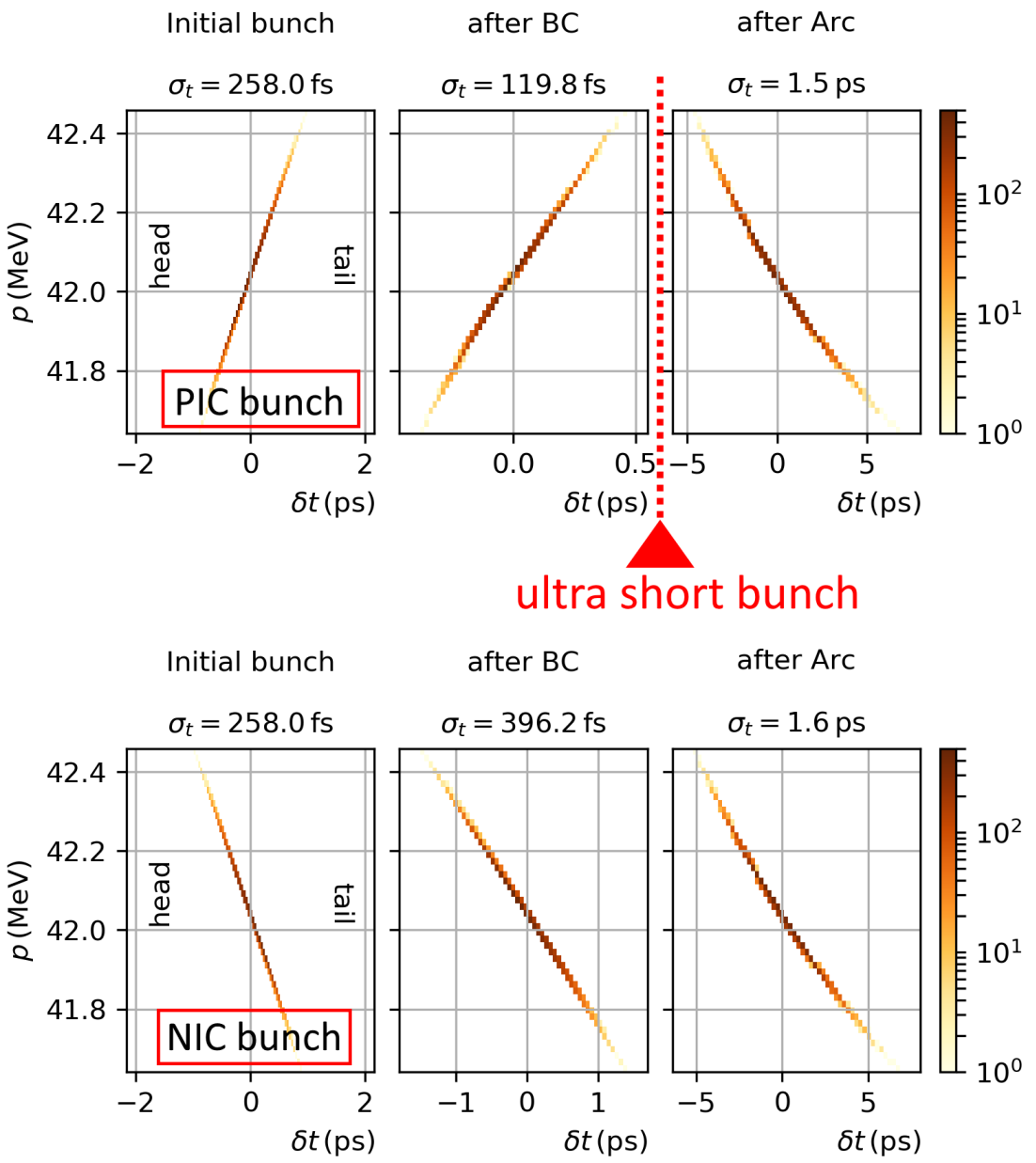

Figure 7.11.: Evolution of the bunch while tracking through the first half of the transfer line. The top row shows a PIC bunch, the bottom row a NIC bunch. The arc changes the sign of the chirp for the PIC from positive to negative. This can lead to an ultra-short bunch within the arc.

Time-of-flight effects: The transfer line in Layout B has a total length of $S = 26.4\,\mathrm{m}$, measured from the starting point to the injection point. At an energy of 41.5 MeV, non-relativistic time-of-flight effects are visible. A higher energetic particle passes the transfer line in a shorter time than a lower energetic particle and therefore moves towards the head of the bunch during the transport. This results in a shearing of the longitudinal phase space, which can be expressed as an additional term of $R_{56,\,\mathrm{ToF}}(S)$ which is proportional to the length S of the transfer line. The effect can be calculated with

$$R_{56,\,\mathrm{ToF}}(S) = \frac{\Delta z}{\delta_p} = \frac{s_- - s_+}{\delta_p} \tag{7.2}$$

where $s_\pm$ are the path lengths for two particles with a momentum offset of $\pm\delta_p$. Considering exclusively the time-of-flight effect, each particle travels along the same orbit with the

Table 7.5.: Values to calculate ToF

S	26.4 m
δ_p	0.2%
$v(p_+)$	$(1 - 7.35 \times 10^{-5}) \times c$
$v(p_0)$	$(1 - 7.39 \times 10^{-5}) \times c$
$v(p_-)$	$(1 - 7.43 \times 10^{-5}) \times c$
$R_{56,\,\mathrm{ToF}}(26.4\,\mathrm{m})$	-0.4 cm

same length S. Yet they require different times for the same path. Therefore Δz can be understood as the longitudinal offset for the off-momentum particles, derived from the differences in their velocity while traveling a given time. The time t_0 the reference particle needs to pass S is given by

$$t_0 = \frac{S}{v(p_0)}. \tag{7.3}$$

The velocity is lower than the speed of light and can be calculated from the particle momentum. The momentum dependent velocity can be calculated by Eq. (2.2) to Eq. (2.4). In this time t_0, the off-momentum particles pass the distances $s_\pm$ depending on their individual velocity.

$$s_\pm = t_0 v(p_\pm) = S\frac{v(p_\pm)}{v(p_0)} \tag{7.4}$$

Then R_{56} can be calculated with the following equation.

$$R_{56,\,\mathrm{ToF}}(S) = \frac{S}{\delta_p}\frac{v(p_-) - v(p_+)}{v(p_0)} \tag{7.5}$$

The numerical values evaluated for the FLUTE bunch are listed in Tab. 7.5 together with the resulting R_{56} parameter for the transfer line of Layout B. The contribution of the time-of-flight effects are added to the sum of all R_{56} values for the transfer line in Tab. 7.4 and the full compression condition in first order is fulfilled.

Second order longitudinal optics: The natural T_{566} value of each section is positive and the full compression condition in second order is not fulfilled. Although the second order full compression condition for a NIC bunch demands a total value of T_{566} of 5 cm, the sum of the transfer line will be matched to zero in a first step, and optimized to the best value in a second step. The arc is required to have a T_{566} of -69.5 cm to bring the sum of all T_{566} values to zero. In order to reduce the T_{566} contribution of the arc section, a sextupole component is included into the central quadrupoles of each DBA cell of the HBA module. Their sextupole strengths were increased simultaneously in steps of $50\,\mathrm{m}^{-2}$ and the resulting T_{566} value of the module was calculated. The relation between the sextupole strengths and the T_{566} value was found to be linear, the simulated data and a linear fit function is plotted in Fig. 7.12. According to the linear fit, all three sextupole components needs to be set on a strength of $834\,\mathrm{m}^{-2}$ to meet the required value to fulfill the second order full compression condition, indicated by the horizontal line in Fig. 7.12. The resulting sum of T_{566} contributions of the transfer line equals zero as expected.

An additional optimization function was executed, which optimizes all three sextupole components individually for a minimum bunch length. The resulting sextupole strenghts are $K_2 = 1063\,\mathrm{m}^{-2}$ for the combined function magnet in the first cell, $K_2 = 751\,\mathrm{m}^{-2}$ in the

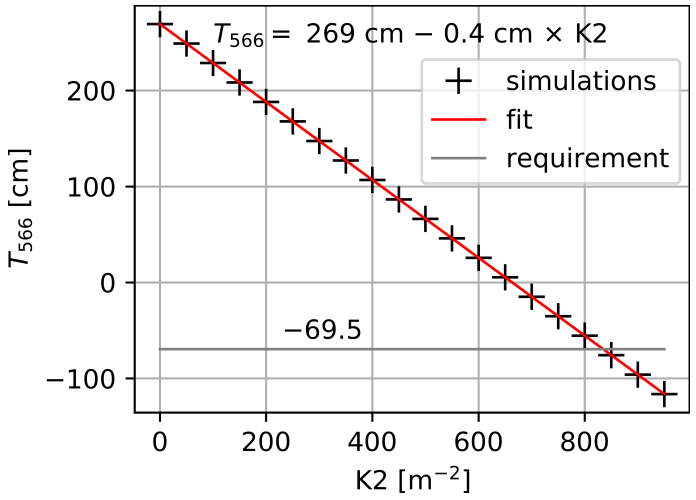

Figure 7.12.: T_{566} values of the HBA for increasing the sextupole components in all three central quadrupoles simultaneously including a linear fit through the data. If the arc is set to have a T_{566} value as indicated by the gray horizontal line, the full compression condition in second order is fulfilled.

Table 7.6.: Sextupole strengths and T_{566} values of the arc and the transfer line for both, the linear fith method and the optimization method.

	Linear fit optics	Optimized optics
K_2 in cell 1	835 m^{-2}	1062.5 m^{-2}
K_2 in cell 2	835 m^{-2}	751.4 m^{-2}
K_2 in cell 3	835 m^{-2}	940.3 m^{-2}
Average K_2	835 m^{-2}	918 m^{-2}
$T_{566,\,\mathrm{HBA}}$	−69.5 cm	−85.4 cm
$T_{566,\,\mathrm{TL}}$	0 cm	−15.9 cm

second and $K_2 = 940\,\mathrm{m}^{-2}$ in the third cell. This leads to a higher negative T_{566} value of −85.4 cm and as a consequence to a negative sum of T_{566} for the transfer line of −15.9 cm. This differs from the expected value of 4.9 cm. Also the optics in Layout A were optimized to a comparable T_{566} value, the reason for this difference to the full compression condition was not investigated in this thesis. One possible reason is that this difference optimizes the bunch length by compensating third order effects. As already mentioned in the discussion about Layout A, an offset in the order of 10 cm in the second order is negligibly small.

The optics resulting from the sextupole strengths set according to the linear fit function will be referenced as linear fit optics, while the optimization function delivered the optimized optics. The sextupole strengths in both optics and the resulting T_{566} values can be compared in Tab. 7.6.

7.3. Tracking

The longitudinal optics were developed by four steps starting from the DBA optics.
(a) DBA optics: Guides the bunches to the injection point.
(b) Negative dispersion optics: Fulfills the first order full compression condition for a NIC bunch and the transverse plane is matched to perform a periodic solution in cSTART.
(c) Linear fit optics: Fulfills the second order full compression condition exactly.
(d) Optimized optics: Fine tunes the second order longitudinal optics.

Table 7.7.: R_{56} and T_{566} of the transfer line for different optics including all sections contributions and also ToF effects.

Optics	$R_{56,\,\mathrm{TL}}$	$T_{566,\,\mathrm{TL}}$
DBA optics	26.1 cm	156.9 cm
Negative dispersion optics	2.9 cm	338.7 cm
Linear fit optics	2.9 cm	0 cm
Optimized optics	2.9 cm	−15.9 cm

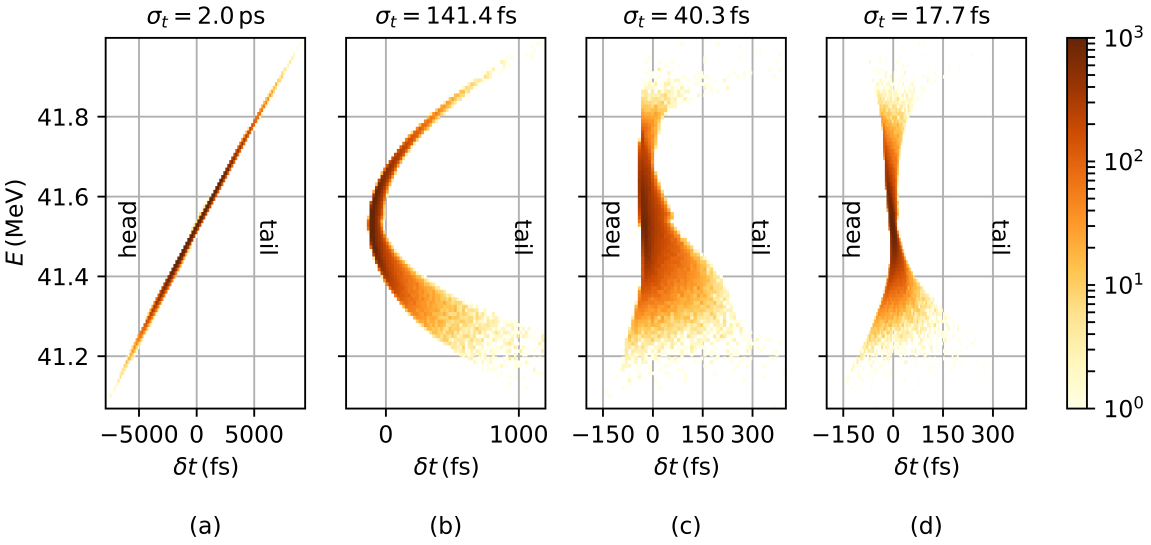

Figure 7.13.: Longitudinal phase space of the NIC bunch after tracking to the injection point in DBA optics (a), negative dispersion optics (b), linear fit optics (c) and optimized optics (d).

For each step the sum of R_{56} and T_{566} values are compared in Tab. 7.7. A tracking simulation was executed for each optics with a NIC bunch, the final bunch shown in the longitudinal phase space is plotted in Fig. 7.13. The simulations includes 100.000 particles, tracked from the starting point over 26.4 m all the way up to the injection point in cSTART. In the DBA optics (a) the first order effects are dominant, the final distribution is linear and chirped in the longitudinal phase space. After correcting the first order with the negative dispersion optics (b) the linear effects are corrected and the bunch is aligned vertically. With a vanishing inverse chirp, the second order effects become dominant and the remaining curvature of the distribution becomes visible. The fulfilling of the second order compression condition with the linear fit methode (c) reduces the curvature and the bunch length is compressed to only 40 fs. The bunch length is dominated by the longitudinal spread of the bunch. Finally the optimization function (d) found settings in the HBA sextupole components which result in less longitudinal spread and the bunch length is further reduced to only 17.7 fs.

The optimized optics shown in (d) are tracked again, including radiation effects for a charge of 1 pC. The results are shown in Fig. 7.14, with synchrotron radiation and incoherent synchrotron radiation considered in run (a), coherent synchrotron radiation in run (b) and all three effects combined in run (c). The three radiation types were discussed in chapter 3.3. As expected, synchrotron radiation and incoherent synchrotron radiation do not have a significant effect with the bunch energy of 41.5 MeV. Coherent synchrotron radiation

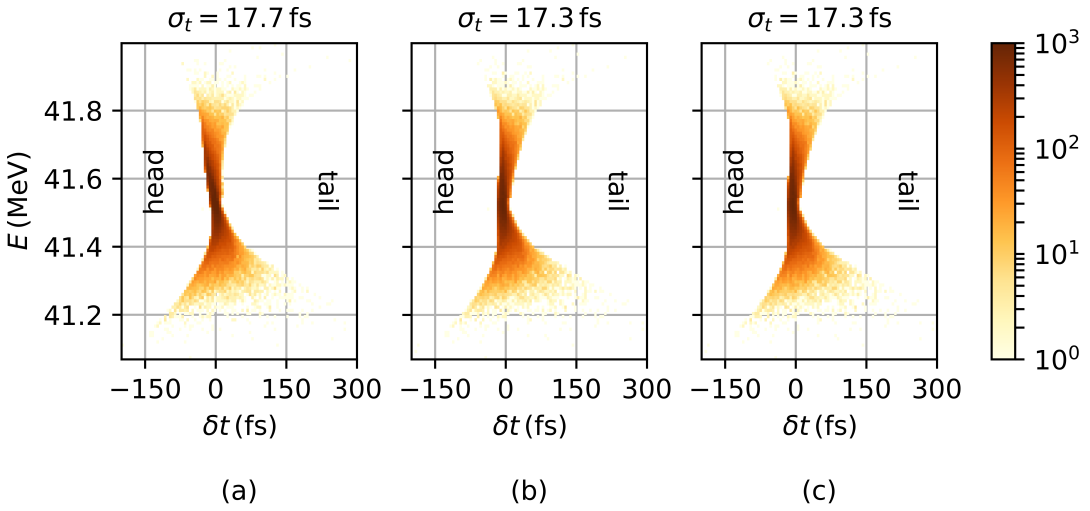

Figure 7.14.: The NIC bunch at the injection point shown in the longitudinal phase space after tracking through the optimized optics including SR und ISR effects (a), CSR effects (b) and all three radiation types (c).

does have a very small but visible effect. Particles with an energy higher than the reference energy appear to fall back in the bunch while particles with a lower energy seems to slip to the head of the bunch. This leads to a slightly shorter bunch of 17.3 fs. The reason for the low impact of coherent synchrotron radiation can be found in the evolution of the bunch length across the transfer line plotted in Fig. 7.15. The data shown is derived from the tracking run resulting in Fig. 7.14 subfigure (c), which already includes all radiation effects. The longitudinal phase space of the NIC bunch is sheared counter clockwise in the bunch compressor and the arc, which enlarges the bunch length. An exception are the three reductions of the bunch length within the arc, coming from the dipoles which are located in regions of positive dispersion. The dogleg parts then shear the phase space clockwise and therefore reduces the bunch length until the injection dipole performs the final compression to an ultra-short bunch. Since the final compression happens at the very end in the injection dipole, no significant amount of coherent synchrotron light is radiated in the transfer line.

The transverse optics were derived using two rotations with $+17.8°$ and $-25.8°$ of the coordinate system in order to describe the optics in a decoupled plane section per section. The tracking simulation on the other hand is able to calculate the influence of rotated elements correctly. Therefore one total rotation with $-8°$ is executed in order to align the bunch's coordinate system to the coordinate system of cSTART. This single rotation is executed again in the middle of the dogleg. For the tracking simulation through the optimized optics, the transverse beam size are shown in Fig. 7.16. The transverse beam size again is a superposition of the beta function and the dispersion function. The step of the beta functions at $S = 20\,\mathrm{m}$ from the rotation is barely visible due to the small total rotation angle of $-8°$.

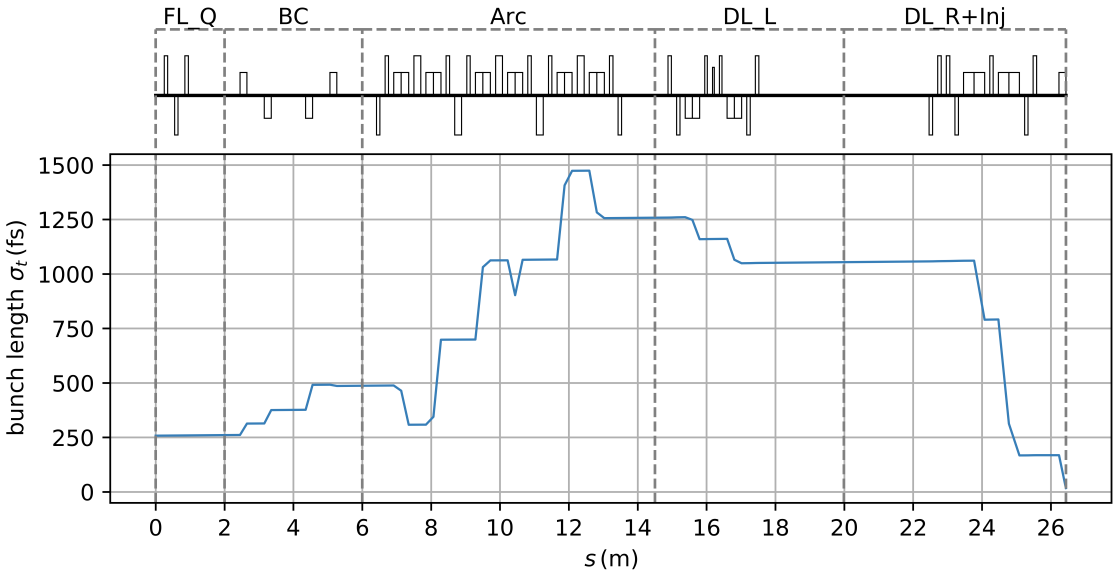

Figure 7.15.: Evolution of the bunch length of a NIC bunch with 100,000 particles tracked through the optimized optics including SR, ISR and CSR effects.

Longitudinal flexibility: The transfer line has two degrees of freedom left to fine-tune the longitudinal beam dynamics. This is the bunch compressor deflection angle which is set to 8° in the optimized optics. Its dipoles can be switched off, which leads to a deflection angle of 0°. This reduces the linear contribution of the bunch compressor to $R_{56,\,\mathrm{BC}}(0°) = 0\,\mathrm{cm}$ but also its second order contribution to zero. By increasing the deflection angle to its maximum of 11.3°, both values grow to $R_{56,\,\mathrm{BC}}(11.3°) = -5\,\mathrm{cm}$ and $T_{566,\,\mathrm{BC}}(11.3°) = 7.7\,\mathrm{cm}$. In both cases, the changes of the transverse optics can be compensated by the FLUTE quadrupole triplet.

The second degree of freedom is the sextupole in the DLL part. With its sextupole strength set to $K_2 = \pm 3000\,\mathrm{m}^{-2}$ it changes the T_{566} value of the section by $\Delta T_{566} = \pm 32\,\mathrm{cm}$. This sextupole strength is close to the maximum possible value calculated in the chapter 4.1.

The R_{56} and T_{566} values for both the bunch compressor and the sextupole set on their extreme values are listed in Tab. 7.8. A tracking study is executed for any combination of these extreme settings, the longitudinal plane of the final bunch for every setup is shown in Fig. 7.17. The left column shows tracking results with the bunch compressor set to a lower R_{56} value, the longitudinal phase space of the bunch in this column are sheared to the left. Accordingly the longitudinal phase space of the bunch in the column on the right side is sheared to the right. For the middle row the sextupole is switched off, while in the top (bottom) row the sextupole strength is set to the positive (negative) extreme value and therefore the top (bottom) particle distributions are curved to the right (left).

7.4. Conclusion

The transfer line in Layout B is 26.4 m long and injects into one of the two distant symmetry points of cSTART. Its geometry requires the DLL part to have a tilted deflection plane which couples the transverse beam dynamics. By rotating the coordinate system a first time, the horizontal plane of the bunch meets the deflection plane and the subsequent elements can be described without transverse coupling. A second rotation aligns the coordinate system of the bunch in parallel to the coordinate system of cSTART. This method allows to calculate the Twiss parameters all the way through the transfer line and even in the cSTART storage ring. An achromatic horizontal injection scheme was derived, which allows

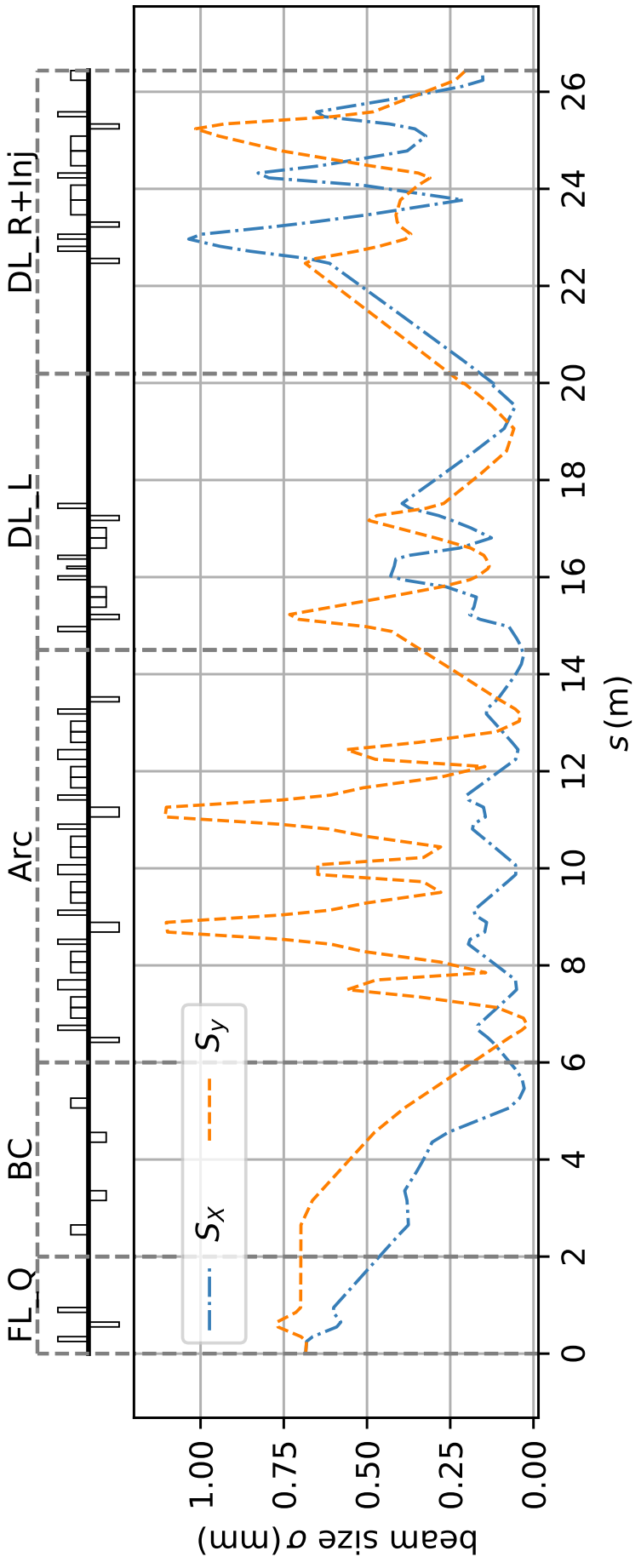

Figure 7.16.: Transverse beam size of the NIC bunch through the transfer line in Layout B, fulfilling both conditions for full compression. The data originate from tracking, including all three types of radiation.

Table 7.8.: R_{56} and T_{566} values of the bunch compressor and the DLL section while changing the degrees of freedom.

Section		R_{56}	T_{566}
Bunch compressor	0°	0 cm	0 cm
	8°	−2.5 cm	3.849 cm
	11.3°	−5.0 cm	7.7 cm
DLL sextupole	$-3000\,\mathrm{m}^{-2}$	−2.4 cm	−17.0 cm
	$0\,\mathrm{m}^{-2}$	−2.4 cm	15.5 cm
	$+3000\,\mathrm{m}^{-2}$	−2.4 cm	47.9 cm

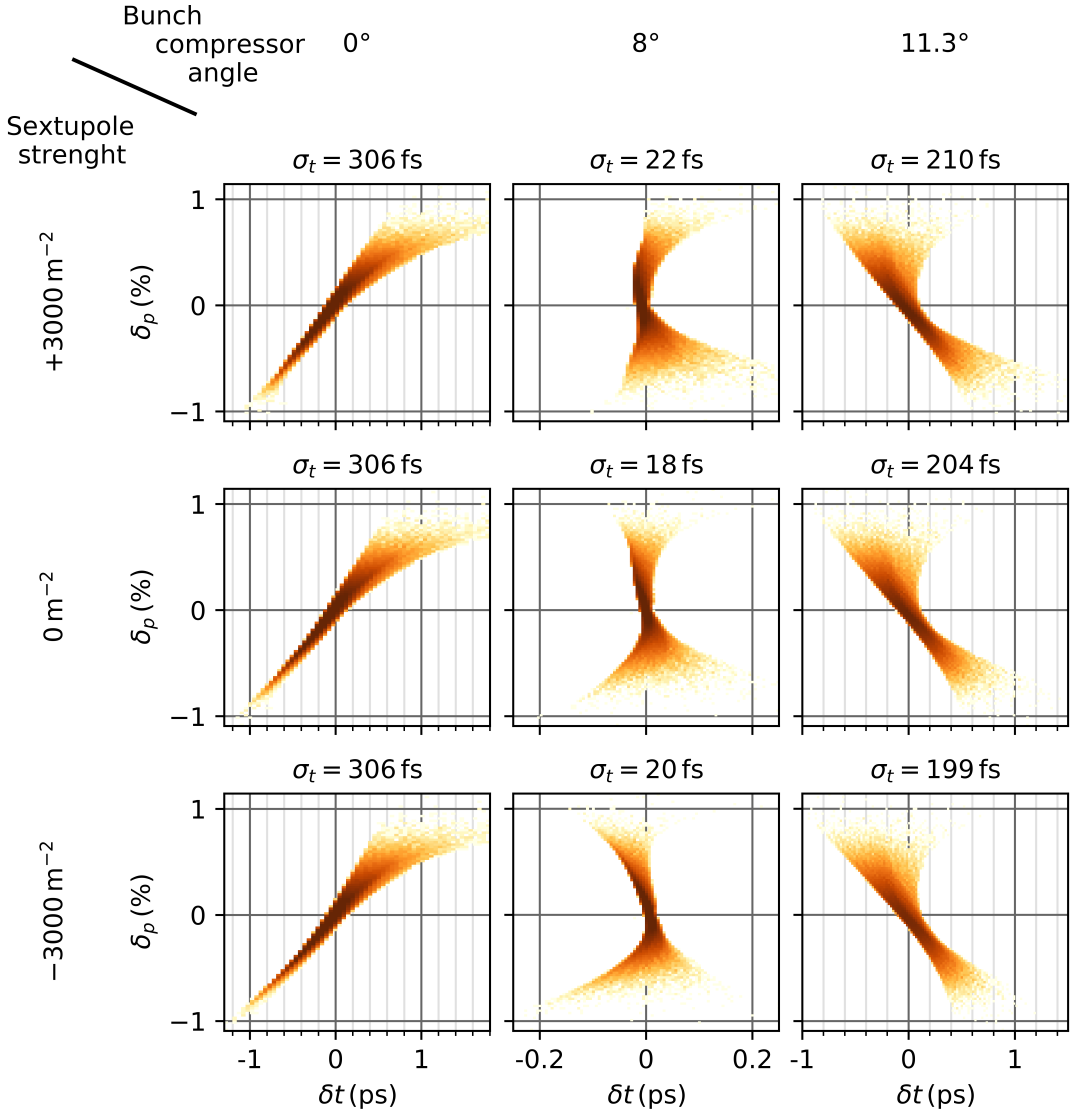

Figure 7.17.: Influence of the variation of the FLUTE bunch compressor deflection angle (columns) and the DLL sextupole (rows) on the final bunch at the injection point. The center plot shows the NIC bunch after tracking through the reference optics as a comparison. The influence of the sextupole is visible best for short bunches in the middle column. Mind the different time scales.

to match all transverse beam parameters at the injection point to the values required by cSTART. As a consequence the Twiss parameters perform a periodic solution within the first cell of cSTART.

The longitudinal optics of the transfer line fulfills the first order full compression condition with the HBA module set to negative dispersion optics. An additional sextupole component at the central quadrupoles of the HBA cells allows to reliably tune T_{566} such that the second order full compression condition is fulfilled as well. A final optimization of the sextupole components in the HBA module further improved the longitudinal optics towards the best compression performance. Tracking studies result in a bunch length of only 17.3 fs, including all radiation effects and edge effects to the second order. During all tracking simulations, not a single particle got lost by the aperture limitations of the vacuum chamber.

In addition, the FLUTE bunch compressor and the sextupole in the DLL part can be used to modify the longitudinal phase space distribution of the bunch at the injection point. The bunch compressor allows to shear the final longitudinal phase space at the injection point, while the FLUTE quadrupole triplet is used to sustain the periodic transverse solution for the cSTART cell while changing the bunch compressor angle. The DLL sextupole can be used for applying an additional warping of the final phase space.

8. Summary and Outlook

The cSTART project will investigate the evolution of ultra-short bunches in a storage ring. In addition to an LWFA, the test facility FLUTE serves as a full energy injector, providing ultra-short bunches with an energy of 42 MeV. In this thesis, a first design of the transfer line to transport the bunches from FLUTE to cSTART was developed. The main goal of the transfer line is to keep the bunches as short as possible at the injection point.

The limited space in the experimental hall and the spatial arrangement of FLUTE and cSTART requires the transfer line to deflect the particle beam multiple times in both transverse planes. Each deflection raises dispersion, which leads to different path lengths for particles with design energy and particles with energy offset. As a consequence, the longitudinal bunch profile changes and the conservation of the ultra-short bunch length is not possible. Therefore, the dispersive effects have to be utilized in such a way that the changes of the bunch profile results into an ultra-short bunch length at the injection point. Then FLUTE itself is not required to provide ultra-short bunches in the first place. This enables several degrees of freedom in FLUTE which were included into the simulations of the transfer line.

The change in path length for off-energy particles was investigated. It was shown that the influence of achromatic lattice modules on the longitudinal profile of a bunch can be calculated by only two parameters found in the module's transport matrices of first and second order. The R_{56} value of a module is proportional to the shearing of the bunch in the longitudinal phase space, while second order effects, represented by the modules T_{566} value, lead to a warping of the bunch in the longitudinal phase space. The bunch is accelerated off-crest by the FLUTE linac which introduces a chirp and a longitudinally correlated energy spread. In order to shear the chirped initial distribution into an upright position in the longitudinal phase space, one R_{56} value can be calculated. The transfer line is required to match this value in its total R_{56} parameter, this is called the first order full compression condition. Since the correlation between energy and longitudinal position of the initial bunch is linear, the transfer line is required to have a vanishing T_{566} value in order to prevent the bunch from growing a curvature in the longitudinal phase space, this is called the second order full compression condition. Two possible layouts of the transfer line were discussed, both consist of achromatic lattice modules which add up their R_{56} and T_{566} contributions to satisfy both full compression conditions.

The transfer line in Layout A guides the bunches into one of the two close symmetry points of cSTART. This layout requires a minimum in space and magnetic components. The transfer line deflects the beam two times using two double bend achromats. Their large R_{56} values are compensated by the FLUTE and an additional four dipole bunch compressors. The geometry requires a vertical injection scheme. The development of such an injection scheme is beyond the scope of this Master's Thesis and is left as a task for future investigations. The transverse optics were set to maintain the transverse bunch size, while the longitudinal optics fulfill both full compression conditions. A tracking simulation

was executed, which results in a final bunch length of 70 fs at the end of the transfer line and in front of the missing injection scheme. The bunch grew a wide spread in the longitudinal phase space and cannot be compressed any further. The reason for this spread are higher order effects which grew from the large dispersion functions coming from the required deflections.

Layout B injects into one of the two distant symmetry points of cSTART, which requires a longer transfer line with more components than in Layout A. The layout starts with an 200° vertical deflecting arc, followed by a dogleg section made by two double bend achromats and a horizontal injection scheme realized by a dipole with a horizontal focusing component. The first double bend achromat in the dogleg section has its deflection plane in between the transverse axis of the bunch coordinate system. This couples the transverse beam dynamics and the transverse optics could not be calculated for the transfer line in one piece. With a tracking based method, the transverse optics could be derived section per section for the whole transfer line including the injection scheme. This method allowed to set the transverse optics to match the final Twiss parameters to the parameters required in cSTART. The final Twiss parameters were propagated into cSTART and evaluated for the first cell of the storage ring where they performed a symmetrical solution. The arc section is made of an hexa bend achromat module, which was designed to tune its R_{56} and T_{566} values in a wide range by changing the optics. With this unique feature, both full compression conditions can be fulfilled. A tracking simulation through the transfer line in Layout B confirmed the conservation of the initial correlated energy spread. As a consequence the final bunch length is compressed to only 17 fs including higher order effects, edge effects and radiation effects. The clean shape of the final bunch is considered to be a result of the low dispersion functions in Layout B in comparison to Layout A. The peak dispersions of the two layouts differ by a factor of two. The lattice in Layout B even has one degree of freedom left open for each, the longitudinal optics in first and in second order. The final bunches' longitudinal shape can therefore be manipulated with an additional shearing and warping while keeping the transverse solution to match the requirements of cSTART.

Both Layouts A and B prove the possibility of injecting an ultra-short bunch from FLUTE to cSTART. Then Layout A is a space and cost saving solution to the transport challenge, while Layout B requires more elements but, in return, results in a shorter bunch length and a higher flexibility. Although all simulations were executed with bunches at the energy of 42 MeV, all magnetic multipole strengths are kept within such limitations that bunches with energies of up to 100 MeV can be transported within the same optics. This provides the possibility of future upgrades of FLUTE to join the cSTART energy acceptance of 50 MeV. Simulations of FLUTE creating bunches with an energy of 50 MeV and additional tracking studies through the transfer line at this energy are necessary tasks of future investigations in order to investigate, if besides the optics, also the performance of the transfer line is energy invariant. Although the optics of the transfer line are invariant within this scope of energy, simulations of FLUTE creating bunches with an energy of 50 MeV and pursuing tracking studies through the transfer line needs to be tasks of future investigations. Also misalignment studies for the transfer line elements and a scan of the dynamic aperture acceptance will be necessary future steps for the project.

A. Appendix

A.1. Transfer line lattice in Layout A

Elegant lattice definition of the transfer line in Layout A, including the reference optics and set up for simulating SR, ISR and CSR effects:

```
! ---------- table of simulation elements ----------

FL_0850:      MARK,      FITPOINT=1
FL_1085:      MARK,      FITPOINT=1
FL_1475:      MARK,      FITPOINT=1
TL_M:         MARK,      FITPOINT=1
M_A5:         MARK,      FITPOINT=1
M_B5:         MARK,      FITPOINT=1
AMP:          MAXAMP,    X_MAX=0.019,Y_MAX=0.019
ROT1:         ROTATE,    TILT=0.785
TL_CHARGE:    CHARGE,    TOTAL=1e-12


! ---------- table of physical elements ----------

ARC_D0:       DRIF,   L=0.5
ARC_D1:       DRIF,   L=0.15
ARC_D2:       DRIF,   L=0.0375
BC2_D1:       DRIF,   L=0.1
BC2_D2:       DRIF,   L=0.5
BC2_D3:       DRIF,   L=0.5
BC2_D4:       DRIF,   L=0.6

FL_D_0850_Q1:     CSRDRIFT,   L=0.25,N_KICKS=10,USE_STUPAKOV=1
FL_D_Q1_Q2:       CSRDRIFT,   L=0.2,N_KICKS=10,USE_STUPAKOV=1
FL_D_Q3_1085:     CSRDRIFT,   L=1.4,N_KICKS=10,USE_STUPAKOV=1
BC_D_1085_B1:     CSRDRIFT,   L=0.1,N_KICKS=10,USE_STUPAKOV=1
BC_D_B1_B2:       CSRDRIFT,   L=0.5041162041194569,N_KICKS=10,USE_STUPAKOV=1
BC_D_B2_B3_5:     CSRDRIFT,   L=0.1998,N_KICKS=10,USE_STUPAKOV=1
BC_D_B4_1475_5:   CSRDRIFT,   L=0.2,N_KICKS=10,USE_STUPAKOV=1


FL_Q1:      KQUAD,   L=0.1,K1=3.394,N_KICKS=30,SYNCH_RAD=1,ISR=1,
                     EDGE1_EFFECTS=2,EDGE2_EFFECTS=2
FL_Q2:      KQUAD,   L=0.1,K1=-9.400825214191414,N_KICKS=30,SYNCH_RAD=1,ISR=1,&
                     EDGE1_EFFECTS=2,EDGE2_EFFECTS=2
FL_Q3:      KQUAD,   L=0.1,K1=4.384555235472567,N_KICKS=30,SYNCH_RAD=1,ISR=1,&
                     EDGE1_EFFECTS=2,EDGE2_EFFECTS=2
ARC_Q_A1:   KQUAD,   L=0.1,K1=-15.79705985909695,SYNCH_RAD=1,ISR=1,&
                     EDGE1_EFFECTS=2,EDGE2_EFFECTS=2
ARC_Q_A2:   KQUAD,   L=0.1,K1=17.65068231822433,SYNCH_RAD=1,ISR=1,&
                     EDGE1_EFFECTS=2,EDGE2_EFFECTS=2
ARC_Q_A4:   KQUAD,   L=0.1,K1=17.65068231822433,SYNCH_RAD=1,ISR=1,&
                     EDGE1_EFFECTS=2,EDGE2_EFFECTS=2
```

```
ARC_Q_A5: KQUAD,    L=0.1,K1=-15.79705985909695,SYNCH_RAD=1,ISR=1,&
                    EDGE1_EFFECTS=2,EDGE2_EFFECTS=2
ARC_Q_B1: KQUAD,    L=0.1,K1=-15.79705985909695,SYNCH_RAD=1,ISR=1,&
                    EDGE1_EFFECTS=2,EDGE2_EFFECTS=2
ARC_Q_B2: KQUAD,    L=0.1,K1=17.65068231822433,SYNCH_RAD=1,ISR=1,&
                    EDGE1_EFFECTS=2,EDGE2_EFFECTS=2
ARC_Q_B4: KQUAD,    L=0.1,K1=17.65068231822433,SYNCH_RAD=1,ISR=1,&
                    EDGE1_EFFECTS=2,EDGE2_EFFECTS=2
ARC_Q_B5: KQUAD,    L=0.1,K1=-15.79705985909695,SYNCH_RAD=1,ISR=1,&
                    EDGE1_EFFECTS=2,EDGE2_EFFECTS=2

ARC_Q_A3: KQUSE,    L=0.2,K1=16.73352364544501,K2=220.2235023180644,TILT=1.57,&
                    SYNCH_RAD=1,ISR=1
ARC_Q_B3: KQUSE,    L=0.2,K1=15.39273199074215,K2=99.7268621568326,TILT=1.57,&
                    SYNCH_RAD=1,ISR=1


BC2_R1:     SBEN,     L=0.2028508379009515,ANGLE=0.5249033392548849,&
                      E1=0.2624516696274424,E2=0.2624516696274424
BC2_R2:     SBEN,     L=0.2028508379009515,ANGLE=-0.5249033392548849,&
                      E1=-0.2624516696274424,E2=-0.2624516696274424
BC2_R3:     SBEN,     L=0.2028508379009515,ANGLE=-0.5249033392548849,&
                      E1=-0.2624516696274424,E2=-0.2624516696274424
BC2_R4:     SBEN,     L=0.2028508379009515,ANGLE=0.5249033392548849,&
                      E1=0.2624516696274424,E2=0.2624516696274424

ARC_BEND_A: CSBEND,  L=0.785,ANGLE=0.785,TILT=1.57
ARC_BEND_B: CSBEND,  L=0.872,ANGLE=0.872,TILT=1.57

BC_B1:  CSRCSBEND,   L=0.2016827459751336,ANGLE=0.1972222,E2=0.1972222,&
                     N_KICKS=30,SYNCH_RAD=1,BINS=600,SG_HALFWIDTH=1,&
                     SGDERIV_HALFWIDTH=1,ISR=1
BC_B2:  CSRCSBEND,   L=0.2016827459751336,ANGLE=-0.1972222,E1=-0.1972222,&
                     N_KICKS=30,SYNCH_RAD=1,BINS=600,SG_HALFWIDTH=1,&
                     SGDERIV_HALFWIDTH=1,ISR=1
BC_B3:  CSRCSBEND,   L=0.2016827459751336,ANGLE=-0.1972222,E2=-0.1972222,&
                     N_KICKS=30,SYNCH_RAD=1,BINS=600,SG_HALFWIDTH=1,&
                     SGDERIV_HALFWIDTH=1,ISR=1
BC_B4:  CSRCSBEND,   L=0.2016827459751336,ANGLE=0.197222301841422,E1=0.1972222,&
                     N_KICKS=30,SYNCH_RAD=1,BINS=600,SG_HALFWIDTH=1,&
                     SGDERIV_HALFWIDTH=1,ISR=1

! ---------------------- table of segments ----------------------

START:  LINE=(AMP,TL_CHARGE,FL__0850)
FL_Q:   LINE=(FL__D__0850__Q1,FL__Q1,FL__D__Q1__Q2,FL__Q2,FL__D__Q1__Q2,&
             FL__Q3,FL__D__Q3__1085)
FL_BC:  LINE=(FL__1085,BC__D__1085__B1,BC__B1,BC__D__B1__B2,BC__B2,BC__D__B2__B3,BC__B3,&
             BC__D__B1__B2,BC__B4,BC__D__B4__1475,FL__1475)
DBA_1:  LINE=(TL_M,ARC_D0,ARC_D1,ARC_Q_A1,ARC_D1,ARC_Q_A2,ARC_D1,ARC_BEND_A,&
             ARC_D1,ARC_Q_A3,ARC_D1,ARC_BEND_A,ARC_D1,ARC_Q_A4,ARC_D1,ARC_Q_A5,&
             M_A5,ARC_D2,ARC_D2,TL_M)
DBA_2:  LINE=(ARC_D2,ARC_D2,ARC_Q_B1,ARC_D1,ARC_Q_B2,ARC_D1,ARC_BEND_B,ARC_D1,&
             ARC_Q_B3,ARC_D1,ARC_BEND_B,ARC_D1,ARC_Q_B4,ARC_D1,ARC_Q_B5,M_B5,&
             ARC_D1,TL_M)
BC_2:   LINE=(BC2__D1,BC2__R1,BC2__D2,BC2__R2,BC2__D3,BC2__R3,BC2__D2,BC2__R4,BC2__D1,&
             BC2__D4,TL_M)

TRANSFER_LINE: LINE = (START,FL_Q,FL_BC,DBA_1,ROT1,DBA_2,BC_2)
```

A.2. Transfer line lattice in Layout B

Elegant lattice definition of the transfer line in Layout B, including the reference optics and set up for simulating SR, ISR and CSR effects:

```
! ---------- table of simulation elements ----------

FL_0850:     MARK,     FITPOINT=1
FL_1085:     MARK,     FITPOINT=1
FL_1475:     MARK,     FITPOINT=1
TL_M:        MARK,     FITPOINT=1
ARC_M:       MARK,     FITPOINT=1
DL_L_M:      MARK,     FITPOINT=1
DL_R_M:      MARK,     FITPOINT=1
AMP:         MAXAMP,   X_MAX=0.019,  Y_MAX=0.019
ROT_A:       ROTATE,   TILT=0.3129792268113461
ROT_B:       ROTATE,   TILT=-0.45051429522529074
TL_CHARGE:   CHARGE,   TOTAL=1e-12


! ---------- table of physical elements ----------

DL_L_S:      KSEXT,  L=0.05,TILT=0.3129792268113461,SYNCH_RAD=1,ISR=1

FL_Q1:       KQUAD,   L=0.1,K1=5.184776190874386,N_KICKS=30,SYNCH_RAD=1,ISR=1,&
                      EDGE1_EFFECTS=2,EDGE2_EFFECTS=2
FL_Q2:       KQUAD,   L=0.1,K1=-8.146937847344917,N_KICKS=30,SYNCH_RAD=1,ISR=1,&
                      EDGE1_EFFECTS=2,EDGE2_EFFECTS=2
FL_Q3:       KQUAD,   L=0.1,K1=4.041271950071343,N_KICKS=30,SYNCH_RAD=1,ISR=1,&
                      EDGE1_EFFECTS=2,EDGE2_EFFECTS=2

ARC_Q_A1:    KQUAD,   L=0.1,K1=-4.512081553620915,N_KICKS=30,SYNCH_RAD=1,ISR=1,&
                      EDGE1_EFFECTS=2,EDGE2_EFFECTS=2
ARC_Q_A2:    KQUAD,   L=0.1,K1=20.61077906618818,N_KICKS=30,SYNCH_RAD=1,ISR=1,&
                      EDGE1_EFFECTS=2,EDGE2_EFFECTS=2
ARC_Q_A4:    KQUAD,   L=0.1,K1=24.84041923677122,N_KICKS=30,SYNCH_RAD=1,ISR=1,&
                      EDGE1_EFFECTS=2,EDGE2_EFFECTS=2
ARC_Q_AB:    KQUAD,   L=0.2,K1=-19.47516550867683,N_KICKS=30,SYNCH_RAD=1,ISR=1,&
                      EDGE1_EFFECTS=2,EDGE2_EFFECTS=2
ARC_Q_B2:    KQUAD,   L=0.1,K1=22.5346760987694,N_KICKS=30,SYNCH_RAD=1,ISR=1,&
                      EDGE1_EFFECTS=2,EDGE2_EFFECTS=2
ARC_Q_B4:    KQUAD,   L=0.1,K1=22.5346760987694,N_KICKS=30,SYNCH_RAD=1,ISR=1,&
                      EDGE1_EFFECTS=2,EDGE2_EFFECTS=2
ARC_Q_BC:    KQUAD,   L=0.2,K1=-19.47516550867683,N_KICKS=30,SYNCH_RAD=1,ISR=1,&
                      EDGE1_EFFECTS=2,EDGE2_EFFECTS=2
ARC_Q_C2:    KQUAD,   L=0.1,K1=24.84041923677122,N_KICKS=30,SYNCH_RAD=1,ISR=1,&
                      EDGE1_EFFECTS=2,EDGE2_EFFECTS=2
ARC_Q_C4:    KQUAD,   L=0.1,K1=20.61077906618818,N_KICKS=30,SYNCH_RAD=1,ISR=1,&
                      EDGE1_EFFECTS=2,EDGE2_EFFECTS=2
ARC_Q_C5:    KQUAD,   L=0.1,K1=-4.512081553620915,N_KICKS=30,SYNCH_RAD=1,ISR=1,&
                      EDGE1_EFFECTS=2,EDGE2_EFFECTS=2

DL_L_Q1:     KQUAD,    L=0.1,K1=29.9996986046588,TILT=0.3129792268113461,&
                       N_KICKS=30,SYNCH_RAD=1,ISR=1,EDGE1_EFFECTS=2,EDGE2_EFFECTS=2
DL_L_Q2:     KQUAD,    L=0.1,K1=-30.9531656972587,TILT=0.3129792268113461,&
                       N_KICKS=30,SYNCH_RAD=1,ISR=1,EDGE1_EFFECTS=2,EDGE2_EFFECTS=2
DL_L_Q3_A:   KQUAD,    L=0.075,K1=34.3721260494656,TILT=0.3129792268113461,&
                       N_KICKS=30,SYNCH_RAD=1,ISR=1,EDGE1_EFFECTS=2,EDGE2_EFFECTS=2
DL_L_Q3_B:   KQUAD,    L=0.075,K1=34.3721260494656,TILT=0.3129792268113461,&
                       N_KICKS=30,SYNCH_RAD=1,ISR=1,EDGE1_EFFECTS=2,EDGE2_EFFECTS=2
DL_L_Q4:     KQUAD,    L=0.1,K1=-31.39756008850459,TILT=0.3129792268113461,&
                       N_KICKS=30,SYNCH_RAD=1,ISR=1,EDGE1_EFFECTS=2,EDGE2_EFFECTS=2
DL_L_Q5:     KQUAD,    L=0.1,K1=28.28969435313239,TILT=0.3129792268113461,&
                       N_KICKS=30,SYNCH_RAD=1,ISR=1,EDGE1_EFFECTS=2,EDGE2_EFFECTS=2

DL_R_Q0A:    KQUAD,   L=0.1,K1=-14.84468705990734,N_KICKS=30,SYNCH_RAD=1,ISR=1,&
                      EDGE1_EFFECTS=2,EDGE2_EFFECTS=2
DL_R_Q0B:    KQUAD,   L=0.1,K1=5.766225884832668,N_KICKS=30,SYNCH_RAD=1,ISR=1,&
```

```
                    EDGE1_EFFECTS=2,EDGE2_EFFECTS=2
DL_R_Q1:    KQUAD,  L=0.1,K1=19.61840488685653,N_KICKS=30,SYNCH_RAD=1,ISR=1,&
                    EDGE1_EFFECTS=2,EDGE2_EFFECTS=2
DL_R_Q2:    KQUAD,  L=0.1,K1=-4.268824545787954,N_KICKS=30,SYNCH_RAD=1,ISR=1,&
                    EDGE1_EFFECTS=2,EDGE2_EFFECTS=2
DL_R_Q3:    KQUAD,  L=0.1,K1=37.66592845322037,N_KICKS=30,SYNCH_RAD=1,ISR=1,&
                    EDGE1_EFFECTS=2,EDGE2_EFFECTS=2
DL_R_Q4:    KQUAD,  L=0.1,K1=-26.38898500824571,N_KICKS=30,SYNCH_RAD=1,ISR=1,&
                    EDGE1_EFFECTS=2,EDGE2_EFFECTS=2
DL_R_Q5:    KQUAD,  L=0.1,K1=33.62958636915386,N_KICKS=30,SYNCH_RAD=1,ISR=1,&
                    EDGE1_EFFECTS=2,EDGE2_EFFECTS=2


BC_B1:      CSRCSBEND,  L=0.2016542099064272,ANGLE=0.1395860730215989,&
                        E2=0.1395860730215989,N_KICKS=30,SYNCH_RAD=1,BINS=600,&
                        SG_HALFWIDTH=1,SGDERIV_HALFWIDTH=1,ISR=1
BC_B2:      CSRCSBEND,  L=0.2016542099064272,ANGLE=-0.1395860730215989,&
                        E1=-0.1395860730215989,N_KICKS=30,SYNCH_RAD=1,BINS=600,&
                        SG_HALFWIDTH=1,SGDERIV_HALFWIDTH=1,ISR=1
BC_B3:      CSRCSBEND,  L=0.2016542099064272,ANGLE=-0.1395860730215989,&
                        E2=-0.1395860730215989,N_KICKS=30,SYNCH_RAD=1,BINS=600,
                        SG_HALFWIDTH=1,SGDERIV_HALFWIDTH=1,ISR=1
BC_B4:      CSRCSBEND,  L=0.2016542099064272,ANGLE=0.1395860730215989,&
                        E1=0.1395860730215989,N_KICKS=30,SYNCH_RAD=1,BINS=600,
                        SG_HALFWIDTH=1,SGDERIV_HALFWIDTH=1,ISR=1
ARC_B2:     SRCSBEND,   L=0.218166156499,ANGLE=0.29088820866,&
                        TILT=1.570796326794897,N_KICKS=30,SYNCH_RAD=1,BINS=600,
                        SG_HALFWIDTH=1,SGDERIV_HALFWIDTH=1,ISR=1
DL_L_B_2:   CSRCSBEND,  L=0.20946446954,ANGLE=-0.20946446954,FINT=0,N_KICKS=30,&
                        SYNCH_RAD=1,BINS=600,SG_HALFWIDTH=1,SGDERIV_HALFWIDTH=1,&
                        ISR=1
DL_R_B_2:   CSRCSBEND,  L=0.3054326190990077,ANGLE=0.3054326190990077,&
                        K1=-1.091642435110967,FINT=0,N_KICKS=30,SYNCH_RAD=1,&
                        BINS=600,SG_HALFWIDTH=1,SGDERIV_HALFWIDTH=1,ISR=1
IN_B:       CSRCSBEND,  L=0.2,ANGLE=0.3490658503988659,K1=10,N_KICKS=30,ISR=1&
                        SYNCH_RAD=1,BINS=600,SG_HALFWIDTH=1,SGDERIV_HALFWIDTH=1

FL_D_0850_Q1:   CSRDRIFT,   L=0.25,N_KICKS=10,USE_STUPAKOV=1
FL_D_Q1_Q2:     CSRDRIFT,   L=0.2,N_KICKS=10,USE_STUPAKOV=1
FL_D_Q3_1085:   CSRDRIFT,   L=1.4,N_KICKS=10,USE_STUPAKOV=1
BC_D_1085_B1:   CSRDRIFT,   L=0.1,N_KICKS=10,USE_STUPAKOV=1
BC_D_B1_B2:     CSRDRIFT,   L=0.5039011074296673,N_KICKS=10,USE_STUPAKOV=1
BC_D_B2_B3_5:   CSRDRIFT,   L=0.1998,N_KICKS=10,USE_STUPAKOV=1
BC_D_B4_1475_5: CSRDRIFT,   L=0.2,N_KICKS=10,USE_STUPAKOV=1
ARC_D:          CSRDRIFT,   L=0.15,N_KICKS=5,USE_STUPAKOV=1
DL_D_ARC_L_6:   CSRDRIFT,   L=0.1746810923105685,N_KICKS=5,USE_STUPAKOV=1
DL_D:           CSRDRIFT,   L=0.15,N_KICKS=5,USE_STUPAKOV=1
DL_D_L_R_10:    CSRDRIFT,   L=0.4647744878273111,N_KICKS=5,USE_STUPAKOV=1
DL_D_R_I_4:     CSRDRIFT,   L=0.125,N_KICKS=5,USE_STUPAKOV=1


ARC_QS_1:       KQUSE,  L=0.2,K1=31.81480766718458,K2=1062.477777777778,&
                        TILT=1.570796326794897,N_KICKS=30,SYNCH_RAD=1,ISR=1
ARC_QS_2:       KQUSE,  L=0.2,K1=31.81480766718458,K2=751.3666666666668,&
                        TILT=1.570796326794897,N_KICKS=30,SYNCH_RAD=1,ISR=1
ARC_QS_3:       KQUSE,  L=0.2,K1=31.81480766718458,K2=940.2555555555555,&
                        TILT=1.570796326794897,N_KICKS=30,SYNCH_RAD=1,ISR=1

! ---------------------- table of segments ----------------------
START:  LINE=(AMP,TL_CHARGE,FL_0850)
FL_Q:   LINE=(FL_D_0850_Q1,FL_Q1,FL_D_Q1_Q2,FL_Q2,FL_D_Q1_Q2,&
            FL_Q3,FL_D_Q3_1085)
```

```
FL_BC:   LINE=(FL_1085,BC_D_1085_B1,BC_B1,BC_D_B1_B2,BC_B2,BC_D_B2_B3,BC_B3,&
              BC_D_B1_B2,BC_B4,BC_D_B4_1475,FL_1475)
ARC:     LINE=(TL_M,ARC_D,ARC_Q_A1,ARC_D,ARC_Q_A2,ARC_D,ARC_B*2,ARC_D,ARC_QS_1,&
              ARC_D,ARC_B*2,ARC_M,ARC_D,ARC_Q_A4,ARC_D,ARC_Q_AB,ARC_M,ARC_D,&
              ARC_Q_B2,ARC_D,ARC_B*2,ARC_D,ARC_QS_2,ARC_D,ARC_B*2,ARC_M,ARC_D,&
              ARC_Q_B4,ARC_D,ARC_Q_BC,ARC_M,ARC_D,ARC_Q_C2,ARC_D,ARC_B*2,ARC_D,&
              ARC_QS_3,ARC_D,ARC_B*2,ARC_M,ARC_D,ARC_Q_C4,ARC_D,ARC_Q_C5,ARC_D,&
              TL_M,DL_D_ARC_L_6*3)
DL_L:    LINE=(DL_D_ARC_L_6*3,TL_M,DL_D,DL_L_M,DL_L_Q1,DL_D,DL_L_Q2,DL_D,DL_L_M,&
              DL_L_B,DL_D,DL_L_Q3_A,DL_D,DL_L_S,DL_L_M,DL_D,DL_L_Q3_B,DL_D,DL_L_B,&
              DL_L_M,DL_D,DL_L_Q4,DL_D,DL_L_Q5,DL_L_M,DL_D,TL_M,DL_D_L_R_10*5)
DL_R:    LINE=(DL_D_L_R_10*5,TL_M,DL_D,DL_R_Q0A,DL_D,DL_R_Q0B,DL_D,DL_R_Q1,DL_R_M,&
              DL_D,DL_R_Q2,DL_D,DL_R_M,DL_R_B,DL_D,DL_R_Q3,DL_D,DL_R_B,DL_R_M,&
              DL_D,DL_R_Q4,DL_D,DL_R_Q5,DL_R_M,DL_D,TL_M)
INJ:     LINE=(DL_D_R_I,IN_B,TL_M)

TRANSFER_LINE: LINE = (START,FL_Q,FL_BC,ARC,ROT_A,DL_L,ROT_B,DL_R,INJ)
```

A.3. cSTART lattice

Elegant lattice definition of the cSTART storage ring, provided by A. Papash (2019):

```
! ---------------------- table of elements ----------------------

RING_dd1        : drift,   l = 1.000000
RING_d11        : drift,   l = 0.100000
RING_d21        : drift,   l = 0.100000
RING_db1        : drift,   l = 0.150000
RING_db2        : drift,   l = 0.100000
RING_ds4        : drift,   l = 0.050000
RING_d51        : drift,   l = 0.080000
RING_ds5        : drift,   l = 0.047000
RING_d61        : drift,   l = 0.080000
RING_ds6        : drift,   l = 0.050000
RING_db3        : drift,   l = 0.100000
RING_d81        : drift,   l = 0.075000

RING_dm         : marker

RING_q1         : quad,    l = 0.075000, k1 = -2.138000
RING_q2         : quad,    l = 0.100000, k1 = 6.736000
RING_q3         : quad,    l = 0.075000, k1 = -4.010000
RING_q4a        : quad,    l = 0.075000, k1 = 11.700000
RING_q4b        : quad,    l = 0.075000, k1 = 11.485000
RING_q5a        : quad,    l = 0.075000, k1 = -15.305000
RING_q5b        : quad,    l = 0.075000, k1 = -16.435000
RING_q6a        : quad,    l = 0.075000, k1 = 11.650000
RING_q6b        : quad,    l = 0.075000, k1 = 11.650000
RING_q7         : quad,    l = 0.100000, k1 = -2.437000
RING_q8         : quad,    l = 0.100000, k1 = 8.460000

RING_bend1      : csbend,  l=0.25, angle=0.196350, k1=-3.99, e1 = 0.196350,&
                           e2 = 0, hgap = 0, fint =0
RING_bend2      : csbend,  l=0.25, angle=0.196350, k1=-3.99, e1 = 0,&
                           e2 = 0.196350, hgap = 0, fint =0

RING_s1              : mult, l=0.0, knl = 0.0000, order=2
RING_s11             : mult, l=0.0, knl = 0.0000, order=2
RING_s2              : mult, l=0.0, knl = 0.0000, order=2
RING_s21             : mult, l=0.0, knl = 0.0000, order=2
RING_s3              : mult, l=0.0, knl = 0.0000, order=2
RING_s41             : mult, l=0.0, knl = 0.0000, order=2
RING_s4a             : mult, l=0.0, knl = 4.4200, order=2
```

```
RING_s4              : mult, l=0.0, knl = 4.4000, order=2
RING_s4b             : mult, l=0.0, knl = 4.4000, order=2
RING_s51             : mult, l=0.0, knl = 0.0000, order=2
RING_s5a             : mult, l=0.0, knl = -22.5000, order=2
RING_s5              : mult, l=0.0, knl = -22.5000, order=2
RING_s5b             : mult, l=0.0, knl = -22.5000, order=2
RING_s61             : mult, l=0.0, knl = 0.0000, order=2
RING_s6a             : mult, l=0.0, knl = 4.2200, order=2
RING_s6              : mult, l=0.0, knl = 4.2200, order=2
RING_s6b             : mult, l=0.0, knl = 4.2200, order=2
RING_s62             : mult, l=0.0, knl = 0.0000, order=2
RING_s7              : mult, l=0.0, knl = 0.0000, order=2
RING_s81             : mult, l=0.0, knl = 0.0000, order=2
RING_s8              : mult, l=0.0, knl = 0.0000, order=2

RING_oc1             : mult, l=0.0, knl = 0.0000, order=3
RING_oc11            : mult, l=0.0, knl = 0.0000, order=3
RING_oc2             : mult, l=0.0, knl = 0.0000, order=3
RING_oc21            : mult, l=0.0, knl = 0.0000, order=3
RING_oc3             : mult, l=0.0, knl = 0.0000, order=3
RING_oc41            : mult, l=0.0, knl = 0.0000, order=3
RING_oc4             : mult, l=0.0, knl = 0.0000, order=3
RING_oc51            : mult, l=0.0, knl = 0.0000, order=3
RING_oc5             : mult, l=0.0, knl = 0.0000, order=3
RING_oc61            : mult, l=0.0, knl = 0.0000, order=3
RING_oc6             : mult, l=0.0, knl = 0.0000, order=3
RING_oc62            : mult, l=0.0, knl = 0.0000, order=3
RING_oc7             : mult, l=0.0, knl = 0.0000, order=3
RING_oc81            : mult, l=0.0, knl = 0.0000, order=3
RING_oc8             : mult, l=0.0, knl = 0.0000, order=3

! ---------------------- table of segments ----------------------

halfcell  : line=(RING_dd1,RING_q1,RING_s1,RING_q1,RING_d11,RING_s11,&
                  RING_d11,RING_q2,RING_s2,RING_q2,RING_d21,RING_s21,RING_d21,&
                  RING_q3,RING_s3,RING_q3,RING_db1,RING_bend1,RING_dm,RING_bend2,&
                  RING_db2,RING_s41,RING_db2,RING_q4a,RING_s4a,RING_q4a,RING_ds4,&
                  RING_s4,RING_ds4,RING_q4b,RING_s4b,RING_q4b,RING_d51,RING_s51,&
                  RING_d51,RING_q5a,RING_s5a,RING_q5a,RING_ds5,RING_s5,RING_ds5,&
                  RING_q5b,RING_s5b,RING_q5b,RING_d61,RING_s61,RING_d61,RING_q6a,&
                  RING_s6a,RING_q6a,RING_ds6,RING_s6,RING_ds6,RING_q6b,RING_s6b,&
                  RING_q6b,RING_db2,RING_s62,RING_db2,RING_bend1,RING_dm,&
        RING_bend2,RING_db3,RING_q7,RING_s7,RING_q7,RING_d81,RING_s81,&
        RING_d81,RING_q8,RING_dm)

cell      : line = (halfcell, RING_s8, -halfcell)

RING      : line = (cell, -cell, cell, -cell)
```

Bibliography

[1] M. J. Nasse, M. Schuh, S. Naknaimueang, M. Schwarz, A. Plech, Y.-L. Mathis, R. Rossmanith, P. Wesolowski, E. Huttel, M. Schmelling, and A.-S. Müller, "FLUTE: A versatile linac-based THz source," *Review of Scientific Instruments*, vol. 84, no. 2, p. 022705, Feb. 2013. [Online]. Available: https://doi.org/10.1063/1.4790431

[2] A. Papash, E. Bründermann, and A.-S. Müller, "An Optimized Lattice for a Very Large Acceptance Compact Storage Ring," in *Proceedings, 8th International Particle Accelerator Conference (IPAC 2017): Copenhagen, Denmark, May 14-19, 2017*, 2017, p. TUPAB037.

[3] "European XFEL," https://www.xfel.eu/index_eng.html, [accessed Oktober 01, 2019].

[4] "The SwissFEL X-ray free-electron laser," https://www.psi.ch/en/media/the-swissfel-x-ray-free-electron-laser, [accessed Oktober 01, 2019].

[5] "Karlsruhe Research Accelerator KARA," http://www.ibpt.kit.edu/1654.php, [accessed Oktober 01, 2019].

[6] "MAX IV," https://www.maxiv.lu.se, [accessed Oktober 01, 2019].

[7] Borland M., Emery L., Shang H., Soliday R., "User's Guide for SDDS Toolkit." [Online]. Available: https://ops.aps.anl.gov/manuals/SDDStoolkit/SDDStoolkit.html

[8] B. Marchetti, R. Assmann, U. Dorda, and J. Zhu, "Conceptual and Technical Design Aspects of Accelerators for External Injection in LWFA," *Applied Sciences*, vol. 8, p. 757, 05 2018.

[9] J. Schäfer, B. Härer, A. Papash, and A.-S. Müller, "Transfer line for ultra short bunches from FLUTE to cSTART," Vortrag gehalten auf DPG-Frühjahrstagung der Sektion Materie und Kosmos (SMuK), Arbeitskreis Beschleunigerphysik (2019), München, Deutschland, 17.–22. März 2019, 2019.

[10] K. Wille, *Physik der Teilchenbeschleuniger und Synchrotronstrahlungsquellen - Eine Einführung*. Wiesbaden: Springer-Verlag, 1996.

[11] A. Wu Chao, M. K. H., T. M., and Z. F., *Handbook of Accelerator Physics and Engineering*, second edition ed. Singapur: World Scientific, 2013.

[12] A. Wolski, *Beam Dynamics In High Energy Particle Accelerators*. Singapur: World Scientific, 2014.

[13] B. Härer, "Lattice design and beam optics calculations for the new large-scale electron-positron collider FCC-ee," Ph.D. dissertation, Karlsruher Institut für Technologie (KIT), 2017.

[14] A. S. Müller, "Description of Beam-Matter Interaction in the Covariance Matrix Formalism: Application to Modification of Emittance and Twiss Parameters; rev. version," CERN, Geneva, Tech. Rep. CERN-PS-2001-013-AE, May 2001. [Online]. Available: https://cds.cern.ch/record/499590

[15] M. Borland, "elegant: A Flexible SDDS-Compliant Code for Accelerator Simulation," September 2000, Advanced Photon Source LS-287, elegant stands for ELEctron Generation ANd Tracking".

[16] ——, "Simple method for particle tracking with coherent synchrotron radiation," *Phys. Rev. ST Accel. Beams*, vol. 4, p. 070701, Jul 2001. [Online]. Available: https://link.aps.org/doi/10.1103/PhysRevSTAB.4.070701

[17] D. Zhou, K. Sokendai, J. Y Tang, Y. Chen, N. Wang, P. R Beijing, and C. , "Explicit maps for the fringe field of a quadrupole," *IPAC 2010 - 1st International Particle Accelerator Conference*, 01 2010.

[18] M. Yan, A.-S. Müller, M. Nasse, M. Schuh, and M. Schwarz, "Optimization of THz Radiation Pulses at FLUTE," in *Proc. of International Particle Accelerator Conference (IPAC'16), Busan, Korea, May 8-13, 2016*, ser. International Particle Accelerator Conference, no. 7. Geneva, Switzerland: JACoW, June 2016, paper WEPOY037, pp. 3067–3069, doi:10.18429/JACoW-IPAC2016-WEPOY037. [Online]. Available: http://jacow.org/ipac2016/papers/wepoy037.pdf

[19] T. Schmelzer *et al.*, "Diagnostics and First Beam Measurements at FLUTE," in *Proc. 10th International Partile Accelerator Conference (IPAC'19), Melbourne, Australia, 19-24 May 2019*, ser. International Partile Accelerator Conference, no. 10. Geneva, Switzerland: JACoW Publishing, Jun. 2019, paper WEPGW010, pp. 2484–2486, https://doi.org/10.18429/JACoW-IPAC2019-WEPGW010. [Online]. Available: http://jacow.org/ipac2019/papers/wepgw010.pdf

[20] Floettmann K., "Astra, a space charge tracking algorithm." [Online]. Available: http://www.desy.de/~mpyflo/

[21] A. Papash, E. Bründermann, A.-S. Müller, R. Ruprecht, and M. Schuh, "Design of a very large acceptance compact storage ring," *Proceedings of the 9th Int. Particle Accelerator Conf.*, vol. IPAC2018, p. Canada, 2018. [Online]. Available: http://jacow.org/ipac2018/doi/JACoW-IPAC2018-THPMF071.html

[22] *Handbook of Accelerator Physics and Engineering (2nd Edition).* World Scientific Publishing Company, 2013.

[23] H. Wiedemann, *Particle Accelerator Physics - Basic Principles and Linear Beam Dynamics.* Berlin Heidelberg New York: Springer-Verlag, 1993.

[24] J. P. Delahaye and J. Jäger, "Variation of the dispersion function, momentum compaction factor, and damping partition numbers with particle energy deviation," *Part. Accel.*, vol. 18, no. SLAC-PUB-3585, pp. 183–201. 30 p, Feb 1985. [Online]. Available: https://cds.cern.ch/record/159404

[25] CERN, "Cern yellow reports: School proceedings, vol 1 (2018): Proceedings of the cas-cern accelerator school on free electron lasers and energy recovery linacs," 2018. [Online]. Available: https://e-publishing.cern.ch/index.php/CYRSP/issue/view/47

[26] P. Schreiber, A. Papash, A. Mochihashi, B. Härer, M. Schuh, M. Brosi, and T. Boltz, "Status of operation with negative momentum compaction at kara," Vortrag gehalten auf DPG-Frühjahrstagung der Sektion Materie und Kosmos (SMuK), Arbeitskreis Beschleunigerphysik (2019), München, Deutschland, 17.–22. März 2019, 2019.

Acknowledgements

I would like to thank all the people that have contributed to this thesis. First of all, I want to express my gratitude to Prof. Dr. Anke-Susanne Müller for providing me the opportunity to write my thesis at such an interesting field at IBPT, KIT.

Also I want to thank Prof. Dr. Ulrich Husemann for reviewing my Thesis.

I would like give my sincere thanks to my advisor, Dr. Bastian Härer, for countless discussions about every last detail and his encouraging enthusiasm for the physics of accelerators.

Abschließend möchte ich meinen Eltern für die andauernde Unterstützung während der gesammten Studienzeit hinweg herzlichst danken.